

DOTTORATO DI RICERCA IN

INGEGNERIA CIVILE, CHIMICA, AMBIENTALE E DEI MATERIALI Ciclo 37

Settore Concorsuale: 08/B2 – Scienza delle Costruzioni

Settore Scientifico Disciplinare: ICAR08 – Scienza delle Costruzioni

MECHANICAL PERFORMANCE OF ARUNDO DONAX ENGINEERED PANELS: EXPERIMENTAL AND NUMERICAL APPROACHES

Presentata da: Giovanni Donini

Coordinatore Dottorato Supervisore

Enrico Sassoni Luisa Molari

Co-supervisori

Vincent Placet

Stefania Manzi

Esame finale anno 2025

Be like bamboo.
On the outside, it is hard and compact,
inside, it is soft and hollow.
Its roots are firmly anchored in the ground
and intertwine with those of other plants
to strengthen and support each other.
The stem allows itself to be freely swayed by the wind,
and instead of resisting, it bends.
What bends is much harder to break.

Buddhist Mantra

Preface

For centuries, humanity has attempted to modify nature, bending it to its will, seeing it as a fierce, cruel, and relentless stepmother. This led humans to emancipate themselves from nature. This emancipation, initially viewed as a triumph of humanity over nature and labeled as "progress," eventually alienated humans from nature, causing them to lose the intimate connection they once had with it. Mankind isolated itself in forests of steel and concrete, traveling in plastic and aluminum vessels on rivers of asphalt.

It would be nice to say that humanity realized the error of its ways, but that would not be truthful. It was nature that awakened us, reminding us that we are part of something greater, with which we must not only live but also coexist. The task before all of us is to relearn a basic yet fundamental concept: "We are nature, and nature is us".

This research work, which lasted three years, fits precisely into this context and aims to make a small contribution to this journey.

The research project was based on the study of engineered panels made using a plant, or more precisely, a native grass of the Italian peninsula, *Arundo donax* (AD).

Three research projects were carried out, each differing mainly in the type of panel studied. The first focused on honeycomb panels, where a fiber-composite material was used for the skins and AD rings for the core. The second project involved particleboard sandwich panels, made with a mix of recycled wood chips and AD. This project was conducted in collaboration with the company Gruppo Saviola, based in Viadana, Mantova, which operates in the production of non-structural particleboard panels and the chemical industry. The third project focused on studying an innovative particleboard panel that does not use adhesives or other chemical additives. In this case, the project was carried out in collaboration with the start-up My.Fibers, based in Modena.

The research project aimed to demonstrate the feasibility and advantages of using AD to manufacture various types of panels, highlighting its strengths and weaknesses, and exploring potential applications in the construction field as an alternative to traditional building materials.

The general objectives of the PhD project were to contribute to the green transition that the construction sector is called upon to achieve. The project aimed to design engineered elements for the construction industry using natural and local materials that have been used for centuries in our peninsula, such as AD, as an alternative to traditional building materials.

This doctoral project was carried out at the University of Bologna with important collaboration from several Italian companies, including Linificio e Canapificio Nazionale, Gruppo Saviola, and My.Fibers. Additionally, a period of six months was spent at the FEMTO-ST Institute at the University of Besançon. The doctoral projects allowed for forging significant relationships with the national industrial sector, and have facilitated connections with International Universities, such as the FEMTO-ST Institute of the University of Besançon.

INDEX

Preface	3
1. INTRODUCTION	11
2. ARUNDO DONAX	12
3. HONEYCOMB PANEL	17
3.1 Introduction	17
3.2 Materials	18
3.3 Manufacture	19
3.4 Methods	22
3.4.1 Roughness analysis of AD cross-section	22
3.4.2 Pull-off Test	23
3.4.3 Three-points bending test	23
3.4.4 Analytical Model	24
3.4.5 Finite Element Model (FEM)	25
3.5 Results and Discussions	27
3.5.1 Analysis of the cross-section surface	27
3.5.2 Pull-off tests	28
3.5.3 Three-points bending tests	29
3.5.4 Results of Analytical and Finite Element Modelling on Flexural Behaviour	32
3.6 Conclusion	38
4. PARTICLEBOARD PANEL	40
4.1 Introduction	40
4.2 Wave 1	41
4.2.1 Materials	42
4.2.2 Manufacturing process	42
4.2.3 Methods	44
4.2.4 Results	48
4.2.5 Discussion	52
4.3 Wave 2	54
4.3.1 Materials	55
4.3.2 Methods	56
4.3.3 Results	57
4.3.4 Discussion	65
4.4 Conclusions	66
5. BINDERLESS PARTICLESBOARD	68
5.1 Introduction	68
5.2 Manufacture and Methods	70

5.3.1 Physical properties	5.3 Results	72
5.3.2 Mechanical properties	5.3.1 Physical properties	72
6. Conclusions83		
	5.4 Conclusion	81
Appendix A	6. Conclusions	83
1 pp • 11 d 1 / 1 1 1 1 1 1 1 1 1 1 1 1 1 1 1	Appendix A	85
References	References	98

Figure Index

Figure 1. Spread of Arundo donax around the world	12
Figure 2. Arundo donax.	13
Figure 3. Cross sections of a culm of Arundo donax, in longitudinal and transverse directions	
Figure 4. (a) Unpolished lateral surface; (b) P120 polished lateral surface; (c) Z80 polished surface.	lateral
Figure 5 . Core rings distribution and dimensions. Inner and outer diameter was measured for crings	orange
Figure 6. (a) Flax/epoxy composite skin; (b) AD rings for core in a frame (300mm x200mm) polishing the cross-section surface; (c) Polishing setup.	before
Figure 7. Detail of panel's components	
Figure 8. (a) Thermohydraulic press; (b) Sandwich panel core focus; (c) Sandwich panel skin	focus.
Figure 9. (a) Sample in the oven at 100 °C before the pull-off test; (b) Samples after the pull-off test;	ff test.
Figure 10. Three-point bending test setup.	24
Figure 11 . Finite Element Model (FEM) of a sandwich beam under a three-point bending test. Figure 12. (a). Unpolished cross section's surface; (b) Polished cross section's surface with sandpaper	P120
Figure 13. (a) Depth [μm] vs Surface Portance [%] for polished specimens; (b) Depth [μm] vs S Portance [%] for unpolished specimens	urface
Figure 14 . (a) Unpolished cross section analysis after the pull-off test, images collected using Eclipse LV150 with a 5x lens; (b) P120 polished cross section analysis after the pull-off test, it collected using Nikon Eclipse LV150 with a 5x lens.	mages
Figure 15. Load-displacement curves for all the specimens.	
Figure 16. (a) Failure mode for unpolished lateral surface; (b) Failure mode for P120 polished surface; (c) Failure mode for Z80 polished lateral surface.	lateral
Figure 17. Comparison of the Load-Displacement curves from the average experimental Equivalent Plate Theory and Sandwich Panel Theory for: (a) Experimental average Unpolished (b) Experimental average P120 Polished (P120).	data, l (UP),
Figure 18. Comparison between the load-displacement curves: (a) Average of Unpo ecperimental samples and the Finite Element Model; (b) all the Unpolished experimental spec and Finite Element Model.	
Figure 19. Load-displacement for Exp. P120 Average and the P120 Finite Element Model (FEM1).	35
Figure 20. Comparison between the load-displacement curve: (a) Average of P120 experir samples and the P120-FEM2; b) all the P120 experimental specimens and the P120-FEM2 c) Available for the experiment Unpolished and Polished specimens.	verage
Figure 21 . Steps followed for the particleboard production process: (a) mechanical mixing materials, (b) preforming the particleboard by applying manual pressure, (c) hot molding particleboard	of the
Figure 22. (a) Immersion of the specimens in the water bath. (b) Thickness swelling test on a s with a cross-section area of 50 x 50 mm	45
Figure 23. (a) Test preparation. (b) Surface soundness test on a sample Thickness swelling test sample with a cross-section area of 50 x 50 mm.	46
Figure 24. (a) Test preparation. (b) Internal bond test on a sample Thickness swelling test on a swith a cross-section area of 50 x 50 mm	46
Figure 25. Three-point bending test on a sample of 300 x 50 x 22 mm.	47

Figure 26. The trend of (a) Thickness swelling 2 h (TS 2 h), (b) Surface soundness and (c) Internal
bond (IB), for the three densities and the variation of the quantity of AD in the core of the
particleboard49
Figure 27. Bending strength (σm) of the particleboard over the quantity of AD in the core according
to the density of the board51
Figure 28. Bending strength (σm) of the particleboard over the Density of the board according to the
percentages of AD in the core51
Figure 29. A response surface with two input variables, the density and the Arundo donax percentage
and the output being the bending strength σm .
Figure 30. Comparison with normative limits for different types of particleboard panels for the
following characteristics: (a) bending strength σm , (b) Modulus of elasticity E_m and (c) Internal bond
(IB)53
Figure 31. Size of particles of sieve-fractionated particles of wood recycled chips: (a) $d < 0.5$ mm;
(b) between $0.5 < d < 1$ mm; (c) between $1 < d < 2$ mm; (d) between $2 < d < 4$ mm
Figure 32. Size of particles of sieve-fractionated particles of Arundo donax chips: (a) $d < 0.5$ mm;
(b) between $0.5 < d < 1 \text{ mm}$; (c) between $1 < d < 2 \text{ mm}$; (d) between $2 < d < 4 \text{ mm}$; (e) between $4 < d < 4 \text{ mm}$;
d < 8 mm
Figure 33. Trend of Slenderness Ratio (SR) with the granulometry for: (a) Arundo donax and (b)
recycle wood.
Figure 34. Trend of Aspect Ratio (AR) with the granulometry for: (a) Arundo donax and (b) recycle
wood58
Figure 35. (a) Slenderness Ratio (SR) and (b Aspect Ratio (AR) AD for the different groups of
particleboards
Figure 36. Trend of average values for (a) thickness swelling 2 h (TS 2 h), (b) water absorption 2 h
(WA 2 h), (c) surface soundness and (d) Internal bond (IB), for 20 % (orange line) and 35 % (blue
line) of AD content. The black dot line represents the value of the specific physical-mechanical
property associated with the A0 specimen60
Figure 37. Box plots for the 20 % AD content, for physical and mechanical properties: (a) Thickness
swelling 2 h; (b) Water absorption 2 h; (c) Surface soundness; (d) Internal bond61
Figure 38. Box plots for the 35 % AD content, for physical and mechanical properties: (a) Thickness
swelling 2 h; (b) Water absorption 2 h; (c) Surface soundness; (d) Internal bond62
Figure 39. (a) Bending strength (σm) and (b) Modulus of elasticity (E_m) for 20 % (orange line) and
35 % (blue line) of Arundo donax content. The black dot line represents the value of the specific
physical-mechanical property associated with the A0 specimen64
Figure 40. Box plots for the 20 % Arundo donax content: (a) Bending strength (σm) ; (b) Modulus
of elasticity (E_m)64
Figure 41 . Box plots for the 35 % Arundo donax content: (a) Bending strength (σm) ; (b) Modulus
of elasticity (E_m) .
Figure 42 . Trend of average values of thickness swelling 2 h (TS 2 h) and 24 h (TS 24 h) for the
forming pressure of: (a) 0.2 MPa, (b) 0.5 MPa and (c) 1 MPa
Figure 43. Trend of average values of water absorption 2 h (WA 2 h) and 24 h (WA 24 h) for the
forming pressure of: (a) 0.2 MPa, (b) 0.5 MPa and (c) 1 MPa
Figure 44. Comparison with normative limits for different types of particleboards for: (a) TS 24 h
and (b) WA 24 h. The red line represents the standard limits associated with the P4 class74
Figure 45. (a) Specimens setup; (b) Setup for the surface soundness test; (c) Setup for the internal
bond test
Figure 46. Comparison with normative limits for different types of particleboards for: (a) surface
soundness test and (b) internal bond (IB). The red lines represent the standard limits associated with
the P1 and P2 classes

Figure 47 Optical microscope images of the fracture surfaces after the IB test, for the specimens
with a pressing pressure of 1 MPa and the different types of aggregates: (a)-(b) Arundo donax; (c)-
(d) Bamboo; (e)-(f) Hemp; (g)-(h) Hemp with a ratio of matrix/aggregate of 60/4078
Figure 48. Setup of the three-point bending test
Figure 49 . Bending strength (σm) for different values of forming pressure: (a) 0.2 MPa, (b) 0.5 MPa
and (c) 1 MPa80
and (c) 1 MPa
MPa and (c) 1 MPa80
Figure 51. Comparison with normative limits for different types of particleboards for: (a) Bending
strength (σm) and (b) Modulus of elasticity (E_m) . The red lines represent the standard limits associated with the P1 and P2 classes.
Figure 52. Microscopic images: (a) hemp woven fabric and (b) single hemp fiber
Figure 53. The sequence of the lamination phases
Figure 54. On the left, is the Galdabini Machine used for the tensile test. On the right, are the Digital
Image Correlation instruments
Figure 55. Histograms of: (a) volume percentage of the matrix, fibres and voids of all the types of
composites and (b) weight percentage of the matrix and fibres
Figure 56. (a) Stress-Strain in the longitudinal direction and (b) Elastic modulus- N/N _{max} for the
generic samples 1A190
Figure 57. Images obtained from the Scanning Electron Microscope (SEM) for the fracture surfaces
of some of the specimens tested with tension test: (a) are reported the specimens 1A1; (b) are reported
the specimens 1B2; (c) are reported the specimens 2B4; (d) are reported the specimens 1C3; (e) are
reported the specimens 2C591
Figure 58. Images obtained from the Scanning Electron Microscope (SEM) for the fracture surfaces
of the specimens 1A2 tested with tension test
Figure 59. Images obtained from the Scanning Electron Microscope (SEM) for the fracture surfaces
of the specimens 1B2 tested with tension test
Figure 60. Box plots of the mechanical properties for all the tested species: (a) Strength σ ; (b)
coefficient of Poisson; (c) Elastic modulus E for 0.1 N/N _{max} ; (d) Elastic modulus E for 0.6 N/N _{max} .
94

Table Index

Table 1. Average and standard deviation of the density and mechanical properties of Arundo dor	
Table 2. Average and standard deviation of the density and mechanical properties of Arundo dor	nax.
Table 3. Weights of the different manufactured panels.	
Table 4. Engineering constants are considered in the FE model for the facial and core materials.	
Table 5 Cohesive zone parameters were used in the model.	
Table 6. Pull-off test results in term of Maximum load and σ	
Table 7. Three-point bending tests: deflection, load, core shear stress, skin bending stress	
modulus of elasticity	30 30
Table 8. Analysis of variance (ANOVA). Table 9. Average geometrical and mechanical data for unpolished and polished P120 specimen	
Table 10. Output data of the average of the Unpolished, polished P120 specimens and the relative	tive
equivalent panel model and Sandwich model	
Table 11. Cohesive zone parameters for the Unpolished Model.	
Table 12. Comparison output data between the specimen average Unpolished and the Unpolished Element Model (FEM).	
Table 13. Cohesive zone parameters for the P120 Polished model 1	
Table 14. Cohesive zone parameters for the Polished P120 model 2	
Table 15. Comparison output data between the P120 specimen average and the P120 Finite Elem Model 2 (P120-FEM2).	
Table 16. EE sensitivity index, the sensitivity of the outputs to the percentage variations of the inp	
Table 17. Average and standard deviation of the density and mechanical properties of Arundo dor	nax.
	42
Table 18. Nomenclature of the particleboards manufactured.	
Table 19. Type of tests carried out, standard associated to each test, number and dimensions of specimens required for the physical-mechanical tests.	
Table 20. Average values and standard deviations for thickness swelling 2 h (TS 2 h), surf	
soundness and Internal bond (IB) for all specimens.	
Table 21. Average values and standard deviations in brackets for the maximum load, bending stren	
σm , Modulus of elasticity E_m and the density for the different types of particleboards	50
Table 22. Comparison of values of Modulus of rupture (MOR), Modulus of elasticity (MOE)	and
Internal bond (IB) of particleboard manufactured with Arundo donax or a mixture of Arundo do	nax
and wood, found in literature and results obtained in this work.	
Table 23. Types of particleboard panels.	
Table 24. Type of tests carried out, standard associated to each test, number and dimensions of	
specimens required for the physical-mechanical tests.	
Table 25. Average values and standard deviations for slenderness ratio (SR) and aspect ratio (A	
for Arundo donax and recycled wood.	
Table 26. Average values and standard deviations for slenderness ratio (SR) and aspect ratio (All Standard Deviations)	
for the different particles of the AD used for the different types of particleboard	
Table 27. Average values and standard deviations for density, thickness swelling 2 h (TS 2 h), we have the same time 2 h (TS 2 h), we have the same time 2 h (TS 2 h).	
absorption 2 h (WA 2 h), surface soundness and internal bond.	
Table 28. Test ANOVA for the results of the tests. Table 29. Average values and standard deviations in brackets for the maximum load, bending strend	
Table 29. Average values and standard deviations in brackets for the maximum load, behaing stren σ m, Modulus of elasticity E_m and the density for the different types of particleboards	_
Table 30. Test ANOVA for the results of the tests	
INDIA DO: 1001 111 10 111 101 HIC LONGIN OF HIC HOND,	0.

Table 31. Chemical of hemp, flax, bamboo and Arundo donax	70
Table 32. Types of particleboard panels.	71
Table 33. Type of tests carried out, standard associated to each test, number and dimension	ns of the
specimens required for the physical-mechanical tests	72
Table 34. Average values and standard deviations for density, thickness swelling (TS) a	
absorption (WA) after 2 and 24 h of immersion.	
Table 35. Average values and standard deviations for surface soundness and internal bond	76
Table 36. Average values and standard deviations in brackets for the maximum load, bending	g strength
σm, Modulus of elasticity E _m and the density for the different types of particleboards	79
Table 37. Comparison of Modulus of rupture (MOR), Modulus of elasticity (MOE), Inter	nal bond
(IB), TS 24 h and WA 24 h of binderless particleboards found in literature, those obtained in	1 Chapter
4 for the density 550-600 kg/m ³ and results obtained in this Chapter	
Table 38. Physical properties of the hemp woven fabric used.	
Table 39. Differences between the two series.	88
Table 40. Four groups of composites. The amount of liquid matrix, used during the improcess, is reported as the ratio of the mass of the resin to the mass of fibers, both expressed	_
Table 41. Average and standard deviation, in brackets, of displacement, maximum load,	
longitudinal and transverse direction, tensile strength, Coeff. of Poisson, Young modulus	
N/N_{max} , Young modulus at 0.6 of N/N_{max} , for all the composites	
Table 42. P-values for σ . Values lower than 0.05 are indicated in bold.	
Table 43. P-values for Poisson coefficient. Values lower than 0.05 are indicated in bold	
Table 44. P-values for E _{0.1} . Values lower than 0.05 are indicated in bold	
Table 45 . P-values for E _{0.6} . Values lower than 0.05 are indicated in bold	95
Table 46. Values of tensile stress and Young's modulus for composites manufactured in	
research found in literature and data of the composite relating to series 1 group B, manufa	ctured in
this research	96

1. INTRODUCTION

Climate change represents one of the most urgent and complex challenges of our time, with profound implications for the environment, societies, and economies worldwide. In recent decades, rising global temperatures, the intensification of extreme weather events, and the rapid melting of glaciers are just a few of the clear signals of an accelerating process, primarily due to the increase in anthropogenic greenhouse gas emissions [1, 2]. This phenomenon has a devastating impact on ecosystems, causing ocean acidification, biodiversity loss, and the desertification of vast areas, threatening species' survival and the food security of millions of people.

The use of renewable and sustainable resources is becoming increasingly important in the design and construction of infrastructure, in response to the need to reduce the environmental impact of civil works and promote the use of eco-friendly materials. The environmental impact associated with construction is strongly influenced by the production, transport and assembly of building materials.

A new approach to architecture and civil engineering has emerged, placing significant emphasis on the use of natural and local materials. This approach draws inspiration from ancient building materials and techniques that evolved in the Mediterranean area, while also integrating the latest scientific and technical advancements to optimize material performance. One notable trend is the revival of traditional natural materials such as bamboo, *Arundo donax* and straw bales [3, 4, 5].

Natural material is defined as one with minimum energy expenditure between the raw material and the semi-finished product, as well as low disposal costs at the end of the building's life. Another characteristic of a natural material, which ensures its effective use in bioarchitecture, is that it must be sourced from areas close to where it is used.

This thesis focuses on the use of natural materials in the construction sector; materials like bamboo or AD can serve as viable alternatives to conventional construction materials like steel, concrete and wood [6, 7].

The objectives of this work are to thoroughly explore the potential of a viable building material for panel applications. This involves a comprehensive analysis of its physical and mechanical properties, its compatibility with other construction materials, and its suitability for possible structural and non-structural applications.

The doctoral thesis focused on the production and physical-mechanical characterization of panels where AD was one of the main materials. Three are the involved projects:

- 1. The first focused on the study of a honeycomb panel, in which AD was used in the core of the panel. This project was carried out in collaboration with the University of Besançon, France.
- 2. The second project, conducted in collaboration with the company Gruppo Saviola S.r.l. of Mantova, focused on a sandwich-type particleboard, consisting of three layers. Part of the wood chips were replaced with AD chips.
- 3. The third project involved a very innovative field, that of panels without the use of binders. The study focused on a binderless particleboard made in collaboration with the Start-Up My.Fibers of Modena. In this case, AD was added as reinforcement, while the matrix was composed of hemp fibers.

2. ARUNDO DONAX

Arundo donax is a perennial herbaceous plant that belongs to the family of Poaceae, it has been indicated as one of the 15 invasive species that have had the greatest impact in the Mediterranean area by the European Commission within the Ecosystem Vulnerability Key Action [8].

Originating from Central Asia, it has progressively spread and established itself in the countries bordering the Mediterranean Sea, in South and Central America and South Africa (Figure 1), thanks to its high tolerance to different climates and soil conditions [9]. In the 17th century, AD was introduced into the USA and specifically in 1820 into the Los Angeles area, to control erosion in canals. Since 1900, it has become an invasive plant in large portions of the United States, particularly in the state of California. In Italy, this plant is widely spread in marshy areas, along the edges of rivers, lakes, and canals and can be more commonly found in the central and southern regions, while in the northern regions, its presence is more limited, as it prefers temperate and subtropical climates.

There are two varieties of AD: AD variegata and AD versicolor. Both species, which are wind-pollinated (anemogamous), bloom in September-October, producing feathery, fusiform panicles ranging in color from pale green to violet, measuring 40–60 cm in length, and with an upright habit. The flowers are monoecious, the seeds are rarely fertile, and reproduction mostly occurs vegetatively, thanks to the presence of rhizomes underground, which form the plant's root system. The aerial part of the plant dries out and falls to the ground in autumn, only to regenerate in the spring from the rhizomes, with the first shoots emerging in March. The rhizomes are capable of germinating regardless of their size and in most environmental conditions, since they are highly tolerant to saline conditions and can adapt well to the accumulation of salt in the soil [10]. This vegetative spread appears to be an effective adaptation to the occurrence of floods.

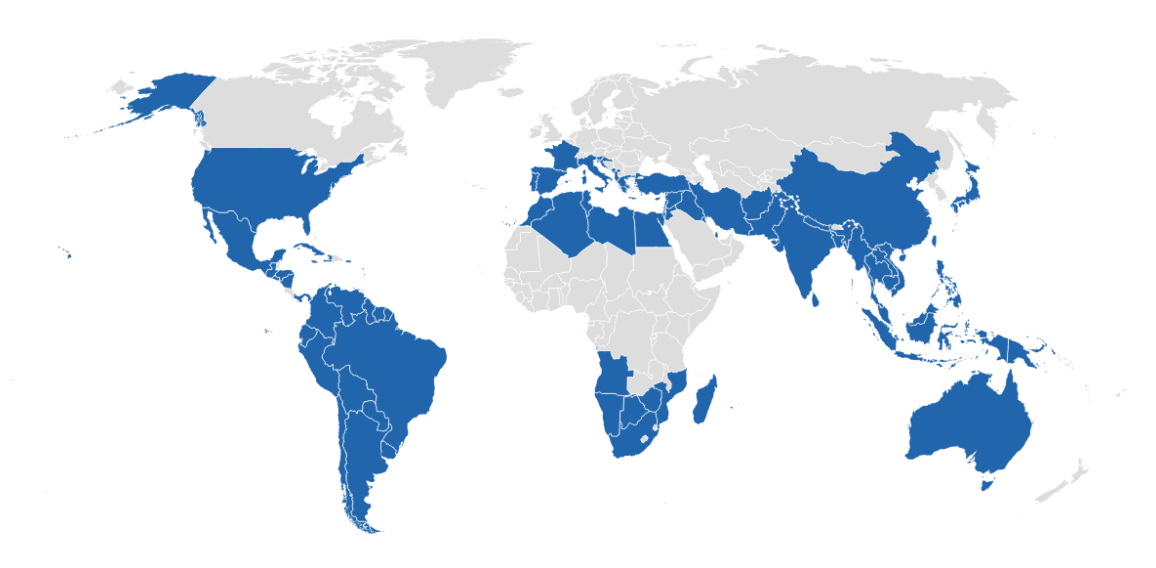


Figure 1. Spread of Arundo donax around the world.

In riverbeds, the force of the water can break the rhizomes, acting as a dispersing agent, but also obstructing the free flow of water in river courses and causing serious problems to waterworks and bridges. The species is primarily spread by the growth of scattered fragments of the rhizome. One of its particularities is the rapid rate of growth. Under optimal conditions, it can grow up to 5 cm per day, which is why it is considered one of the most important sources of vegetable material for biomass and cellulose production. Through vegetative reproduction, this species occupies new areas

and forms dense masses (reed beds) which can cause a profound transformation of the ecosystems it invades, and the detriment of other native species.

Cultivations of AD have the advantage of not requiring artificial irrigation, except in the initial phase, and do not need pesticides, allowing cultivation in areas unsuitable for other species, resulting in significant economic savings [11, 12].

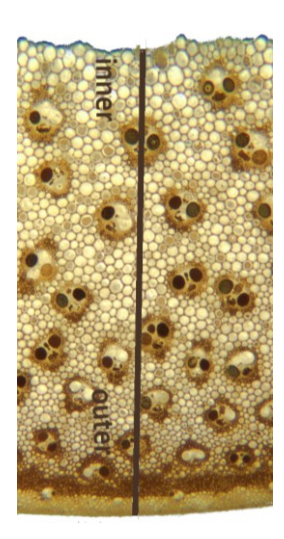
Its root system consists of thick, knotted rhizomes with very strong, deep adventitious roots. These rhizomes are branched, with distinct nodes and internodes, and equipped with buds that produce new culms [13]. The roots can provide substantial natural soil reinforcement. For this reason, giant reeds are used to consolidate the soil, stabilize slopes, and protect hillsides and land from erosion caused by water.

AD stem, called culm, can reach a height of 6-8 meters, Figure 2; it is hollow, with diameters ranging from 10 to 30 mm, which varies along the longitudinal axis of the culm, being maximum at the base and minimum at the top, while the thickness of the walls ranges between 1 and 4.5 mm. The culm of AD is divided into sections called internodes by diaphragms called nodes, as is the case with bamboo. The latter stabilizes and strengthens the entire culm versus the local buckling due to bending forces, such as those due to the wind [14]. The mass proportion of nodes within the culm varies in the range of 10–25%, depending on the length of the internodes, which, in turn, varies between 10 and 30 cm [15]. The leaves are alternate, gray-green in color, 300–600 mm long, and 20–60 mm wide, with a lanceolate shape tapering to a point.



Figure 2. Arundo donax.

Inside the culm wall, sclerenchymatous fibres strengthen vascular bundles and are embedded in a matrix of lignified parenchyma [16] giving a good mechanical performance. The fibers present in the culm of AD are longitudinally oriented along the axis of the culm. The fiber density varies both across the thickness and along the height of the culm. Along the thickness, (Figure 3), two zones are distinguishable: the inner one, in which vascular bundles are rather homogeneously embedded in the ground parenchyma, and the second, in the neighbourhood of the outer culm wall, in which the ring of sclerenchymatic tissue divides the cortical parenchyma from the rest of the section [17, 18].



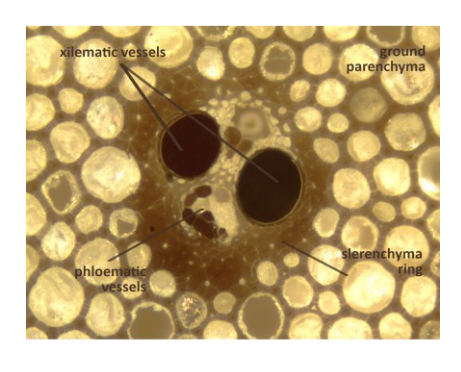


Figure 3. Cross sections of a culm of Arundo donax, in longitudinal and transverse directions [17].

The described microscopic characteristics directly influence the macroscopic properties of the culm, contributing to its marked orthotropy. This orthotropy is evident in the culm's ability to better withstand stresses applied along the longitudinal axis, where the fibre orientation provides greater stiffness and strength. This structural arrangement is optimized for supporting mechanical loads and ensuring the plant's stability under environmental conditions such as, for example, strong winds. Furthermore, the difference between the inner and outer zones of the culm helps optimize the balance between flexibility and robustness, allowing the plant to combine structural lightness with high mechanical performance.

In [6], a physical-mechanical characterization of AD was conducted. This research involved compression, tensile, shear and circumferential bending tests on C-shaped specimens.

The average density of AD was found to be 647.37 kg/m³ with a standard deviation of 0.04 kg/m³. In compression tests, the load-displacement curve revealed an elastoplastic trend, indicating a ductile behaviour of the material under this type of stress. Moreover, the maximum load and the stiffness of the material were independent of the presence of nodes in the culm.

In tensile tests, the specimens exhibited elastic behaviour with brittle failure of the material. In this case, the presence of nodes significantly reduced the maximum load the specimen could withstand. Shear curves demonstrated elastic behaviour followed by a brief ductile zone preceding a quasi-brittle failure. The presence of nodes increased the maximum load, showing the opposite effect compared to the tensile tests.

As for circumferential bending tests, the presence of nodes resulted in greater variability in the results. In Table 1, the results obtained from this research are presented in tabular form [6].

Table 1. Average and standard deviation of the density and mechanical properties of Arundo donax.

Parameters	Value
Density ρ [kg/m ³]	647.7 (±0.04)
Compression stress σ_c [MPa]	57.04 (±0.05)
Compression Young modulus Ec [GPa]	$13.40 (\pm 0.33)$
Tensile stress, parallel to the fiber $\sigma_{t,0}$ [MPa]	$111.70 (\pm 0.12)$
Tensile Young modulus parallel to the fiber $E_{t,0}$ [GPa]	$15.29\ (\pm0.07)$
Tensile stress, perpendicular to the fiber $\sigma_{t,90}$ [MPa]	$11.22 (\pm 0.14)$
Tensile Young modulus perpendicular E _{t,90} [GPa]	$1.05 (\pm 0.16)$
Shear stress τ [MPa]	$18.40 \ (\pm 0.12)$
Shear elastic modulus G [GPa]	2.96 (±0.23)

AD has been and continues to be used in other applications such as manufacturing paper [19], extracting xylose [20], producing activated carbon [21], processing compost [22], generating biomass [23], producing biogas [24], obtaining biofuel [25, 26], forming lignocellulosic films [27], preparing composites [28], designing reinforcements for cement mortar [29] and constructing particleboards [16].

The lightness of its stem combined with its fair mechanical strength as well as its high flexibility, which is due to the tubular shape of the stem, have allowed different uses of AD in many human activities: for the construction of tools; as building material; as raw material for artifacts; for the manufacture of musical instruments and even as a drug.

The earliest architectures built using giant reeds can be traced back to the Upper Paleolithic (approximately 40,000 to 16,000 years ago). Archaeological and Paleontological studies have discovered huts made with plastered branches in the temperate areas of continental Europe and East Asia during that period. This technique shows strong similarities with construction methods used in Andean settlements, where buildings were made of giant reeds tied together with ropes [30].

In Mediterranean architecture, AD was primarily used in structural elements such as beams or panels. These were typically made of parallel culm reinforced in the other direction with perpendicular culm elements or, more commonly, with mortar, plaster, or raw earth. In Italy, an example of this application can be found in the Baraccas of Oristano, in western Sardinia. These buildings were used by local fishermen as storage spaces for equipment and as places for rest. The load-bearing structure was made of wood, while the walls were constructed from large-diameter culms of AD, layered to form a lattice. The covering was made of falasco, a marsh grass known locally as "cruccuri" [31]. The roof was made of wood or slats of AD, covered with overlapping AD culms to form a 'bundle,' on which terracotta tiles were then placed.

In southern Italy, the culms of AD were extensively used in construction for internal partitions and vertical closures, particularly in Calabria after the seismic events of 1783 that devastated the Kingdom of the Bourbons. After this catastrophic event, the Bourbon government initiated an experimental reconstruction program, which saw widespread use of giant reeds, especially for the construction of internal partitions and external walls. These walls consisted of a wooden load-bearing structure to which two layers of giant reeds mixed with flax and clay were attached.

Another example of the use of AD was the Mudhif, structures originating from the Mesopotamian region. These buildings were made entirely of giant reeds, with load-bearing parabolic arch structures formed by opposing pairs of bundles of culms. The earliest Mudhif constructions date back to the Sumerian period, 5,000 years ago, but they were still built and used until 1993, when Saddam Hussein began draining the marshes. Following the U.S. invasion of Iraq in 2003, maintenance of the marshland ceased, and the areas became flooded again, returning to their original marshy state.

The use of these raw materials is limited by their shapes and dimensions. Their use in laminated structures or panels can overcome this issue. In the field of panel engineering, García-Ortuno et al. [16] demonstrated the feasibility of producing particleboard in the engineering field using shredded AD particles as aggregates and urea formaldehyde resin as an adhesive, Cintura et al. [32] conducted a study on the physical and mechanical characteristics of particleboard panels made with chips of sodium silicate as resin.

Over the years, more eco-friendly alternatives have also been studied regarding the resin, such as the use of non-modified starches [33] and the study of panels without the use of resin [34].

AD is a native and widely distributed material in the south Europe, and its industrial use would contribute to economic development by triggering local production chains. The data present in the literature demonstrate the feasibility of using this material on an industrial scale assessing a production ranging from 20 Mg DM ha⁻¹ to 51.4 Mg DM ha⁻¹, where the unit of measurement Mg DM ha⁻¹ represents the amount of dry matter in megagrams (or tonnes) per hectare [35, 36, 37].

Currently, no data are available on the national availability of *Arundo donax*, nor are there studies analyzing its potential availability in quantitative terms for industrial use. However, given its characteristics—being one of the most invasive plant species in the country and exhibiting rapid growth—there is a strong basis for its industrial application, especially considering its high dry matter yield per hectare.

Regarding sustainability, analyzing the life cycle of AD compared to pure wood shows that the growing time and the land use are lower, as well as the demand for water for production. The use of AD would bring significant environmental and economic benefits It has phytoremediation capability, meaning it can phytoextract heavy metals and/or induce the degradation of organic compounds in contaminated soils [38, 39, 40], and it can also be used as a biofilter for the treatment of contaminated water or wastewater [41].

3. HONEYCOMB PANEL

3.1 Introduction

The project stems from a collaboration between the University of Bologna in Italy and the University of Besançon in France.

Honeycomb panels are a specific type of sandwich panel, consisting of three layers: two thin and highly rigid external layers, and a thick internal layer with a honeycomb geometric structure, from which the panel derives its name. The physical and mechanical properties of honeycomb panels can vary considerably, not only due to the wide range of materials that can be used for the core and skins but also because of geometric variations that can be controlled during panel fabrication. These variations include the thicknesses, the geometric shape of the core cells, and how they are connected to the skins [42].

Honeycomb sandwich structures possess lightweight characteristics, high stiffness-to-weight and strength-to-weight ratios, effective thermal insulation, and strong load-bearing capabilities [43]. They find extensive applications in civil, mechanical, and aerospace engineering due to their versatility [44].

To minimize the environmental impact of structures, the use of eco-friendly materials is increasingly encouraged. Several examples of such applications in honeycomb panels can be found in the literature. Gato et al. [45] explore the use of discarded bottle caps as the core material, paired with hybrid glass fiber composite skins. This reuse of bottle caps demonstrates a circular approach to material consumption. A similar approach, utilizing bottle caps in the core but combining them with flax-based laminates for the skins, is studied by Oliveira et al. [46]. Antony et al. [47] employ bio-based materials, specifically hemp and polylactic acid (PLA), to create a 3D-printed hemp/PLA honeycomb sandwich structure. Napolitano et al. [48] present an example of partially bio-based sandwich panels featuring a bamboo core and synthetic aluminium skins. Fully bio-based sandwich panels are examined by Darzi et al. [49], who use plywood faces and a bamboo core, experimenting with different configurations of one or two bamboo layers in the core. Another fully bio-based solution is investigated by Fu et al. [50], involving flax fiber-reinforced polymer (FRP) skins and a paper honeycomb core.

In this study, bio-based sandwich honeycomb panels with a core made of AD rings, bonded with foaming epoxy resin to flax fiber-reinforced epoxy composite skins, are investigated. This concept is inspired by the work of Oliveira et al. [51], where bamboo rings were used for the core.

The use of fiber composites is driven by their lightweight nature combined with high mechanical strength. Natural fibers, particularly for skins, offer several advantages over synthetic alternatives, including sustainability [52], biodegradability, renewability [53], low cost [54], low density, and mechanical properties that are well-suited for secondary structural applications. Additionally, they provide poor electrical conductivity, good thermal and acoustic insulation. Among plant fibers, flax is widely used due to its excellent mechanical properties and versatility. Flax (Linum usitatissimum) has been utilized since prehistoric times [55, 56], it is one of the most widely used bio-fiber, is particularly notable, because it has a reasonable tensile strength (500–1500 MPa) and tensile modulus (25.6 GPa) [57], while at the same time possessing an embodied energy of only 2.75 MJ/kg [57]. Its good mechanical properties and versatility make it a choice for polymeric matrix reinforcement [58]. Several reviews of the use of flax in composites can be found in the literature [59, 60, 61, 55]. For their mechanical properties and lightness flax fiber composites are well-suited for use as skins in biobased sandwich and honeycomb structures. There are several examples in the literature of biobased sandwich panels made of cork with flax composite skins [62, 63, 64].

Another crucial point for the mechanical performance of these sandwich structures is the skin-core bonding. The commonly used bonding method in composite structures is the adhesive which is easily applicable and allows a good load distribution.

The strength of bonded joints depends on several factors such as the characteristics of the adhesive and the geometry of the joint but also the treatment of the surface to be bonded. Specifically, microscale phenomena like the roughness significantly influence the macroscopic behavior of the joint [65]. Although there are several experimental studies on this topic, and despite the existing literature on the mechanical behavior of flax/epoxy adhesive joints with metallic and carbon-fiber reinforced composite substrates [66], there is a gap in research regarding the effects of surface roughness on flax/epoxy adhesive joints with other biomaterials [67].

This study aims to design and demonstrate the feasibility of using a honeycomb panel made with low environmental impact technologies and materials, particularly AD, highlighting how the final mechanical properties of the panel comply with industry standards.

The key properties of the proposed panel include its lightness, achieved through honeycomb technology; its low environmental impact ensured using bio-based materials such as flax and AD; and its strong mechanical performance, attributed to the use of AD rings and foaming epoxy resin. The adhesion between the rings and the skins is enhanced by polishing the lateral surfaces of the AD rings before bonding. The research focuses on the effect of the surface roughness of the rings on the bending mechanical properties of the panels, specifically, the adhesion between the skin and core, as well as between individual AD rings within the core. The pull-off method is employed to assess adhesion between the AD rings and the flax/epoxy composite skin, while three-point bending tests are used to characterize the mechanical behavior of the sandwich structure.

In addition to experimental tests, numerical finite element analyses are conducted to predict, once calibrated, bonding strength (consequently structures capacity) and the relationship with surface roughness. Two models are developed, one for the case of unpolished and one for the case of polished core rings surfaces. The adhesive layer is commonly modeled as a cohesive interface [67] which simplifies the representation of the damage interface and fracture propagation zone. However, the identification of the key parameters can be challenging [68].

The cohesive parameters were determined starting from the unpolished model. The damage initiation stress was derived from the pull-off test. The penalty stiffness and fracture energy values were optimized through a tuning process. In the polished model, the tuned values of the penalty stiffness and fracture energy are maintained, while the damage initiation stress is increased to account for enhanced adhesion due to the foam resin.

The goal is to create a relatively simple FE model that accurately simulates the panel's behavior up to failure, which can be used for future parametric studies focusing on the panel's core.

3.2 Materials

The skins of sandwich panels are made of a combination of unidirectional flax fibre fabric reinforcement with an aerial weight of 110 g/m^2 (FlaxTapeTM-110-36) manufactured by LINEO®, and the matrix used is composed of the epoxy polymer SR Green Poxy 56, and the hardener SD 7561, provided by Sicomin (France), with a mass proportion of 100/36 in g.

The core of the panel is made of internode portions of AD, with a height of 13 mm, which corresponds with the height of the core of the Honeycomb panel, with a ring form, each ring is cut with a circular saw. Giant reed was collected from a cultivation of the Department of Agricultural and Food Sciences, of the University of Bologna, in Cadriano, Bologna, Italy. Before processing, the apical and basal parts of the culms, as well as the leaves, were removed.

The density and mechanical properties of AD are reported in Table 2 [6].

Table 2. Average and standard deviation of the density and mechanical properties of Arundo donax.

Parameters	Value
Density ρ [kg/m ³]	647.7 (±0.04)
Compression stress σ _c [MPa]	57.04 (±0.05)
Compression Young modulus Ec [GPa]	$13.40 \ (\pm 0.33)$
Tensile stress, parallel to the fiber $\sigma_{t,0}$ [MPa]	111.70 (±0.12)
Tensile Young modulus parallel to the fiber $E_{t,0}$ [GPa]	$15.29 \ (\pm 0.07)$
Tensile stress, perpendicular to the fiber $\sigma_{t,90}$ [MPa]	11.22 (±0.14)
Tensile Young modulus perpendicular to the fiber E _{t,90}	1.05 (±0.16)
[GPa]	
Shear stress τ [MPa]	18.40 (±0.12)
Shear elastic modulus G [GPa]	2.96 (±0.23)

AD was dried using an oven at a temperature of T = 85 °C until reaching a mass variation of less than 0.1% after 24 h in the oven [69]. The weight loss of the dry material ranged from 28% to 43%.

The resin used to connect the rings and skins is a foaming adhesive composed of 59.1 g of PB 170 glue and 18.8 g of DM02 hardener.

3.3 Manufacture

The first phase involved the production of skins made of flax fibre, used in the form of unidirectional fabric. Three layers were used, following the approach of a previous study [64] to obtain values that could later be compared with those from that research.

Composite plates are manufactured through a hand lay-up method, followed by impregnation and a thermocompression process. Each plate consists of three FlaxTape layers arranged to form unidirectional laminates. These layers are impregnated with an excess of the matrix in a steel mould measuring $300 \times 200 \text{ mm}^2$. To prevent resin from adhering to the mould, the metallic surfaces are first coated with Teflon. The impregnation of the FlaxTape layers follows a specific procedure outlined in [70], aimed at optimizing impregnation while minimizing fibre waviness and misalignment. A resin strip is poured at the center of each ply perpendicular to the fibre direction. Under pressure, the matrix flows along the length of the fibres. The mould is then partially closed on two sides to allow excess matrix and air to escape during the pressurization stage.

After this, the mould is placed in an AGILA® Presse 100 kN thermocompression press for the curing phase. When the mould reaches 40 °C, a pressure of 3 bar is applied. After maintaining this condition for 15 minutes, the temperature is raised to 100 °C for the final curing process, which lasts for 1 hour. Once the curing phase is complete, the heating is turned off, and the plate is allowed to cool naturally while the pressure is gradually released. The composite plate then undergoes a post-curing phase in an oven at 100 °C. Both skins of the panel are fabricated at the same time, separated by a Teflon-coated iron sheet.

The culms were cut with a circular saw to obtain the rings. Three different cores were manufactured, one in which the lateral surface of the rings had not undergone any treatments and two in which the lateral surfaces were polished. The polishing of the lateral surface (LS in the notation of the specimens) is done manually before cutting the cane. Two different sandpapers were used: Z80 and P120, as it is reported in Figure 4.

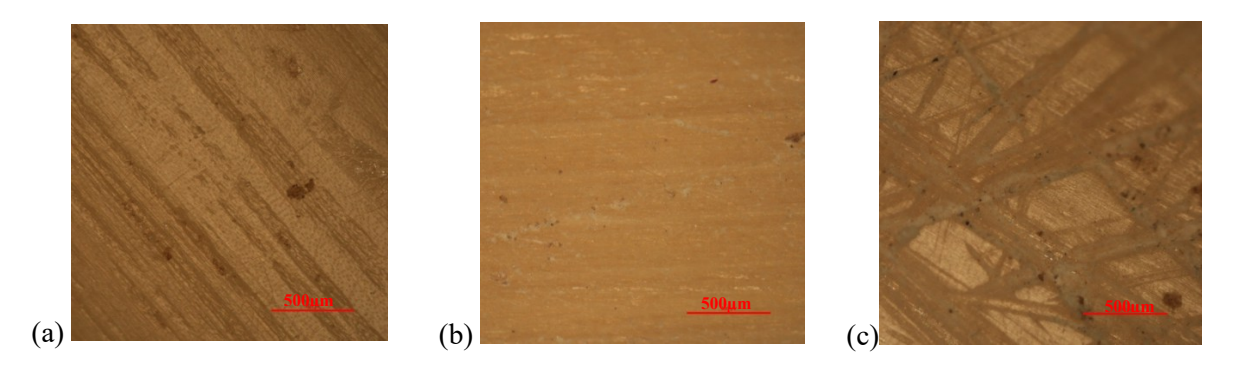


Figure 4. (a) Unpolished lateral surface; (b) P120 polished lateral surface; (c) Z80 polished lateral surface.

Considering 72 randomly taken rings of the core (highlighted in orange) in Figure 5, the outer diameters of the ring ranged from 13 mm to 17.1 mm (mean 15.2 mm), the inner diameters of the core from 8.2 mm to 12.6 mm (mean 10.7 mm) with a thickness from 1.45 mm to 3.5 mm (mean 1.5 mm).

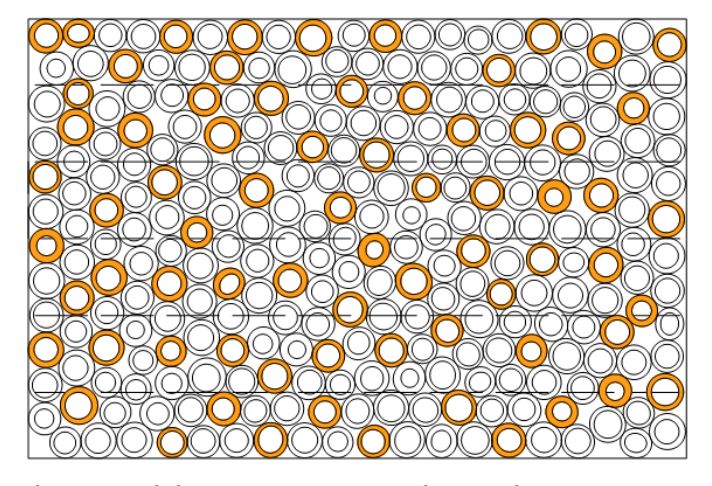


Figure 5. Core rings distribution and dimensions. Inner and outer diameter was measured for orange rings.

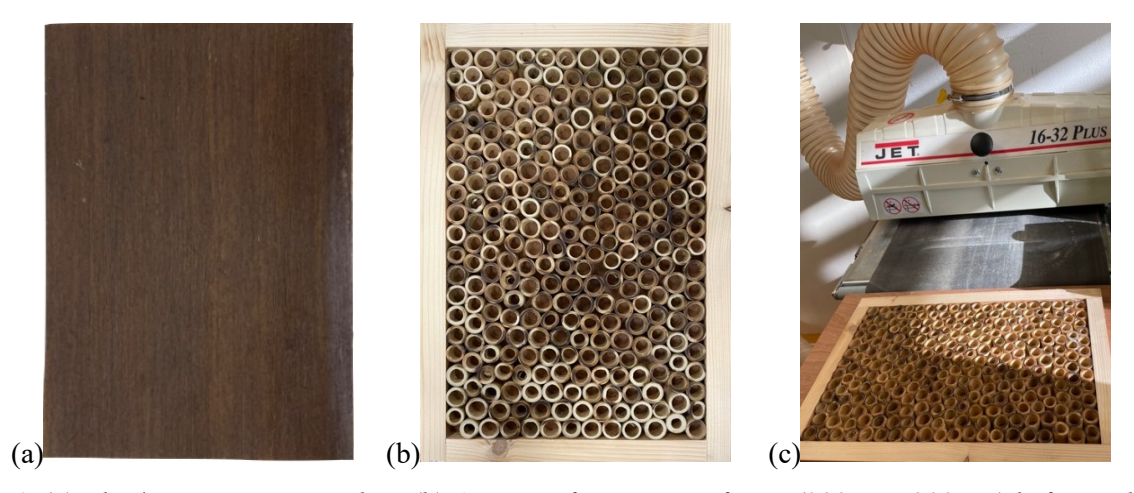


Figure 6. (a) Flax/epoxy composite skin; (b) AD rings for core in a frame (300mm x200mm) before polishing the cross-section surface; (c) Polishing setup.

To build the panels, all the rings constituting the core are posed in a wood frame of the same dimensions as the mould and the skins (300 x 200 mm) (Figure 6 (b)) and polished (Figure 6 (c)) using a sanding and calibrating machine (JET 16-32 Plus) with P120 sandpaper. The sandwich, with dimensions of 300 x 200 mm is then obtained by interposing the skin and the ring core as reported in Figure 7.

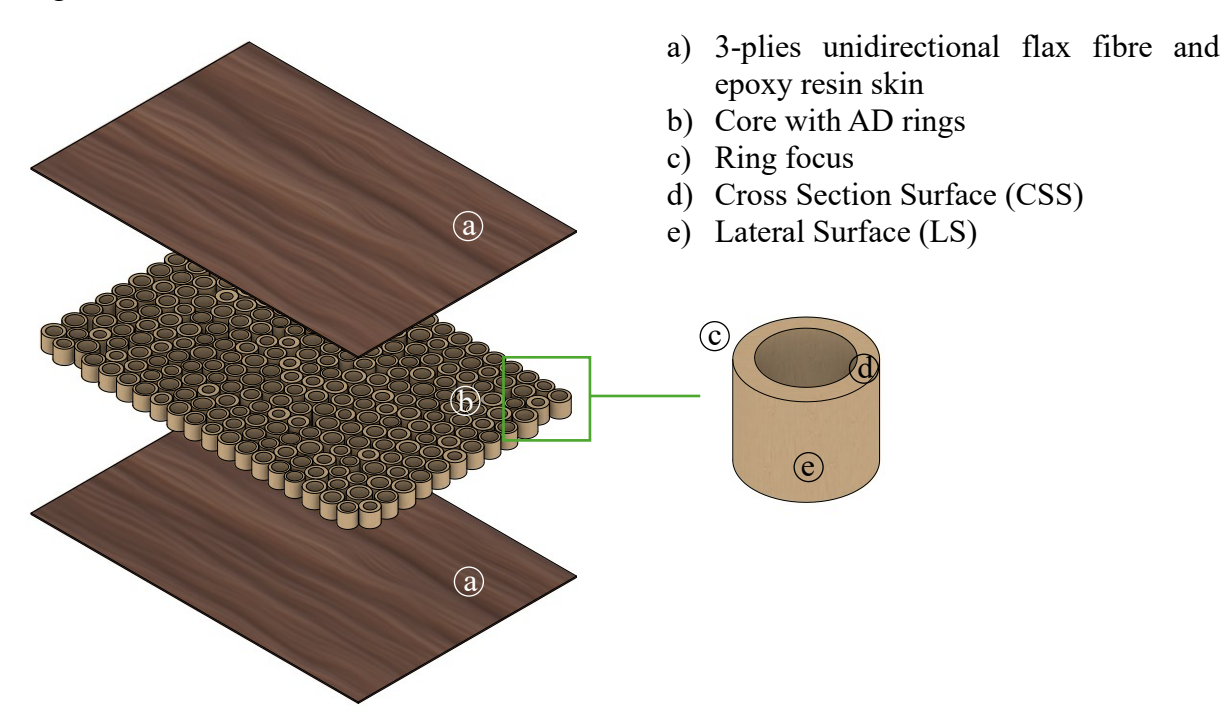


Figure 7. Detail of panel's components.

The skins were glued to the AD rings core with the foaming adhesive composed of 59.1 g of PB 170 glue and 18.8 g of DM02 hardener for one sandwich panel of 300 x 200 mm. The gluing process is applied by maintaining the panel at 100 °C for 1 hour, using a pressure of 3 bar on the panel (Figure 8 (a)). The glue becomes a foam that goes into the voids inside the core (Figure 8 (b) and (c)).







Figure 8. (a) Thermohydraulic press; (b) Sandwich panel core focus; (c) Sandwich panel skin focus.

Three types of panels were produced each differing in the treatment applied to the lateral surfaces of the core rings: the "Unpolished_LS" where the lateral surfaces were left untreated, the "P120_LS" which had the lateral surfaces sanded with P120 sandpaper and the "Z80_LS" where the lateral surfaces were treated with Z80 sandpaper. The Cross Section Surfaces (CSS) of all the rings in the three panels underwent the same polishing process using P120 sandpaper.

For each type of sandwich, four samples were made. Table 2 shows the mean weight of each panel to show the weights of the different components and their ratio. The differences in the weight of the components are due to the natural variation of the elements themselves.

Table 3. Weights of the different manufactured panels.

Rings lateral surface		Weight of sandwich panels		
polishing treatment	Core [g]	Skins x2 [g]	Total glue [g]	
Unpolished_LS	190.7	82.5	70.9	
Z80 LS	200.0	76.3	70.9	
$P12\overline{0}$ LS	197.2	78.3	70.9	

3.4 Methods

3.4.1 Roughness analysis of AD cross-section

The first data collected are related to the surface roughness of the AD ring's cross-section. An Alicona microscope was employed to obtain quantitative measurements and a three-dimensional surface mapping, while a preliminary qualitative analysis was conducted using a Nikon Eclipse LV150 with a 5x lens.

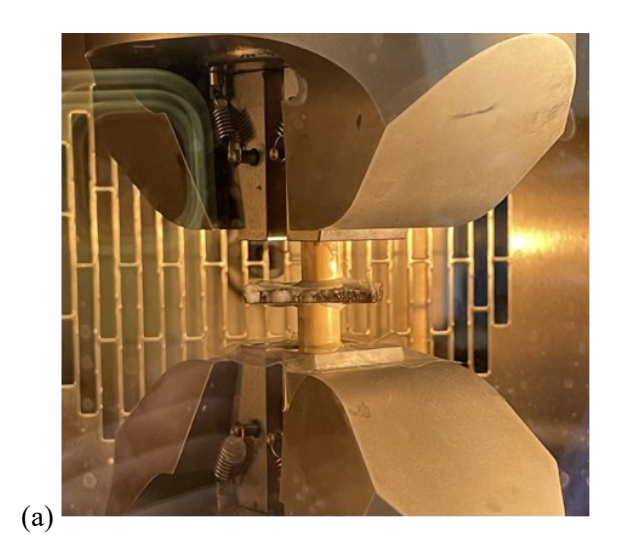
Surface roughness was quantified using the Surface Portance parameter, which represents the percentage of the surface (measured in µm) located above and below the middle plane.

All specimens prepared for the pull-off test were evaluated, three measurements were taken from the surface of each sample.

3.4.2 Pull-off Test

Pull-off tests are performed to understand the influence of the surface treatment of the AD cross-section on the resistance of the panel. There is no specific standard for Arundo, and the test used is an adaptation of the pull-off test in ISO D4541-22.

Two AD rings are bonded to a 3cm x 3cm flax skin, made from 25 layers of flax (approximately 4mm thick), providing sufficient thickness to prevent failure as depicted in Figure 9 (a). A mixture of PB170 (5g) and DM02 hardener (1.8g) is used as foaming adhesive. The samples are placed into clamp supports of the machine, and the adhesive is allowed to solidify for one hour in a preheated oven at 100°C, under a compression load of 50 N (Figure 9 (b)). Pull-off tests were conducted at room temperature using an Instron Electropulse E10000 (Figure 9 (a)) on various samples with different cross-section polishing treatments. Specifically, pull-off tests were carried out on two unpolished samples, two samples polished with P120 sandpaper, and two samples polished with P400 sandpaper. The tests were performed in displacement control mode at a speed of 0.60 mm/min.



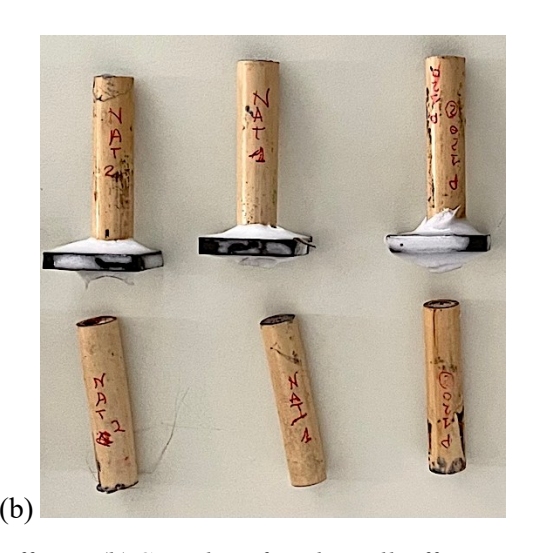


Figure 9. (a) Sample in the oven at 100 °C before the pull-off test; (b) Samples after the pull-off test.

3.4.3 Three-point bending test

The three-point bending tests were conducted on sandwich samples with approximate dimensions of 300mm x 35mm x 14mm. For each manufactured panel, at least four specimens were tested. The procedure follows the ASTM C393-00 [71] standard for the three-point bending test for long beam three-point load (Figure 10). The span length was set at 220mm, with a displacement rate of 6 mm/min. The tests were performed on a universal testing machine, MTS Criterion 45, equipped with a 5 kN full-range load sensor. Mid-span deflection on the specimen's bottom surface was recorded using a laser micrometer sensor (micro-epsilon optoNCDT 1420).



Figure 10. Three-point bending test setup.

The test was performed for all the sandwich samples. The core shear stress, the skin bending stress, the flexural strain and stress and the tangent modulus of elasticity are calculated following the ASTM C393-00 [71] standard. The core shear stress τ is expressed by the equation:

$$\tau = \frac{P}{(d+c)\,b}\tag{1}$$

where P is the load, d is the sandwich thickness, c is the core thickness, and b is the sandwich width. The skin bending stress σ is expressed as:

$$\sigma = \frac{PL}{2t (d+c) b} \tag{2}$$

where t is the skin thickness, and L is the span length.

The modulus of elasticity in bending EB is expressed as:

$$E_B = \frac{L^3 m}{4 b d^3} \tag{3}$$

where *m* is the slope of the tangent to the initial curve of the load-deflection curve.

The data were statistically analyzed using the ANOVA method (Analysis of Variance) to evaluate whether the means of the measured mechanical properties of the different types of honeycomb panels were significantly different from each other. A probability (Pr) was calculated, and the difference between means is considered significant when the Pr is less than 0.05. The method was implemented using Minitab v.18 software [72].

3.4.4 Analytical Model

To study the behaviour of a panel under the three-point bending test, two analytical models were developed: the equivalent panel model, which considers a homogenized material, and the sandwich model which is based on sandwich theory. For both models, a linear elastic behaviour for all the materials is considered.

The sandwich panel theory [72], allows the calculation of the equivalent flexural stiffness (EI)_{eq}, which describes the flexural stiffness of a composite structure, considering the entire panel, under specific assumptions, using the following equation:

$$(EI)_{eq} = \frac{E_{c2}bc^3}{12} + 2 \cdot \frac{E_{f1}bt^3}{12} + 2 \cdot E_{f1}bt \left(\frac{d}{2}\right)^2 \tag{4}$$

where E_{fl} is Young modulus of the skins along the longitudinal axis, E_{c2} is the Young modulus of the core material along the longitudinal axis of the panel. At the foundation of this model, there are two hypotheses $E_{f1} \gg E_{c2}$ and $c \gg 2t$, through which it is possible to simplify Eq. 4:

$$(EI)_{eq} = \frac{E_{f1}btc^2}{2} \tag{5}$$

According to this theory, the skins absorb all the normal stress acting on the panel, while the core absorbs the tangential stress. The normal stress acting in the skin, σ_s using the following equation [72].

$$\sigma_{S} = \frac{M}{h \cdot t \cdot c} \tag{6}$$

where M is the bending moment acting on the beam. The deflection at the midpoint of the beam is given by the sum of a bending contribution related to the skins and a shear contribution associated with the core $\delta = \delta_b + \delta_s$.

$$\delta_b = \frac{P \cdot L^3}{48 \cdot (EI)_{eq}}; \, \delta_S = \frac{P \cdot L}{4 \cdot G_C \cdot A_C} \tag{7}$$

where G_c is the shear modulus of the core, and A_c is the shear area, and P is the load.

The equivalent model is a simplification of the equivalent panel theory in which the panel is considered made of a single equivalent homogeneous and isotropic material with an equivalent Young modulus \tilde{E} obtained by enforcing the equality with the bending stiffness of the sandwich model $(EI)_{eq}$ using this equation:

$$\tilde{E} = \frac{(EI)_{eq}}{\tilde{I}}; \tilde{I} = \frac{bd^3}{12} \tag{8}$$

where \tilde{I} is the inertia moment of the equivalent cross-section of the panel, considered homogeneous.

3.4.5 Finite Element Model (FEM)

A finite element model of the sandwich panel under a three-point bending test is developed not only to compare and benchmark against the experimental results but also to develop a tool for prediction and design. Two finite element models were created using Abaqus software: one for the unpolished panels and another for the polished P120 panels by using Abaqus software localizing the nonlinearity in the adhesion areas.

To simulate three-point bending, half of the panel was modelled with symmetric boundary conditions, as can be seen in Figure 11. The test was carried out in displacement control.

The skin and the AD ring walls were modelled as orthotropic materials, assuming they maintain linear elastic behaviour until the panel fails. The core was represented by rings with a constant diameter of 15 mm, a size chosen to reflect the average ring diameter used in experimental setups. The thickness of the ring walls was defined as 1/10th of the diameter, resulting in 1.5 mm. The rings were arranged in a regular pattern, with three rows covering the entire length of the panel. To simulate the three-point bending, half of the panel was modelled with symmetric boundary conditions.

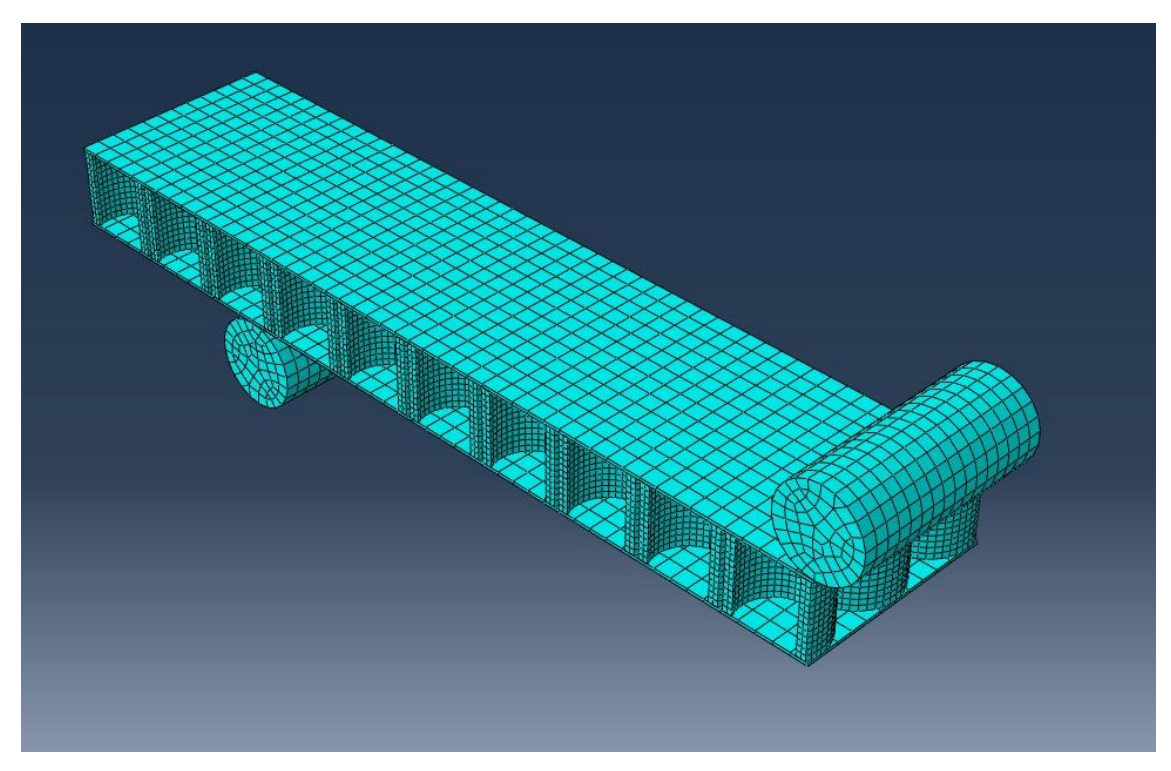


Figure 11. Finite Element Model (FEM) of a sandwich beam under a three-point bending test

The engineering constants of the AD and the flax-reinforced composite used in the FEM are taken from [6] and [73], respectively, and are reported in Table 4.

Table 4. Engineering constants are considered in the FE model for the facial and core materials.

Parameter	Definition	Value	
		Arundo donax	Flax composite
$\overline{E_{11} \text{ [GPa]}}$	Longitudinal elastic modulus	13.4	36.0
$E_{22} = E_{33} [\text{GPa}]$	Transverse elastic modulus	1.05	4.20
$v_{11} = v_{22} = v_{33}$	Poisson's ratio in plane 1-2/1-3/2-3	0.56	0.33
$G_{12} = G_{13} = G_{23}$ [GPa]	Shear modulus in plane 1-2/1-3/2-3	2.96	4.29

A Poisson's ratio equal for the minor and major ratios was used as it was referenced in the article by L. Ávila de Oliveira et al. [64]. The supports of the beam and the load cell are modelled as cylindrical rigid shells, to which boundary conditions are applied through reference points (RP). Constraints were applied to the supports, while the load cell was permitted to move in the direction perpendicular to the specimen's longitudinal axis.

Cohesive surfaces were utilised to model the interaction between the skins and the AD rings of the core and within the rings. Table 5 shows the cohesive parameters: the Damage initiation stress in the normal direction t_1 and the transverse direction t_2 and t_3 expressed in [MPa]; the Penalty stiffness of the cohesive layer in the normal direction K_1 and the transverse direction K_2 and K_3 and the fracture energy in the normal direction G_1 and transversely G_2 and G_3 expressed in [N/mm]. These interface properties are dependent on the type of adhesive utilized. The viscosity coefficient μ stabilizes the material in a softening regime, it is set equal to 0.0005 as suggested by Demir et al. [74] after performing a detailed analysis of the influence of the viscosity coefficient on the results.

Table 5 Cohesive zone parameters were used in the model.

Parameter	Definition	
$t_1; t_2; t_3 [MPa]$	Damage initiation stress	
K_1 ; K_2 ; K_3 [N/mm ³]	Penalty stiffness	
G_1 ; G_2 ; G_3 [N/mm]	Fracture energy	
μ	Viscosity	

The contacts between the skins and the supports as well as between the skin and the indenter were modelled using hard contact in the normal direction and friction in the tangential direction. Flax composite skins and AD rings of the core are modelled using an eight-node linear brick 3D

The difference between the two models lies in different assumptions regarding the connective surfaces. In the unpolished model, it was assumed that there was an adhesion between the core and skins but there was no interaction between the rings inside the core with the belief that the foam resin did not enhance adhesion when penetrating the rings.

In contrast, for the polished model, it was hypothesized that the foam resin did enhance adhesion when penetrating the rings leading to an improved adhesion between the core and the skins and creating an adhesion witing the core.

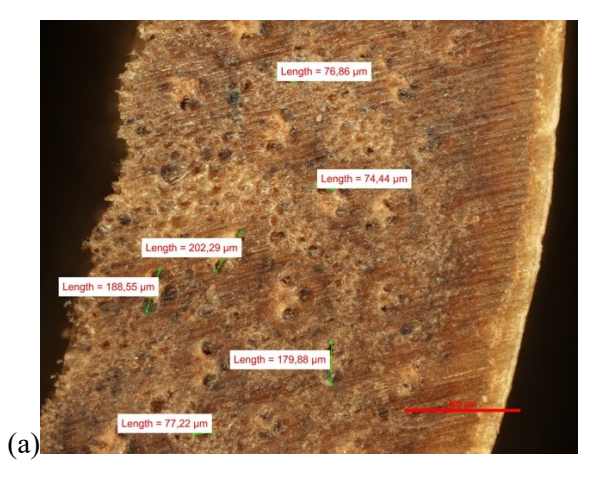
Another difference between the two models concerns the geometric characteristics of the modeled panel which refer to the averages of the tested samples. In the case of the unpolished panel, the base is 32.9 mm and the thickness of the skins is 0.6 mm, while for the polished P120 case, these dimensions are 35 mm and 0.5 mm respectively.

3.5 Results and Discussions

element (C3D8R).

3.5.1 Analysis of the cross-section surface

The analysis of the surface roughness of AD ring cross sections unpolished and polished is performed. Figure 12 (a) and (b) show the images taken with Nikon Eclipse LV150 with a 5x lens cross-section before polishing and after polishing with P120 sandpaper and the difference is evident, and the surface appears more rough.



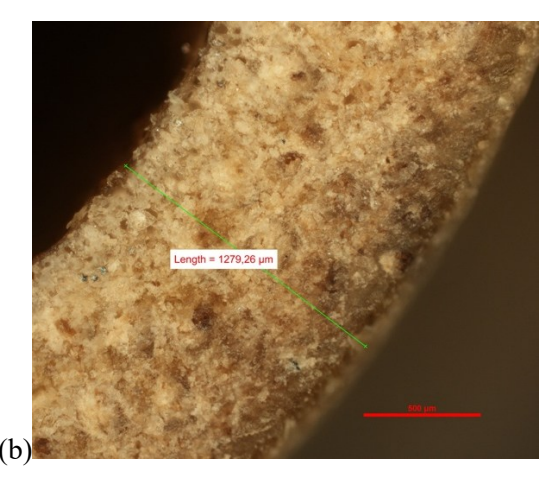
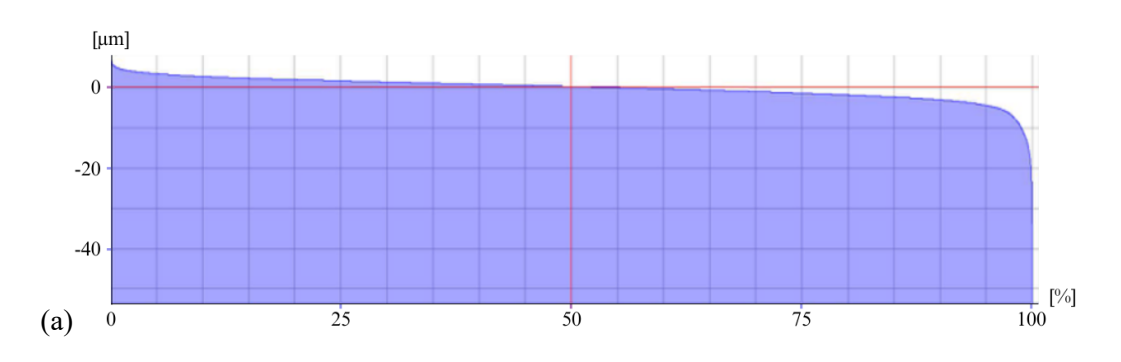


Figure 12. (a). Unpolished cross section's surface; (b) Polished cross section's surface with P120 sandpaper

Figure 13 (a) and (b) report an example of the Surface Portance around a point of unpolished samples and polished samples respectively (the same difference in the graphs is obtained in other points). Figure 13 (b) clearly shows the passage of the sandpaper with a broader variability of the punctual depths and a significantly larger area with notable depth concerning Figure 13 (a).



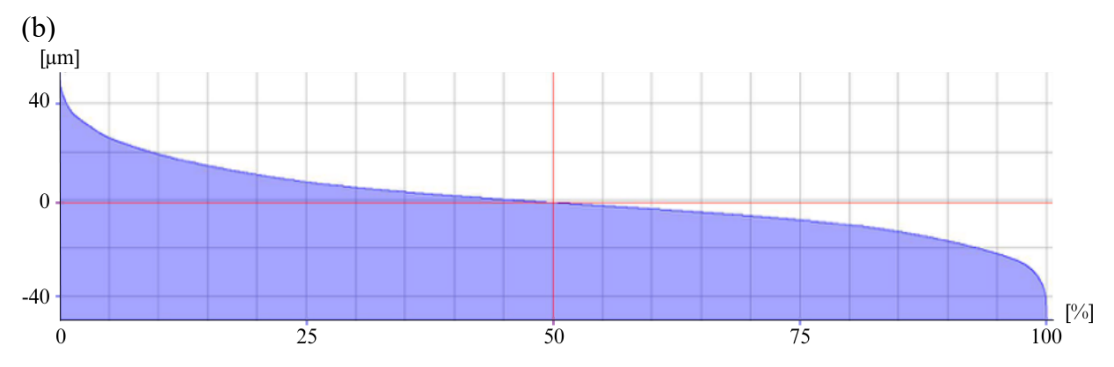


Figure 13. (a) Depth $[\mu m]$ vs Surface Portance [%] for polished specimens; (b) Depth $[\mu m]$ vs Surface Portance [%] for unpolished specimens.

The average arithmetical mean height of the surface, Sa, measured over three points and expressed in μ m, is 3.5 for the unpolished surface and 6.8 for the P120 polished surface. Interestingly, as seen in the Surface Portance, the polished surface exhibits a higher roughness parameter, suggesting that the polishing process introduced new surface features or irregularities.

3.5.2 Pull-off tests

Table 6 summarizes the maximum load and normal stress reached during the pull-off tests for different surface tratments. It highlights that samples polished with P120 sandpaper on the CSS show greater resistance compared to the unpolished samples with an increment of more than 50%. Figure 14 (a) illustrates the unpolished sample, while Figure 14 (b) shows the P120 polished sample. The P120 polished samples display a flax skin substrate covering nearly the entire surface, whereas the unpolished samples exhibit cohesive failure of the adhesive substrate, with only a few flax fibres visible on the surface. For this reason, all the AD rings in the core were polished with P120 sandpaper on their cross-sections.

Table 6. Pull-off test results in term of Maximum load and σ .

Cross-section treatment	Maximum load [N]	Normal stress [MPa]
Unpolished_CS	310,2	6.6
P120Polished_CS	499.1	10.6

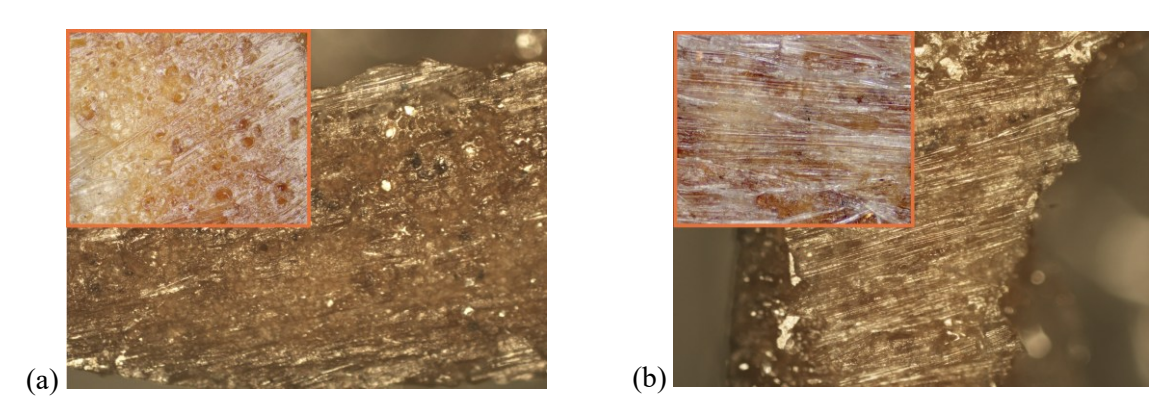


Figure 14. (a) Unpolished cross section analysis after the pull-off test, images collected using Nikon Eclipse LV150 with a 5x lens; (b) P120 polished cross section analysis after the pull-off test, images collected using Nikon Eclipse LV150 with a 5x lens.

3.5.3 Three-point bending tests

Figure 15 shows the load-deflection and Table 7 summarizes deflection, load, core shear stress, skin bending stress and modulus of elasticity.

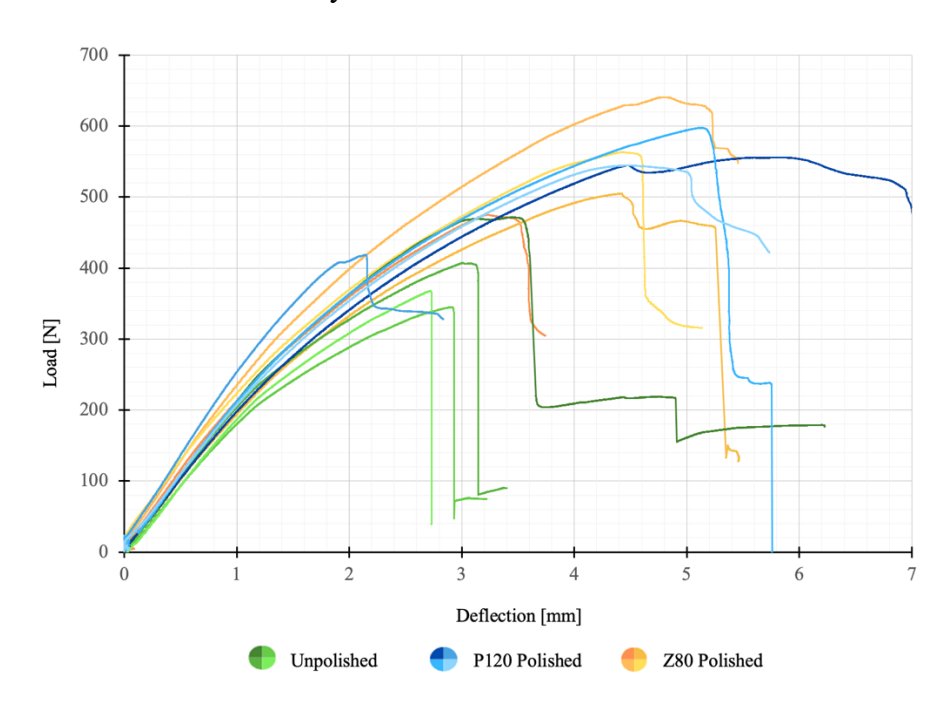


Figure 15. Load-displacement curves for all the specimens.

Table 7. Three-point bending tests: deflection, load, core shear stress, skin bending stress and modulus of elasticity.

Specimens	Deflection [mm]	Load [N]	Core shear stress, τ _c [MPa]	Skin bending stress σ _s [MPa]	Elasticity modulus E _B [GPa]
Unpolished1_LS	3.44	471.1	0.53	96.86	4.93
Unpolished2_LS	3.17	406.4	0.44	81.2	4.39
Unpolished3_LS	2.98	344.7	0.38	70.66	3.86
Unpolished4_LS	2.73	367.6	0.41	74.68	4.14
Mean	3.08	397.5	0.44	80.86	4.33
St.dev	0.30	55.3	0.06	9.98	0.45
Z80 1_LS	3.20	475.0	0.50	99.32	4.98
Z80 2_LS	4.90	640.5	0.66	146.34	5.50
Z80 3_LS	4.42	504.8	0.53	116.1	4.71
Z80 3_LS	4.58	563.3	0.59	129.9	5.05
Mean	4.28	545.9	0.57	122.92	5.06
St.dev	0.74	72.9	0.07	17.33	0.33
P120 1_LS	5.85	555.8	0.59	129.38	4.77
P120 2 LS	2.17	418.2	0.44	96.72	6.03
P120 3_LS	5.11	597.4	0.63	137.74	5.15
P120 4_LS	4.52	544.6	0.57	126.34	4.93
Mean	4.41	529.0	0.56	122.54	5.22
St. Dev.	1.59	77.2	0.08	15.48	0.56

The average maximum load increases from 397.5 N for the unpolished samples to 545.9 N and 529 N for the samples having the rings' lateral surfaces polished with Z80 and P120 sandpapers, respectively. All the mechanical characteristics increase with the polishing treatment of the lateral surface, with an increase from 0.44 MPa to 0.56 MPa and 0.57 MPa for the average values of the core shear stress, from around 80 MPa to around 122 MPa for the skin bending stress, from 4.3 GPa to around 5 GPa for the flexural Young modulus. The results show an increase in both shear and flexural properties.

Table 8 presents the p-values of the ANOVA analysis for the different surface treatments. Statistically distinguishable groups are characterized by p-values less than 0.05, (in bold in Table 5).

We can observe statistically significant differences between the treated samples and the Unpolished samples concerning both the skin bending stress and the maximum load.

Table 8. Analysis of variance (ANOVA).

Specime	ns	Load [N]	Skin bending stress σ _s [MPa]
Unpolished_LS	Z80_LS	0.035	0.016
Unpolished_LS	P120_LS	0.059	0.017
Z80_LS	P120_LS	0.937	1.000

The p-values reported in Table 8 highlight these meaningful differences. Specifically, the comparison between Unpolished and Z80_LS polished specimens as well as between Unpolished and P120_LS specimens show statistically significative difference with a p-value near or below 0.05.

In contrast, no significative differences were observed between Z80_LS and P120_LS polished specimens, indicating that both the treatments have similar effects on the material.

The polishing of the lateral surface not only improves the bonding between the lateral surfaces of the rings, leading to an increase in stiffness and shear resistance but also enhances the adhesion between the core as a whole and the skins, thereby improving the overall flexural performance.

The data obtained with the AD core are higher than those reported in a similar setup using a bamboo ring core in de Oliveira et al. [64], where the average flexural strength reached around 9 MPa and the average flexural modulus was approximately 3.2 GPa.

The difference can be attributed to multiple factors. The first is the internal geometry: AD has much smaller diameters compared to bamboo. Additionally, in the research of de Oliveira et al. [64], the rings were aligned in three parallel rows, whereas in this paper, the rings were arranged to minimize the number of voids within the core. The second significant difference is that in this research, the cross-section surfaces of the rings were roughened using P120 sandpaper, and this treatment was also applied to the lateral surfaces of the rings. The third difference is the use of an expanding epoxy resin that formed a rigid foam, partially filling the voids within the core. In de Oliveira et al. [64], a traditional epoxy resin was used, which provided a connection between the core rings and the skins but did not fill the core's voids and did not build a connection between the rings. The combination of foam resin and the abrasion of the rings' lateral surfaces ensured a proper connection between each ring with the others, which ensured that the core acted as a single monolithic element, significantly increasing the core's stiffness.

The lateral surface polishing treatment setup leads to different failure modes. In the four unpolished samples, as shown in Figure 16 (a), the main failure mode was the debonding between skins and AD rings. The failure starts in the core, at the lateral surfaces of the rings, which consequently leads to the debonding of the skins from the core.

In contrast in the specimens with the treatment of the lateral surface, failure occurs either due to debonding between the core and the skin or due to buckling failure in the skin (as can be seen in Figures 16 (b) and (c)).

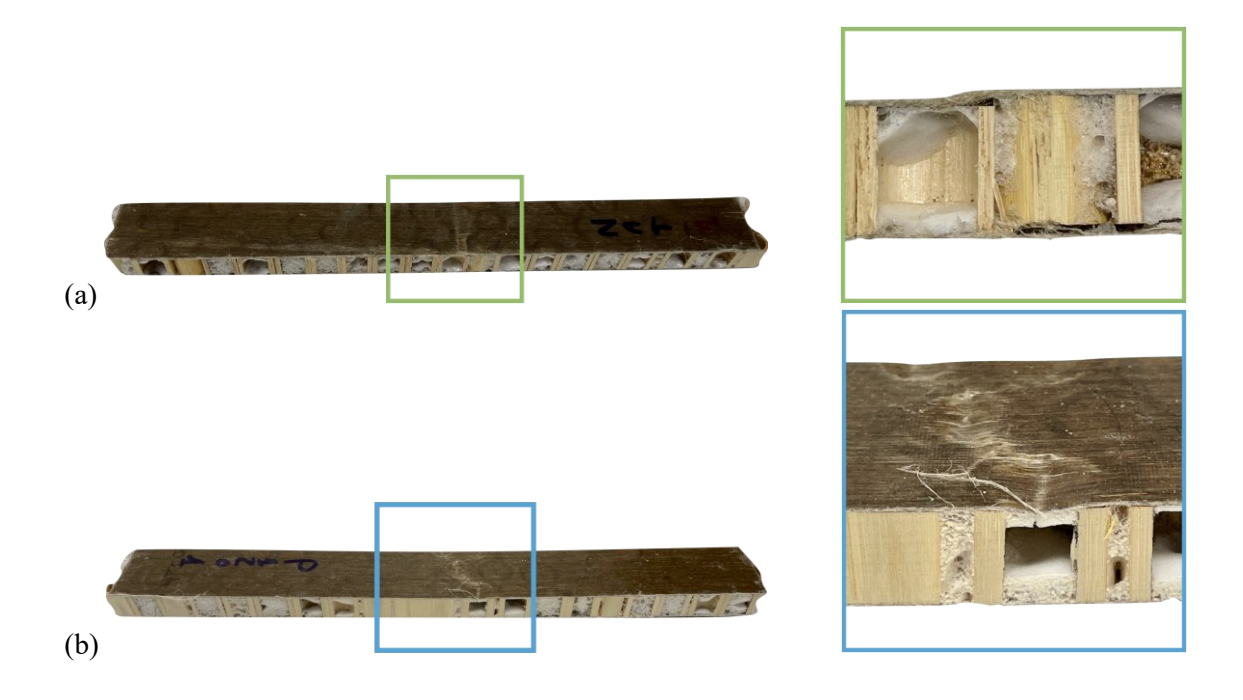




Figure 16. (a) Failure mode for unpolished lateral surface; (b) Failure mode for P120 polished lateral surface; (c) Failure mode for Z80 polished lateral surface.

For the next phase of modelling, it was decided to model the unpolished specimens, as they are simpler to produce and have lower production costs, not requiring the treatment of the lateral surfaces of the rings. As for the polished cases, it was decided to model the specimens polished P120.

3.5.4 Results of Analytical and Finite Element Modelling on Flexural Behaviour

In Table 9 are reported the geometrical and mechanical properties of the unpolished and P120 polished specimens. As for the polished samples, only the P120 case was considered in the modelling process.

Table 9. Average geometrical and mechanical data for unpolished and polished P120 specimen.

Parameter	Unpolished	P120 Polished
Length L_{tot} [mm]	296.5	300.0
Width b [mm]	32.9	35.2
Panel thickness h [mm]	14.3	14.0
Core thickness c [mm]	13.1	13.0
Diameter of the ring D _r [mm]	15	15
Wall thickness of the ring s [mm]	1.5	1.5
Skin thickness t [mm]	0.6	0.5
Mass m $[g]$	53.6	56.3
Equivalent Density $\tilde{\rho}$ [g/cm^3]	0.383	0.382
Young modulus of the skin E _{fl} [MPa]	36000	36000
Young modulus of the core E _{c1} [MPa]	13400	13400
Flexural stiffness of the sandwich panel (EI) _{eq} [Nmm ²]	60976465.2	53248026.24
Young modulus of the equivalent panel \tilde{E} [MPa]	7606	6667.7

Figures 17 (a) and (b) compare load versus displacement curves between the experimental data, the equivalent panel model, and the sandwich theory respectively for the unpolished and P120 polished cases. The related data are reported in Table 10. In both cases the sandwich model replicates the experimental trend in the linear portion of the experimental curve; however, the two trends start to diverge once the nonlinear behaviour of the panel emerges.

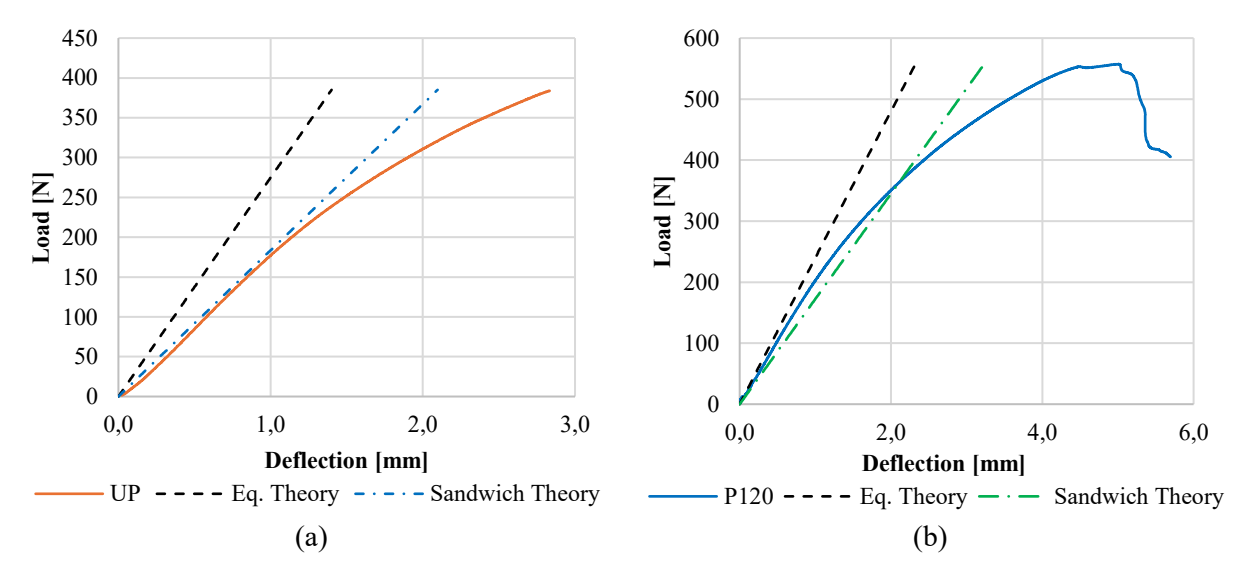


Figure 17. Comparison of the Load-Displacement curves from the average experimental data, Equivalent Plate Theory and Sandwich Panel Theory for: (a) Experimental average Unpolished (UP), (b) Experimental average P120 Polished (P120).

Table 10. Output data of the average of the Unpolished, polished P120 specimens and the relative equivalent panel model and Sandwich model.

UnPolished			P120			
Parameter	Experiment	Equivalent panel	Sandwich panel theory	Experiment	Equivalent panel	Sandwich panel theory
Maximum						
Deflection	2.83	1.40	2.23	5.01	2.32	3.23
δ [mm]						
Maximum Load	383.9	384.0	384.0	557.3	557.0	557.0
P [N]	303.9	364.0	304.0	337.3	337.0	337.0
Strain of the						
panel at failure E	0.502	0.248	0.395	0.865	0.401	0.559
[%]						
The stress of the	78.07	/	81.67	128.91	/	134.21
skin σ_s [MPa]	/ 0.0 /	/	01.07	120.71	1	134.41

As expected, due to the linear elastic hypothesis and the homogeneous core hypothesis, the analytical models of the sandwich panel are only able to predict the bending rigidity in the linear region of the experimental curve.

To better represent the nonlinear behavior of the panel, a FEM model was used. The cohesive parameters were identified starting from the unpolished model. For this case, an additional assumption was made of a total lack of connection between the various rings constituting the core. Specifically, the damage initiation stress is derived directly from the pull-off test (Sect 3.5.2). The value of the penalty stiffness parameters K_i and the fracture energy G_i were obtained through a tuning process of optimizing the model's output results. Specifically, K_i was tuned considering the linear behaviour while G_i considered the non-linear behaviour.

Table 11 summarizes the cohesive zone parameters used for the unpolished model.

Table 11. Cohesive zone parameters for the Unpolished Model.

Parameter	Value	
Penalty stiffness K_1 ; K_2 ; K_3 [N/mm ³]	140	
Damage initiation stress t_1 ; t_2 ; t_3 [MPa]	10.6	
G_1 ; G_2 ; G_3 [N/mm]	2.5	
Viscosity v	0.0005	

Figure 18 (a) reports the comparison in terms of load versus displacement curves between the Experiment (Average Unpolished) obtained by the three-point bending tests and the Unpolished Finite Element Model (FEM).

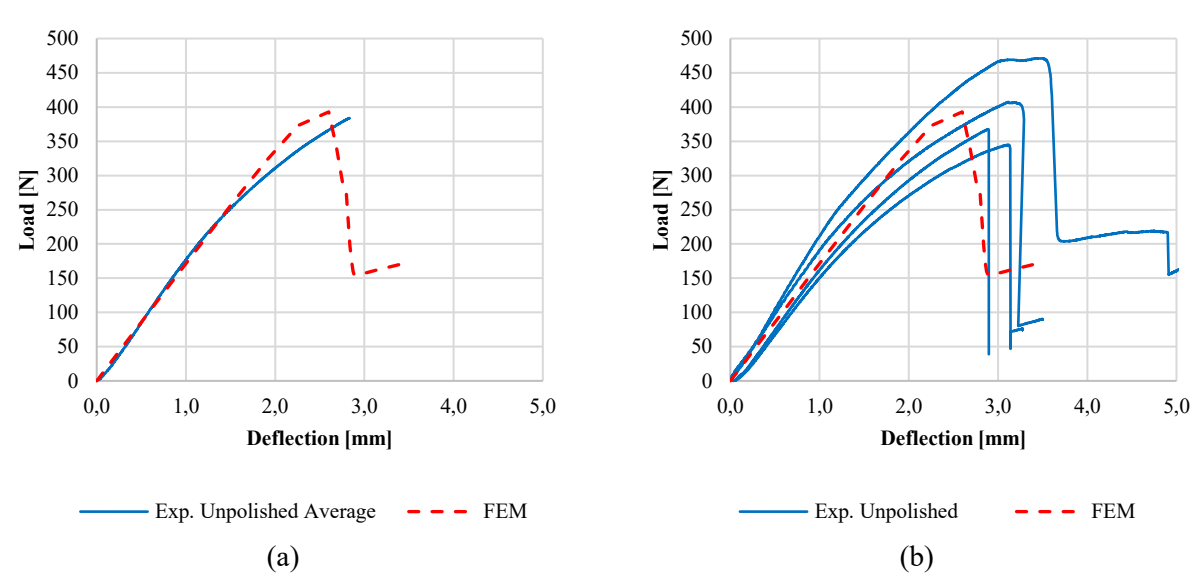


Figure 18. Comparison between the load-displacement curves: (a) Average of Unpolished experimental samples and the Finite Element Model; (b) all the Unpolished experimental specimens and Finite Element Model.

The trend of the load-displacement curve associated with the FEM optimally simulates the linear part of the graph, regarding the nonlinear part, the simulation is less accurate. Nevertheless, the deviation between the average experimental curve and the one related to the FEM falls within the variability of the experimental data for the 4 tested panels, as it is possible to see from Figure 18 (b).

Table 12. Comparison output data between the specimen average Unpolished and the Unpolished Finite Element Model (FEM).

Parameter	Value		
	Unpolished	FEM	
Maximum Deflection δ [mm]	2.83	2.60	
Maximum Load P [N]	383.9	392.9	
Strain of the panel at failure E [%]	0.00502	0.00461	
Stress of the skin σ_s [MPa]	78.07	83.26	

From the data in Table 12, it is evident that the FEM closely replicates the output of the experimental analysis, particularly the value of the maximum load and the stress in the skins. The failure of the panel, in the case of the FEM, occurs in the connection regions between the skins and the core. The

activation of this phenomenon in the model indicates the activation of the failure criteria and degradation law in the cohesive elements of the Finite Element Model (FEM). This is in line with what was obtained experimentally.

Once the modelling associated with the unpolished series panels was completed, modelling was also carried out for the P120 polished specimens. In this case, the initial assumption made for the unpolished samples (total absence of cohesive interaction inside the core between the rings) is no longer valid, and a new assumption has been formulated. The same cohesive interaction present between the skins and the core is now considered to be present between the lateral surfaces of the various rings constituting the core, thanks to the roughening treatment applied to these surfaces using sandpaper. Initially, the same cohesive parameters obtained for the unpolished case, as reported in Table 13 were used.

Table 13. Cohesive zone parameters for the P120 Polished model 1.

Parameter	Value	
Penalty stiffness K_1 ; K_2 ; K_3 [N/mm ³]	140	
Damage initiation stress t_1 ; t_2 ; t_3 [MPa]	10.6	
G_1 ; G_2 ; G_3 [N/mm]	2.5	
Viscosity v	0.0005	

Using these parameters, the results shown in Figure 19 were obtained in terms of load-displacement, in which the P120 Finite Element Model was indicated as P120-FEM1. As can be observed, the model reaches failure much earlier than in the real case. This is because in the polished case, the foam resin is connected both to the skins and to the lateral surfaces (LS) of the rings. This connection causes a change in the internal geometry of the core, effectively increasing the contact area between the core and the skin.

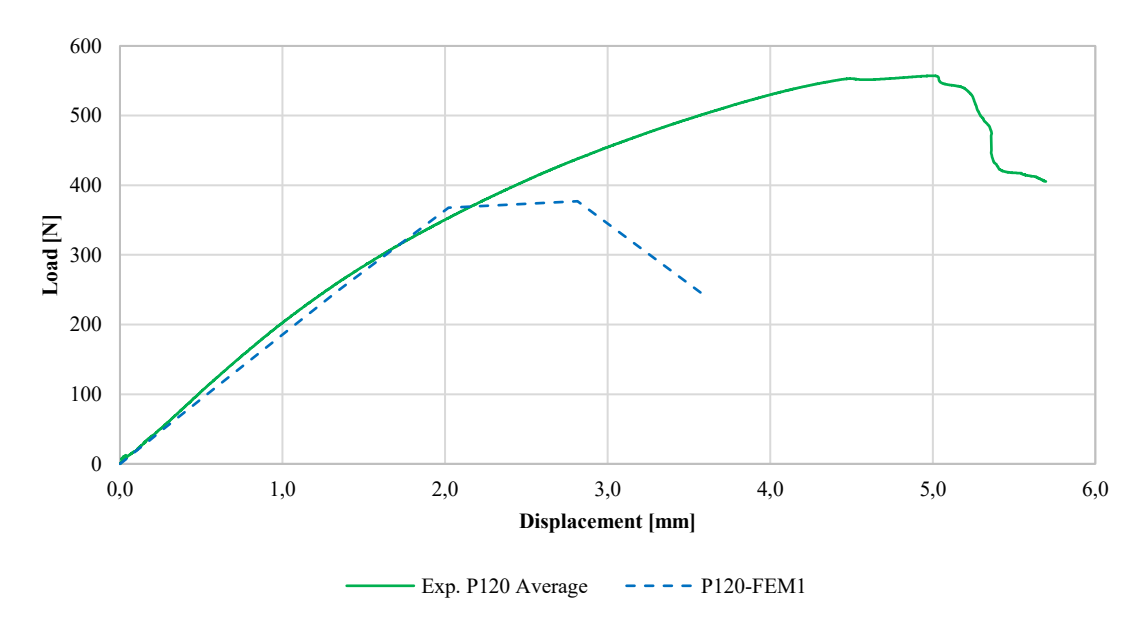


Figure 19. Load-displacement for Exp. P120 Average and the P120 Finite Element Model (P120-FEM1).

Since the goal is to keep the model as simple as possible, it was decided not to modify the internal geometry of the core, but to adjust another parameter instead: the damage initiation stress t. By keeping all other parameters of the cohesive zone constant, the correct value of t was obtained through a tuning process (Table 14). The value of t appears to be significantly greater compared to the

unpolished case, the new P120 Finite Element Model was indicated as P120-FEM2. Figure 20 reports the results.

Table 14. Cohesive zone parameters for the Polished P120 model 2.

Parameter	Value	
Penalty stiffness K_1 ; K_2 ; K_3 [N/mm ³]	140	
Damage initiation stress t_1 ; t_2 ; t_3 [MPa]	38.5	
G_1 ; G_2 ; G_3 [N/mm]	2.5	
Viscosity v	0.0005	

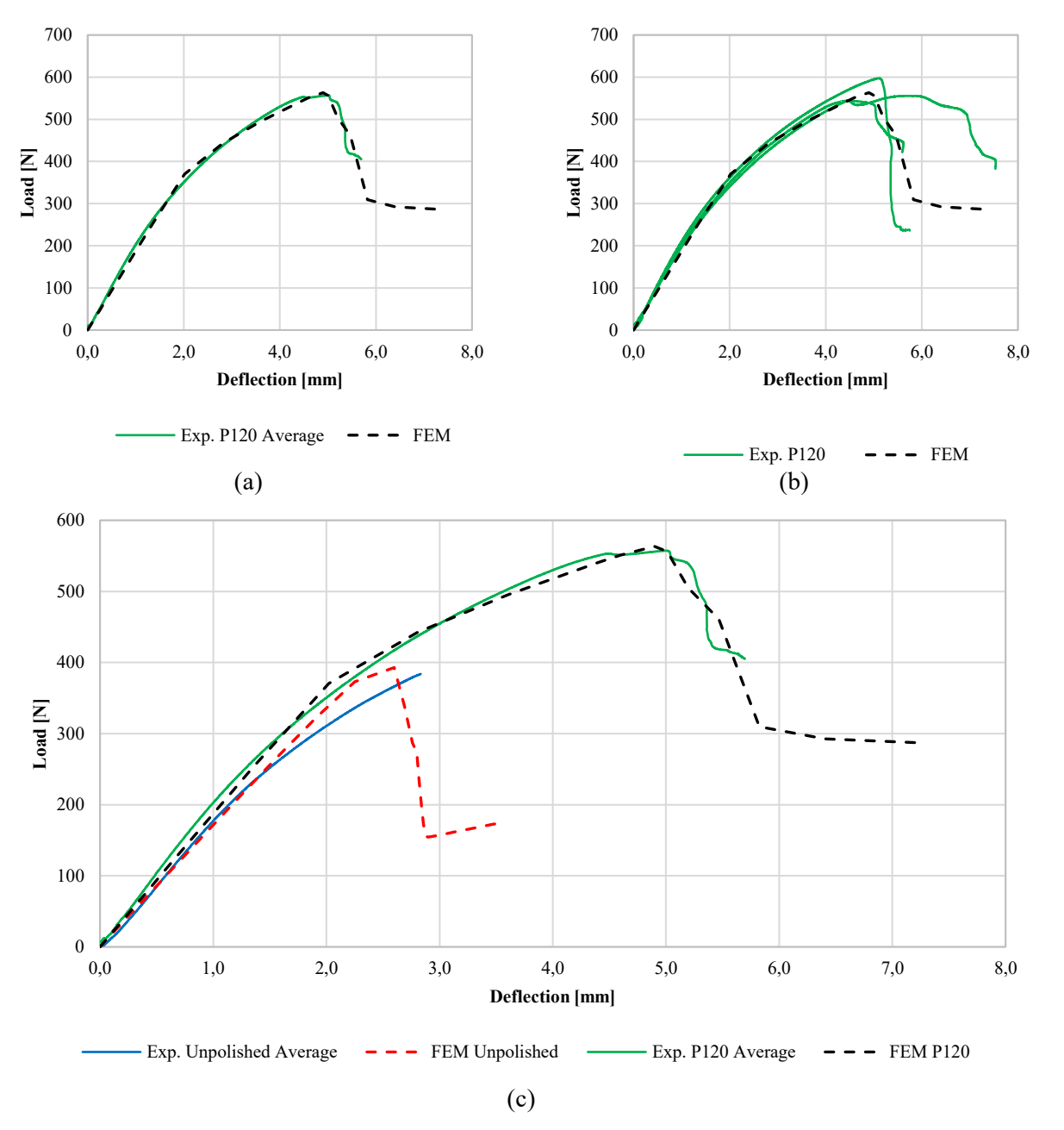


Figure 20. Comparison between the load-displacement curve: (a) Average of P120 experimental samples and the P120-FEM2; b) all the P120 experimental specimens and the P120-FEM2 c) Average and FE models for the experiment Unpolished and Polished specimens.

From Figures 20 (a) and 20 (b), it is possible to observe that the model reproduces the behavior of the panel under a three-point bending test, both in the linear, non-linear and failure parts. The FEM model for specimen P120 presents a very low discrepancy from the experimental values, as can be observed from Table 15, even regarding the stress values in the skins. Figure 20 (c) shows a comparison between the Unpolished and P120 polished, both for the experiment and the model.

Table 15. Comparison output data between the P120 specimen average and the P120 Finite Element Model 2 (P120-FEM2).

Parameter	Value		
	P120	P120-FEM2	
Maximum Deflection δ [mm]	5.01	4.90	
Maximum Load P [N]	557.34	563.25	
Strain of the panel at failure E [%]	0.0087	0.0087	
Stress of the skin σ_s [MPa]	128.91	127.06	

A sensitivity analysis of the FEM models was performed. For the Unpolished model, the analysis focused on the input parameters G and K related to the cohesive zone, which were derived through tuning. For the P120 model, the analysis concentrated on the parameter t, the only one obtained through tuning. The results were obtained by varying each input within a range of -20 % to +20 % and calculating the corresponding percentage variations of the outputs. Table 16 reports the values of the EE sensitivity index, which measures the average rate of output variation when a single input factor is modified (One Factor at a Time analysis).

Table 16. EE sensitivity index, the sensitivity of the outputs to the percentage variations of the inputs.

	Input	Deflection	Load	Skin Stress
EEM Umaliahad	G	0.0318	0.0228	-0.1584
FEM Unpolished	K	-0.0080	0.3799	0.3686
FEM P120	t	1.5457	0.5586	0.5404

The results suggest that, to optimize system performance, special attention should be paid to controlling the input t which has a dominant impact on deflection. Similarly, the inputs K and t are crucial for managing load and skin stress. On the other hand, the input G can be considered less critical due to its low sensitivity to the analysed outputs.

From the data in Table 16, it is evident that the FEM closely replicates the experimental results, particularly in terms of maximum load and stress distribution in the skins. The FEM predicts panel failure in the connection regions between the skins and the core, aligning with experimental observations.

FEM for both Unpolished and P120 polished panels accurately simulate the experimental behaviour. In the Unpolished case, the FEM confirms the hypothesis of a complete lack of adhesion between the resin foam and the rings within the core, effectively representing the experimental material's non-linearity and failure.

The increased material stiffness from Unpolished to polished is attributed to the improved adhesion between the foam resin and the Arundo rings forming the core, which occurs after the lateral surface of the rings undergoes polishing. The foam resin now connects to both the skins and the rings inside the core, transmitting stresses from the skins to the rings. This interaction results in a larger contact surface between the skin and the core, leading to an increase in the material's bending resistance. This is modelled with the link among the cohesive interface of the core ring.

Also, in this case the model can catch the experimental evidence. The cohesive bond between the core and skins, as well as within the core rings, leads to a significant increase in the panel's ultimate strength and a more accurate representation of the panel's stiffness.

As shown in Figures 18 and 20, the model also predicts the drop load of the curves after the maximum load, with the presence of a subsequent residual strength in the numerical and experimental results. In the experimental phase, the drop in resistance after the load peak was significantly more pronounced in the Unpolished case compared to the P120 case, with reductions of 79.0% and 38.1%, respectively. This behavior was also accurately reproduced by the Finite Element model, which predicted a drop in resistance of 60.7% for the Unpolished case and 47.9% for the P120 case.

The lower residual strength, in percentage terms, observed both in the experimental results and in the FEM simulations for the unpolished specimens, is attributable to the lack of adhesion between the foam resin inside the core and the AD rings. This results in the core behaving not as a monolithic element, but as a collection of independent components connected only to the skins. Once the cohesion with the skins is lost, these elements no longer contribute to the structural strength.

3.6 Conclusion

From the unpolished to the polished model, a significant increase in the ultimate strength of the panel was observed in the numerical simulation, closely reflecting the experimental findings. The model, thanks to the presence of the cohesive bond within the core, accurately represents the stiffness of the panel.

The increase in material stiffness from unpolished to polished is due to the proper adhesion between the foam resin and the AD rings constituting the core, which occurs once the lateral surface of the rings undergoes the polishing treatment. This adhesion does not occur in the natural state because of the particularly smooth surface of the material [75]. The adhesion between the foam and the lateral surfaces of the rings not only increases the panel's stiffness, due to the core acting as a single unit but also causes a change in the internal geometry of the core. This change is because the foam resin is simultaneously connected to one of the two skins and the rings inside the core, transmitting the stresses from the skin to the rings and the second skin.

The panel was manufactured and evaluated using a three-point bending test, demonstrating favorable bending properties that met the minimum strength requirements specified in the EN 312 standard [76]. This makes it a suitable candidate for both structural and non-structural panels in the construction industry.

The results indicate that the surface polishing treatments on the lateral and cross-section areas of the AD rings have a significant impact on the panel's mechanical properties. Specifically, the mechanical performance improves with the polishing of the basal and lateral surfaces. Core shear stress, flexural stress, and modulus increased by an average of 30%, while the facing bending stress increased by as much as 52%.

The finite element model (FEM) successfully predicted the load-displacement curves for both unpolished and P120 polished panel series, accurately capturing both the linear and non-linear material behavior, including the failure phase. Initially developed for the unpolished series, the model was adapted to the P120 polished series by introducing a cohesive interaction hypothesis between the rings in the panel core. This interaction was assumed to be the same as the one between the skins and the core. By adjusting just one parameter, the Damage initiation stress t, which was understandably higher in the polished panels, the model performed well for the P120 series. The skins and rings were modeled as homogeneous orthotropic solids, with orthotropic properties chosen to match the panel's stiffness.

In the unpolished model, it was possible to confirm the hypothesis of a complete lack of connection between the foam resin and the lateral surfaces of the rings, meaning that each ring acts as a separate element within the core.

The P120 FE model allowed for the confirmation that following the polishing treatment of the lateral surfaces of the rings, there is proper adhesion between the resin and the rings. This increases the stiffness of the panel and causes a modification in the internal geometry of the core, resulting in an increased contact surface between the core and the skin. This is responsible for the increased bending resistance of this type of panel compared to the untreated case.

The implementation of cohesive interaction within the core, between the rings that constitute it, was crucial for the correct realization of the model. Without this interaction, the material would be much less rigid than it is. It was possible to create a model that accurately represents the mechanical behavior of the material, both in the absence of surface treatment and when surface treatment is applied. This was achieved while keeping the model simple and easily reproducible, which was one of the intended objectives.

The FE model, developed and validated with experimental results, can be used in future studies to improve board design to meet various requirements, such as enhancements in sound or thermal insulation, as well as mechanical performance.

Additionally, the model will be used to conduct a parametric analysis to assess how performance is influenced by geometric parameters, such as ring diameter, length, and the geometric arrangement of the rings within the core.

In addition to all the advantages of bio-based plants, Arundo donax used in the core offers further benefits, such as a high strength-to-weight ratio, good flexibility, and lightweight characteristics. These properties ensure excellent mechanical performance of the panel while keeping its weight lower than that of panels made with alternative materials like metals.

Moreover, Arundo donax naturally grows throughout the Italian peninsula, significantly reducing both economic and environmental transportation costs compared to other natural materials like bamboo or wood, which are less common in central and southern Italy and on the islands. This gives the panel a strong territorial identity and supports the implementation of the "km 0" concept. The use of a natural material does not necessarily imply a lower environmental impact, especially if it needs to be transported over long distances from its place of cultivation or production to the site of use.

Another key improvement introduced and demonstrated by the developed honeycomb panel is the strong correlation between the surface roughness of the bonding areas (skin-to-core and ring-to-ring interfaces within the core) and the panel's flexural performance. Even small increases in roughness led to a significant rise in friction, thereby improving adhesion and, consequently, the mechanical properties under bending.

A critical point regards the choice of adhesive and composite matrix. This project used synthetic, petrochemical-based epoxy resins. There are greener alternatives, such as cashew nut shell liquid (CNL) or polyhydroxyalkanoates (PHA); however, both are prohibitively expensive and have limited production capacity, mostly outside the European Union, which restricts their use in large quantities, at least for the time being.

Another issue encountered concerns the high cost and significant energy consumption required to manufacture the panel skins.

Although flax fibers possess very high mechanical properties, they are much more expensive than other natural fibers, such as hemp fibers (due to a higher agricultural yield).

As for the production process, the one used requires high pressure and temperatures, leading to high economic and environmental production costs for the composite. An alternative option for the skins was studied in Appendix A.

4. PARTICLEBOARD PANEL

4.1 Introduction

This project was born from the collaboration between the University of Bologna and the company Gruppo Saviola, based in Viadana, Mantova, which specializes in the chemical sector and the production of non-structural particleboards. The project aimed to study the feasibility of using *Arundo donax* (AD) in the production of particleboard panels considering the company's desire to improve the mechanical and physical properties of their particleboard without modifying the production process and the quantity and type of resin used.

Particleboard, or particleboard, is a composite material produced by pressing small wood fragments, known as chips, mixed with thermosetting synthetic resins. These panels are manufactured through a process that involves mixing the chips with a binder (typically urea, phenolic, or melamine resins), followed by a thermocompression in moulds. During this phase, the resin undergoes polymerization, creating a solid and compact structure.

Particleboard panels usually have outer layers made of finer chips to improve surface finish and an inner layer of coarser chips to provide mechanical strength. Their physical-mechanical properties depend on the quality of the raw materials used, the size of the chips, the density of the panel, and the type of resin employed.

Particleboard is widely used in the furniture and construction industries due to its cost-effectiveness, versatility, and availability. However, it does have some limitations in terms of mechanical strength and moisture sensitivity compared to other composite materials like Medium-Density Fibreboard (MDF) or plywood.

Particleboards made of wood are extensively utilized in massive furniture production and construction sectors. Despite wood is considered a renewable resource, the growth rate of trees varies by species, ranging from 30 cm to 1 m per year. Trees require from 3 to 40 years to mature before they can be harvested for engineering purposes. The widespread use of wood, combined with its slow regrowth, is contributing to deforestation on a large scale. Over the past two decades, global forest coverage has decreased by 1 million km² (equivalent to 2.4% of the forested area since 2000) [77, 78, 79]. Deforestation of forests is an important global issue because these forests harbor a high percentage of land biodiversity and play a critical role in the global carbon and water cycles [80, 81]. Additionally, the conversion of forests to other land uses is responsible for around 20% of the world's greenhouse gas emissions (GHG), and the accelerating rate of deforestation has a significant impact on global climate change [80].

Countries like Italy are major importers of wood. According to the Economic Observatory of the Italian Ministry of Foreign Affairs, Italy imports approximately 3 to 4 billion euros worth of wood annually (excluding furniture), while its exports are valued at around 1.5 to 2 billion euros [82]. From an economic standpoint, importing such large amounts of wood poses challenges to the trade balance, while from an environmental standpoint wood imports lead to an increase in CO₂ emissions due to the logistics required for transportation, which could be reduced by using autochthonous materials.

Lignocellulosic resources derived from waste, have significant industrial potential but are underutilized and it can help reduce the uncontrolled logging of forests [83, 84]. These resources can be classified into industrial waste (mainly from pulp, paper, and wood processing), forestry waste (residues from forestry and maintenance), agricultural waste (crop residues, nuts, grains, and surplus crops), and urban waste (such as recycled wood, wastepaper, and cardboard). The volume of post-consumer waste wood is rising with urbanization and industrialization. According to Eurostat data from 2014, Europe generates around 60 million tonnes of wood waste annually from various sectors. Germany is the leader in the collection of wood waste in Europe with around 6.6 million tons in 2016, while Italy, the United Kingdom and France produce around 4 million tonnes per year [85]. Despite differences in wood waste management, recycling rates vary from country to country with high

percentages ranging from 85% to 95% in countries such as Sweden, Switzerland, Norway, the Netherlands, and Finland. A great part of this recycled material is then used in particleboard production, Italy leads among European countries with 42% followed by Austria with 33% [85]. Wood waste comes from various sources, making it a non-homogeneous material due to the diversity of wood types, applications, and origins [86]. Waste wood contains physical and chemical contaminants, which pose challenges for recycling processes and affect the properties of the recycled products. Nowadays, several mechanical processes can separate physical contaminants in wood waste, such as plastics, metals, or fabrics. However, chemical contaminants from wood preservatives, paints, and adhesives are more challenging to remove, resulting in the mechanical properties of recycled particleboards being inferior to those made from virgin wood.

In the production of particleboard or particleboard panels, the use of non-wood plants as a substitute for, or supplement to, wood has been studied for decades to provide innovative properties to traditional products. These non-wood materials include hazelnut shells [87, 32], coffee parchment [88], tobacco stalk [89], peanut hull [90], sycamore leaves [91], rice straw [92], recycled wood [93, 94, 95] and in particular AD, that has demonstrated good potential [96, 33, 97, 16].

The project aimed to develop recycled wood particleboards produced by a certified supply chain and enhance their properties by adding AD particles. It has been widely demonstrated in the literature that the use of AD as a substitute for wood provides sufficient mechanical properties to a particleboard panel to ensure its commercialization. Studies have also been conducted on panels where wood particles were partially replaced with AD particles in the case of single-layer panels [98]. Other studies have shown that the use of this material improves the water resistance of particleboard compared to its wood-based counterpart [99].

The starting point of the project was Gruppo Saviola company's particleboard for indoor use, made with recycled wood chips and urea formaldehyde resin, a resin commonly used in this sector because it is the most economical and provides good mechanical performance and durability to particleboard. The special advantages of UF resins compared to other wood adhesive types have been widely reported by several researchers [101, 102]. These mainly concern the high mechanical performance of this type of resin, the strong bond between the resin and the wood (this resin was specifically developed for use in wood particleboard panels), which ensures optimal cohesion between the two components and the very low cost (a fundamental characteristic for an industry with production volumes the order of millions of tons of panels produced Urea-formaldehyde resins generally pose issues related to volatile compound emissions from wood and wood-based panel products. However, these emissions are kept low and within legal limits by the company.

Particleboard is a sandwich panel composed of three layers: two thin outer layers made using a very fine particle size, and a thicker inner layer consisting of coarser particles.

The research was structured into three different phases or Waves, in agreement with the company. In Wave 1, the study focused on the effect of particleboard density and the addition of AD in various percentages within the core. In Wave 2, the effect of varying the size and shape of AD chips in the core was investigated. In future work, AD could be substituted in the outer layers.

4.2 Wave 1

In the first phase, called Wave 1, the recycled wood chips were partially substituted with AD chips only in the core of the particleboard, using different percentages of substitution, to enhance the physical and mechanical characteristics of the particleboards. Different percentages of AD substitution, and three different levels of density were analyzed while maintaining the same type the

amount of resin. Therefore, no changes were made to the production process except for the substitution of part of the recycled wood in the core with AD.

The goals included determining the optimal percentage of AD that corresponds to the best mechanical performance, observing whether this varies with the density of the particleboard and ensuring an enhancement of the mechanical properties of the particleboard while maintaining the same density and adhesive used.

4.2.1 Materials

In the particleboard panels, two different particle size distributions of recycled wood are used: one composed of finer particles in the range $0.1~\mathrm{mm} < \mathrm{d} < 2~\mathrm{mm}$, and one composed of coarser particles in the range $0.5~\mathrm{mm} < \mathrm{d} < 4~\mathrm{mm}$, where d is the particle size. The first particle size distribution is used to manufacture the outer layers of the particleboard, while the second one is used for the core layer. The company's proprietary granulometric distributions were used, which are not reported here for confidentiality reasons. The recycled wood particles were provided by Saviola Group. Giant reed was collected from a cultivation of the Department of Agricultural and Food Sciences, of the University of Bologna, in Cadriano, Bologna, Italy. Before processing, the apical and basal parts of the culms, as well as the leaves, were removed. The AD was processed following four sequential steps: harvesting, during which the leaves and the apical and basal parts of the plants were removed, drying in an oven at 85° C until a constant mass was achieved, defined as less than a 0.5% weight variation between two weighing conducted 24 hours apart [69], shredding using a hammer shredder followed by sieving of the chips to achieve the same granulometric distribution as the recycled wood chips used for the panel's core.

The density and mechanical properties of AD are reported in Table 17 [6].

Table 17. Average and standard deviation of the density and mechanical properties of Arundo donax.

Parameters	Value
Density ρ [kg/m³]	647.7 (±0.04)
Compression stress σ_c [MPa]	57.04 (±0.05)
Compression Young modulus Ec [GPa]	13.40 (±0.33)
Tensile stress, parallel to the fiber $\sigma_{t,0}$ [MPa]	111.70 (±0.12)
Tensile Young modulus parallel to the fiber $E_{t,0}$ [GPa]	15.29 (±0.07)
Tensile stress, perpendicular to the fiber $\sigma_{t,90}$ [MPa]	11.22 (±0.14)
Tensile Young modulus perpendicular to the fiber $E_{t,90}$	1.05 (±0.16)
[GPa]	
Shear stress τ [MPa]	18.40 (±0.12)
Shear elastic modulus G [GPa]	2.96 (±0.23)

AD was dried using an oven at a temperature of T = 85 °C until reaching a mass variation of less than 0.1% after 24 h in the oven [69]. The weight loss of the dry material ranged from 28% to 43%.

Urea formaldehyde resin (Sadecol L) in a liquid form was used for particleboard manufacture together with, the hardener CTZ (Amm. Solfato) The resin and the hardener were supplied by the SADEPAN Company.

4.2.2 Manufacturing process

The manufacturing process is designed to align with the company's production methods while incorporating findings from the literature on particleboards similar to those produced here [100, 101]. The particleboard panels form a sandwich structure with three layers: two thin outer layers and a thick 42

inner layer, the core of the particleboard. The outer layers are made of recycled wood chips with a finer particle size distribution to ensure a uniform and completely planar surface for the nobilization of the particleboard. The composition of these outer layers is the same as that used by the Saviola Company, with no modifications made during this experimental campaign. The core was modified by substituting part of the recycled wood chips with chips of AD.

Various particleboard panels were manufactured with adjustments in density and the percentage of AD in the core. Table 18 shows the 15 types of specimens produced along with their corresponding notation.

Table 18. Nomenclature of the particleboards manufactured.

Type of Board	Quantity of AD particles in the core [%]	Quantity of recycled wood particles in the core [%]	Density [kg/m ³]
A550	0	100	550
A680	0	100	680
A750	0	100	750
B550	10	90	550
B680	10	90	680
B750	10	90	750
C550	20	80	550
C680	20	80	680
C750	20	80	750
D550	35	65	550
D680	35	65	680
D750	35	65	750
E550	50	50	550
E680	50	50	680
E750	50	50	750

The manufacturing of the particleboard panel involved three main phases. In the first phase (Figure 21 (a)) the components were mixed. For the outer layer, recycled wood chips, resin, and water were combined in fixed proportions, consistent across all densities; specific details are not disclosed here for confidentiality. For the core AD and recycled wood chips were mixed varying their percentages as reported in Table 16, the percentage of resin used in the core was the same for all densities.

In the second phase (Figure 21 (b)) the three layers forming the particleboard were manually positioned inside a pre-mold measuring 32x25x30 cm. Pressure was manually applied to create a preform, reducing air content and simulating industrial production conditions.

In the third phase (Figure 21 (c)), the pre-formed material was placed inside a hot press for the molding process. The particleboards were produced through a hot-pressing process with a pressure of 300 bar and a temperature of $190 \sim 210$ °C to ensure the catalysis of the resin inside the particleboard and the evaporation of the water. The particleboard was maintained inside the press at a constant temperature for approximately 4 min.







Figure 21. Steps followed for the particleboard production process: (a) mechanical mixing of the materials, (b) preforming the particleboard by applying manual pressure, (c) hot molding of the particleboard.

This procedure was carried out for all the different types of particleboards reported in Table 16. The density was adjusted by varying the amount of material used for the particleboard manufacturing while the pressure applied by the machine remained the same.

Before proceeding with the testing phase all the particleboards were squared to remove the edges, resulting in particleboards measuring 300 x 200 x 22 mm and they were cut using a circular saw to obtain the specimens for the different tests.

4.2.3 Methods

Four different tests were conducted to perform a mechanical and physical characterization of the particleboard. These specific tests were selected according to the EN 312 standard [76], which provides guidelines for the classification and characterization of various categories of particleboard. Table 19 reports the four tests, the normative associated with the test, the number and the dimensions of the specimens tested for each type of particleboard manufactured according to the standard [102].

Table 19. Type of tests carried out, standard associated to each test, number and dimensions of the specimens required for the physical-mechanical tests.

Test	Normative	Number of Specimens	Dimensions of specimen [mm]
Swelling in thickness	EN 317 (1993)	8	50 x 50 x 22
Surface soundness	EN 311 (2002)	8	50 x 50 x 22
Internal Bond	EN 319 (1993)	8	50 x 50 x 22
Three-point bending	EN 310 (1993)	6	300 x 50 x 22

Before testing the samples were kept for 24 h in a conservation chamber, at a temperature of 20°C and a relative humidity of 65%.

The Swelling in thickness test as specified in the EN 317 (1993) standard was performed to determine the thickness swelling of a specimen with a cross-section of 50 x 50 mm after complete immersion in controlled water, at a constant temperature of 20 °C and a pH of 7 for 2 hours. The specimens were maintained separated from each other, and from the surfaces of the water bath, as reported in Figure 22 (a). For each particleboard type, 8 specimens were tested as suggested by EN 326-1 [102]. The tests were performed with the IMAL testing machine (Model IB600, IMAL, S.R.L., Modena Italy), Figure 22 (b).

During the immersion period, the specimens were covered with 25 mm of water, to ensure proper immersion. For each test, the water in the bath was changed, following the standard recommendation [103]. The swelling in thickness G_t was calculated according to the Eq. 9:

$$G_t = \frac{t_2 - t_1}{t_1} 100 \tag{9}$$

where t_1 is the thickness of the test piece before immersion expressed in millimeters, t_2 is the thickness of the test piece after immersion, also expressed in millimeters.

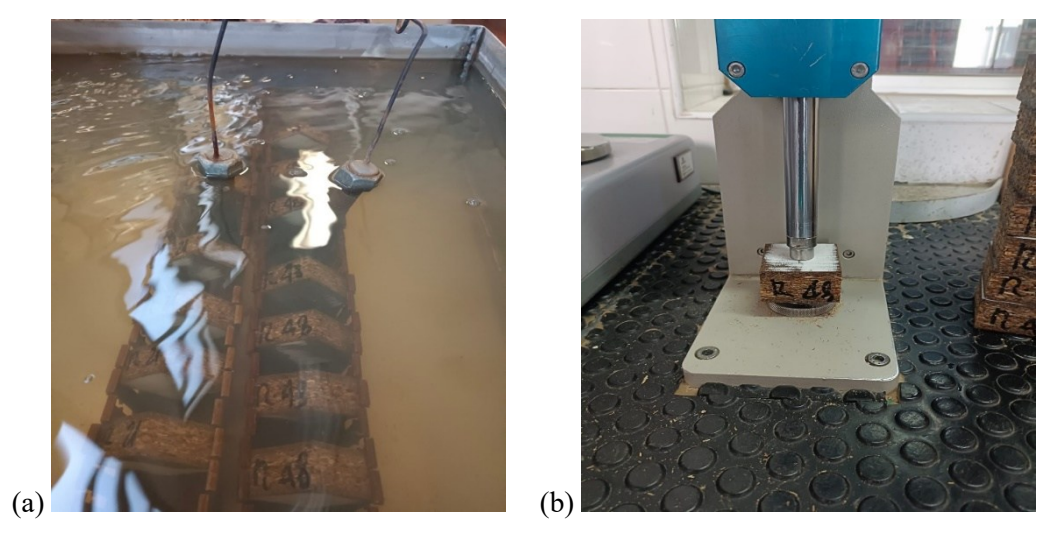


Figure 22. (a) Immersion of the specimens in the water bath. (b) Thickness swelling test on a sample with a cross-section area of 50×50 mm.

The Surface soundness test aimed to determine the tensile strength perpendicular to the surface of the particleboard and the adhesion between the outer and the inner layers of the particleboard. Eight square specimens of 50 x 50 x 22 mm were tested as suggested by the standards EN 326-1 [102]. Circular grooves were cut into the surface of the specimens according to the standard [104]. On the surface of the specimen, a heated steel pad is glued using a hot-melt adhesive with a melting point under 150 °C, Figure 23 (a) shows test preparation: the hot pad is pressed onto the surface of the specimen and held with a light pressure of 0.1 N/mm² to 0.2 N/mm² until the adhesive has cooled and hardened. The tests reported in Figure 23 (b) were carried out at a constant speed, so the failure occurred in 60-90 s [104].





Figure 23. (a) Test preparation. (b) Surface soundness test on a sample Thickness swelling test on a sample with a cross-section area of 50×50 mm.

Figure 24 (b) shows the Internal bond (IB) test, performed to determine the tensile strength perpendicular to the plane of the particleboard. As suggested by the standards EN 326-1 [102], 8 square specimens of 50 x 50 x 22 mm were tested. The specimens were glued to both the surface and metal test blocks, as shown in Figure 24 (a). Excess glue was removed before proceeding with the test. The load was applied at a constant rate of crosshead movement throughout the test and the rate of loading was adjusted so that the maximum load was reached within (60 ± 30) s, as reported in the standard [105].





Figure 24. (a) Test preparation. (b) Internal bond test on a sample Thickness swelling test on a sample with a cross-section area of 50×50 mm.

Tensile strength perpendicular to the plane of the particleboard of each test piece is calculated according to Eq. 10:

$$f_{t\perp} = \frac{F_{max}}{a \cdot b} \tag{10}$$

where F_{max} is the breaking load expressed in Newton, a and b are respectively the length and width of the test piece expressed in millimeters.

The Three-point bending tests were carried out on samples of 300 x 50 x 22 mm. Three specimens were cut for each manufactured particleboard and two particleboards were manufactured for each type of particleboard panel, a total of six specimens were tested, according to the standard EN 326-1 [102]. The test procedure follows the standard EN 310 [106], using a span length of 250 mm.



Figure 25. Three-point bending test on a sample of 300 x 50 x 22 mm.

A strain gauge (KFGS-10-120-C1-11 L1M2R of 10 mm length) was placed on the bottom face of each specimen, the strain gauges were glued with CC-33A adhesive. Figure 25 reported the test, it was conducted under displacement control (displacement rate of 2 mm/min) ensuring that the specimen fracture occurs in approximately 100 s, in compliance with the guidelines outlined in EN 310 [106].

The modulus of elasticity E_m and the bending strength $were\sigma_m$ was calculated following EN 310 [106]. E_m was calculated according to Eq. 11:

$$E_m = \frac{l_1^3 (F_2 - F_1)}{4bt^3 (a_2 - a_1)} \tag{11}$$

where l_1 is the distance between the supports, b is the width of the test piece, t is the thickness of the test specimen (all expressed in millimeters). F_1 and F_2 are the loads at 10% and 40% of the maximum load expressed in Newton, a_1 and a_2 are the deflection at the mid-length of the specimen corresponding to F_1 and F_2 .

The bending strength is expressed according to Eq. 12:

$$\sigma_m = \frac{3F_{max}l_1}{2ht^2} \tag{12}$$

where F_{max} is the maximum load expressed in Newton.

4.2.4 Results

4.2.4.1 Physical and mechanical properties

Table 20 reports the average and standard deviation of thickness swelling, surface soundness and internal bond for the specimens.

Table 20. Average values and standard deviations for thickness swelling 2 h (TS 2 h), surface soundness and Internal bond (IB) for all specimens.

Specimens	TS 2 h [%]	Surface soundness [MPa]	IB [MPa]
A550	$11.78 (\pm 6.20)$	$0.72~(\pm~0.04)$	$0.31~(\pm~0.02)$
B550	$13.95 \ (\pm \ 0.44)$	$0.70~(\pm~0.26)$	$0.37~(\pm~0.11)$
C550	$13.41 (\pm 1.13)$	$0.71~(\pm~0.09)$	$0.36~(\pm~0.05)$
D550	$13.12 (\pm 1.44)$	$0.78~(\pm~0.20)$	$0.31~(\pm~0.01)$
E550	$14.16 \ (\pm \ 0.99)$	$0.54 (\pm 0.22)$	$0.33~(\pm~0.05)$
A680	14.66 (± 1.07)	$1.55~(\pm~0.17)$	$0.56~(\pm~0.08)$
B680	$14.20~(\pm~1.23)$	$1.71~(\pm~0.14)$	$0.38~(\pm~0.05)$
C680	$14.06~(\pm~0.98)$	$1.67 (\pm 0.18)$	$0.48~(\pm~0.04)$
D680	$12.24~(\pm~0.69)$	$1.81 \ (\pm \ 0.08)$	$0.34~(\pm~0.01)$
E680	$11.75~(\pm~0.54)$	$1.59 (\pm 0.23)$	$0.44 (\pm 0.09)$
A750	14.27 (± 1.18)	$1.24~(\pm~0.12)$	$0.38~(\pm~0.08)$
B750	$11.86 \ (\pm \ 0.98)$	$1.20~(\pm~0.08)$	$0.48~(\pm~0.07)$
C750	$10.73~(\pm~0.74)$	$1.13~(\pm~0.31)$	$0.57 \ (\pm \ 0.09)$
D750	$9.99 (\pm 2.00)$	$1.02~(\pm~0.22)$	$0.44~(\pm~0.03)$
E750	$11.31 (\pm 0.49)$	$0.86~(\pm~0.10)$	0.32 (± 0.11)

Figure 26 illustrates the trend of thickness swelling, surface soundness and internal bond concerning the quantity of AD and the densities of 550, 680 and 750 kg/m³.

For the density 550 kg/m³ the different percentages of AD in the core do not influence the value of Thickness swelling, surface soundness and Internal bond (Figure 26 (a), (b) and (c)).

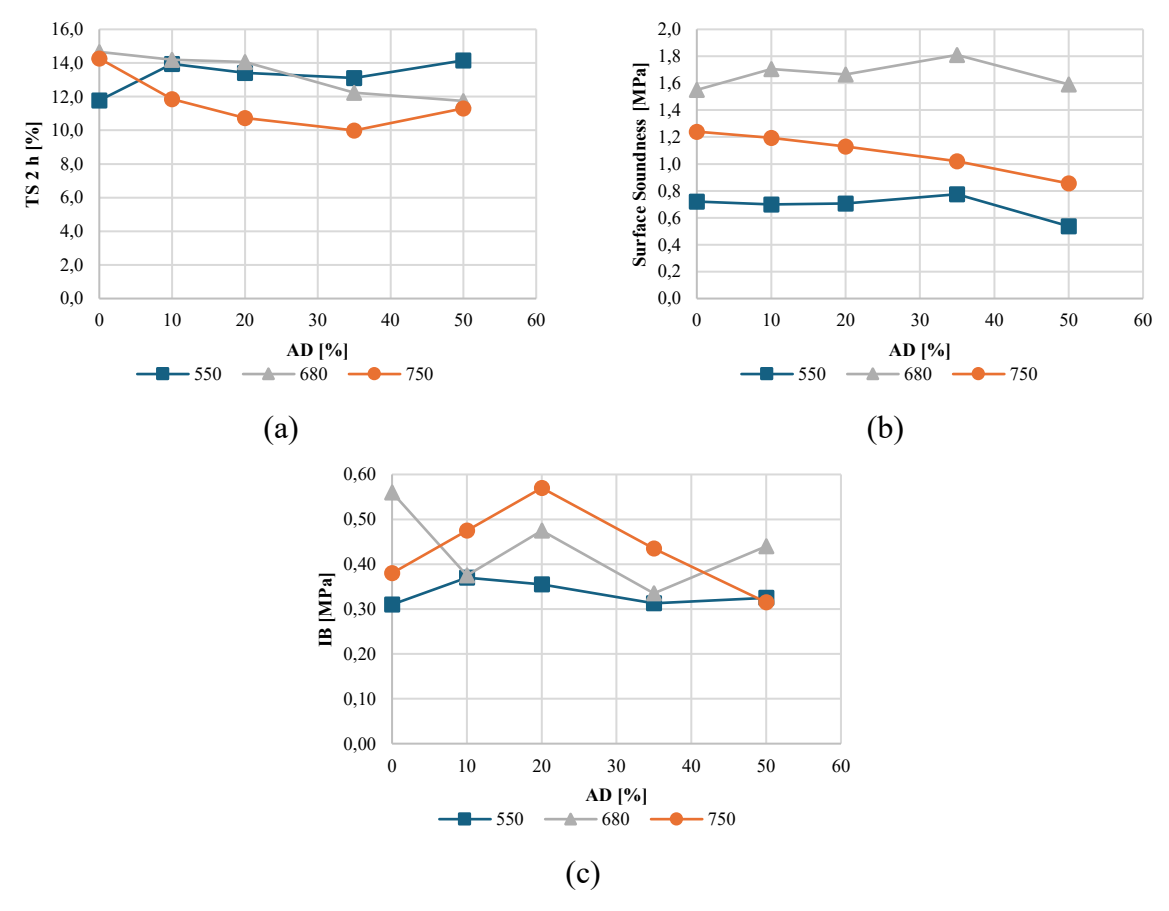


Figure 26. The trend of (a) Thickness swelling 2 h (TS 2 h), (b) Surface soundness and (c) Internal bond (IB), for the three densities and the variation of the quantity of AD in the core of the particleboard.

In the case of 680 kg/m³ density it was observed a slightly decreasing trend for the TS and IB (Figure 26 (a) and (c)) with the increment of the quantity of AD inside the core of the particleboard. Instead, the surface soundness remains constant, as shown in Figure 26 (b). Finally, the specimens with a density of 750 kg/m³ show a parabolic trend for the TS and the IB (Figure 26 (a) and (c)) with a minimum for the TS at 35 % of AD content and a maximum for the IB at 20 %. The surface soundness shows a decrease with the increase in the percentage of AD.

The reason why the 750 kg/m³ density exhibits a countertrend for the IB characteristic compared to the lower densities could be attributed to a better interconnection of the AD within the particleboard, resulting in improved adhesion to the resin due to increased compaction pressure.

4.2.4.2 Three-point bending test

Table 21 presents the mean values and standard deviations of the particleboard panels tested in the three-point bending test. As expected, the performances improve with increasing density.

Table 21. Average values and standard deviations in brackets for the maximum load, bending strength σ_m , Modulus of elasticity E_m and the density for the different types of particleboards.

Specimens	Maximum Load [N]	σ_m [MPa]	E _m [MPa]	Density [kg/m³]
A550	335.19 (± 35.79)	$5.43 \ (\pm \ 0.62)$	$980.27~(\pm43.94)$	538.1 (± 11.72)
B550	388.83 (± 31.46)	$6.29 \ (\pm \ 1.05)$	$1113.42 \ (\pm \ 144.49)$	577.4 (± 16.79)
C550	$373.71 \ (\pm \ 62.40)$	$5.23~(\pm~1.10)$	$901.19\ (\pm\ 70.98)$	$567.2 \ (\pm \ 20.86)$
D550	$398.28\ (\pm\ 105.90)$	$6.19 (\pm 1.89)$	$1077.31 \ (\pm\ 228.68)$	$560.8 \ (\pm \ 19.81)$
E550	335.19 (± 35.79)	$5.43~(\pm~0.62)$	$980.27~(\pm43.94)$	555.2 (± 20.40)
A680	896.07 (± 64.44)	$10.98 (\pm 0.60)$	1829.95 (± 192.65)	665.8 (± 24.66)
B680	$956.58 \ (\pm\ 82.67)$	$13.02 (\pm 1.13)$	$1866.32 (\pm 121.71)$	$675.6 (\pm 19.02)$
C680	$1070.48 \ (\pm \ 104.66)$	$14.20 \ (\pm \ 1.36)$	$1839.96 (\pm 179.20)$	$656.6 \ (\pm \ 20.15)$
D680	$1106.16 (\pm 67.41)$	$15.64 \ (\pm \ 0.68)$	$1937.52\ (\pm\ 197.23)$	$701.6 (\pm 16.58)$
E680	$724.97 \ (\pm \ 84.01)$	$9.35~(\pm~1.02)$	$1408.89\ (\pm\ 220.50)$	649,9 (± 32.18)
A750	1087.10 (± 164.55)	13.81 (± 2.02)	2131.20 (± 279.97)	720.1 (± 30.91)
B750	$1149.01 \ (\pm \ 43.58)$	$15.77~(\pm~0.44)$	$2401.80 \ (\pm \ 140.24)$	$746.3 \ (\pm \ 12.59)$
C750	$1158.71 \ (\pm\ 52.30)$	$15.66 \ (\pm \ 0.73)$	$2470.79 (\pm 104.26)$	$747.9 \ (\pm \ 10.89)$
D750	$1119.35 \ (\pm \ 91.27)$	$14.82 \ (\pm \ 1.42)$	$2282.68 \ (\pm\ 272.53)$	$730.6 \ (\pm\ 36.05)$
E750	$954.20 \ (\pm \ 21.57)$	$12.72~(\pm~0.30)$	$2042.62 \ (\pm \ 184.87)$	728.8 (± 31.68)

Figure 27 shows the trend of σ_m with the percentage of AD for the three different densities. At densities of 680 kg/m³ and 750 kg/m³, a parabolic trend is observed in the bending strength (σ_m) as the percentage of AD in the particleboards increases. The position of the peak is different for the two densities: for the specimens with a density of 750 kg/m³, the peak is reached for AD percentages between 10% and 20%, while for the specimens with a density of 680 kg/m³, the peak is reached for a percentage of 35%.

For the density 550 kg/m³, the bending strength σ_m curve exhibits a constant trend, meaning that the addition of AD does not lead to any variations in bending strength.

For all densities, with the addition of 50% AD content, the bending strength σ_m of the particleboards is lower than at 0% AD (Figure 27). This trend can be explained by the fact that AD exhibits better mechanical performance than recycled wood, and its chips are slimmer than those of recycled wood, which also enhances the mechanical properties of the panels [107, 96]. However, the outer surface of AD chips is very smooth [96] compared to the case of recycled wood where the roughness is significantly higher, this could lead to a reduction of the grip between the chips and the adhesive. Initially, an improvement in the mechanical properties of the particleboard is observed, particularly in flexural strength, due to the superior mechanical properties of AD compared to recycled wood. This results in an increase in bending strength (σ_m) up to a maximum level of AD content. Beyond this point, the positive effects of AD's superior mechanical properties are outweighed by the negative impact of reduced adhesion between the resin and AD, compared to the stronger adhesion between resin and recycled wood, leading to a decline in particleboard performance.

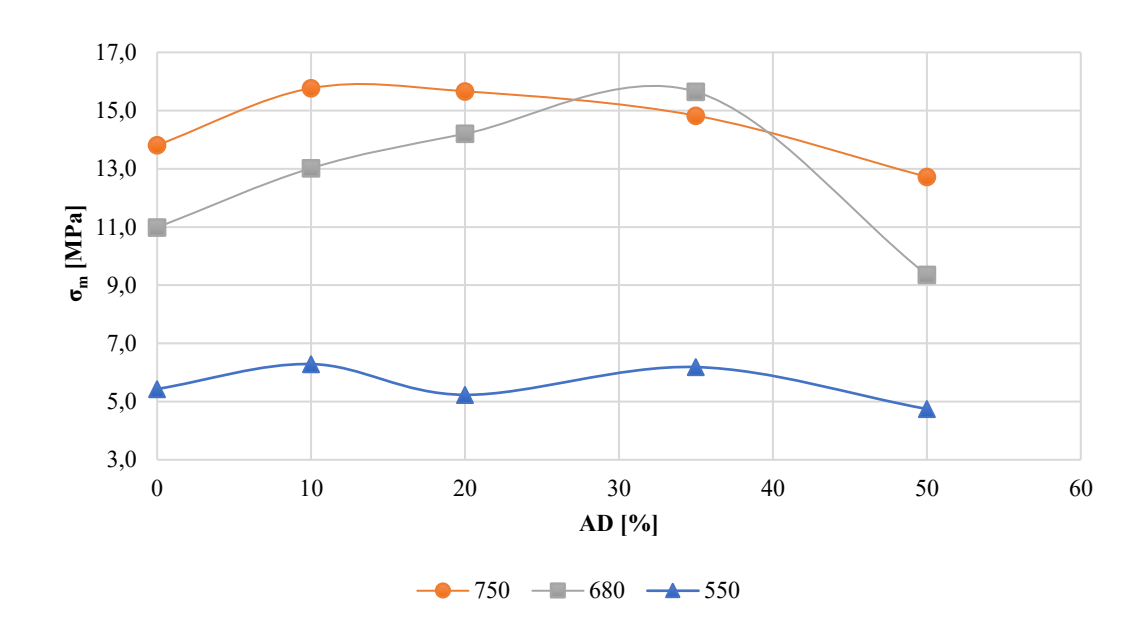


Figure 27. Bending strength (σ_m) of the particleboard over the quantity of AD in the core according to the density of the board.

Figure 28 shows the bending strength σ_m as a function of the density variation for each AD percentage. The curves show a linear trend in the case of 0% AD the trend becomes quadratic for 20% and 30% and returns linear at 50% of AD crops.

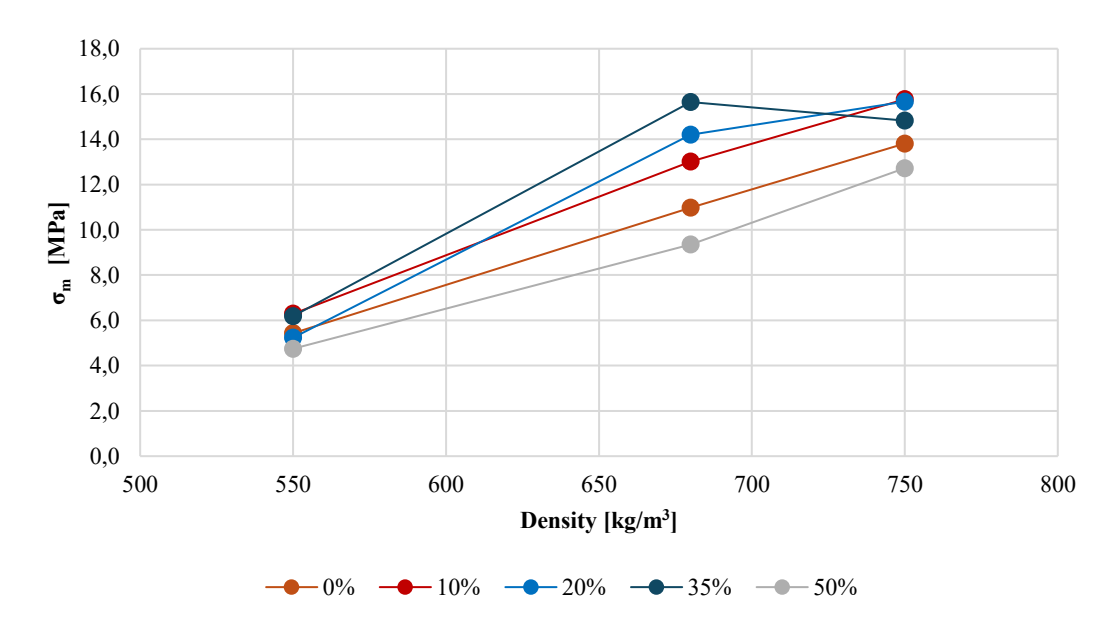


Figure 28. Bending strength (σ_m) of the particleboard over the Density of the board according to the percentages of AD in the core.

Adding AD chips to the core of the particleboard, in percentages ranging from 10% to 35% of the total, leads to an improvement in bending strength for densities of 680 and 750 kg/m³ compared to the 0% AD case. Conversely, at 50% AD, the particleboard properties are lower across all densities compared to the 0% case.

Figure 29 presents a response interpolated surface, a 3D curve illustrating how the output data of bending strength σ_m , change with two inputs: the density and the AD percentage inside the core on

the particleboard. It can be observed that there are two peak points of the surface, in which the surface is colored in yellow: one corresponds to the density of 750 kg/m³ and with 20% of AD in the core, and the second is associated with the density of 680 kg/m³ and with a 35% of AD in the core.

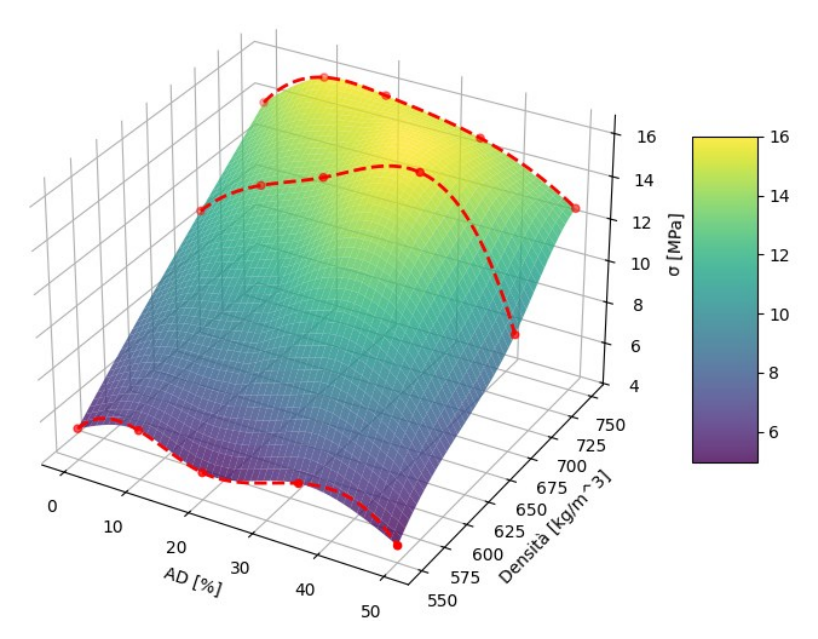


Figure 29. A response surface with two input variables, the density and the Arundo donax percentage and the output being the bending strength σ_m .

4.2.5 Discussion

A key objective of this study was to enhance the mechanical performance of recycled wood particleboard by maintaining the same density and resin while varying the core material, specifically by replacing recycled wood chips with AD chips. This improvement aimed to upgrade the particleboard's classification from P2 to P4. [76]. Class P4 is associated with load-bearing particleboards suitable for use in dry conditions. The properties considered for the comparison of the two classes of particleboards were: bending strength σ_m , modulus of elasticity Em, internal bond (tensile strength perpendicular to the plane of the particleboard).

Specimens with a density of 680 kg/m³ and AD content between 10 % and 35 % demonstrated an average bending strength σ_m that exceeds the minimum requirement associated with the P4 particleboard class, as shown in Figure 30 (a), where the red lines indicate the standard limits for the P2 and P4 particleboard classes. However, when considering the standard deviation, the specimen with 10 % AD does not meet the minimum requirements for P4 classification. Specimens with a density of 750 kg/m³ exhibit average bending strength σ_m values above the standard limit, except for those with an AD percentage of 50 %, Figure 30 (a).

Figure 30 (b) reported the average Modulus of elasticity E_m for all the specimens, in which the red lines represent the standard limits associated with the P2 and P4 classes of particleboard. As can be observed only the specimens with the density of 750 kg/m³ exceed the minimum standard requirement, except those containing 0 % and 50 % of AD.

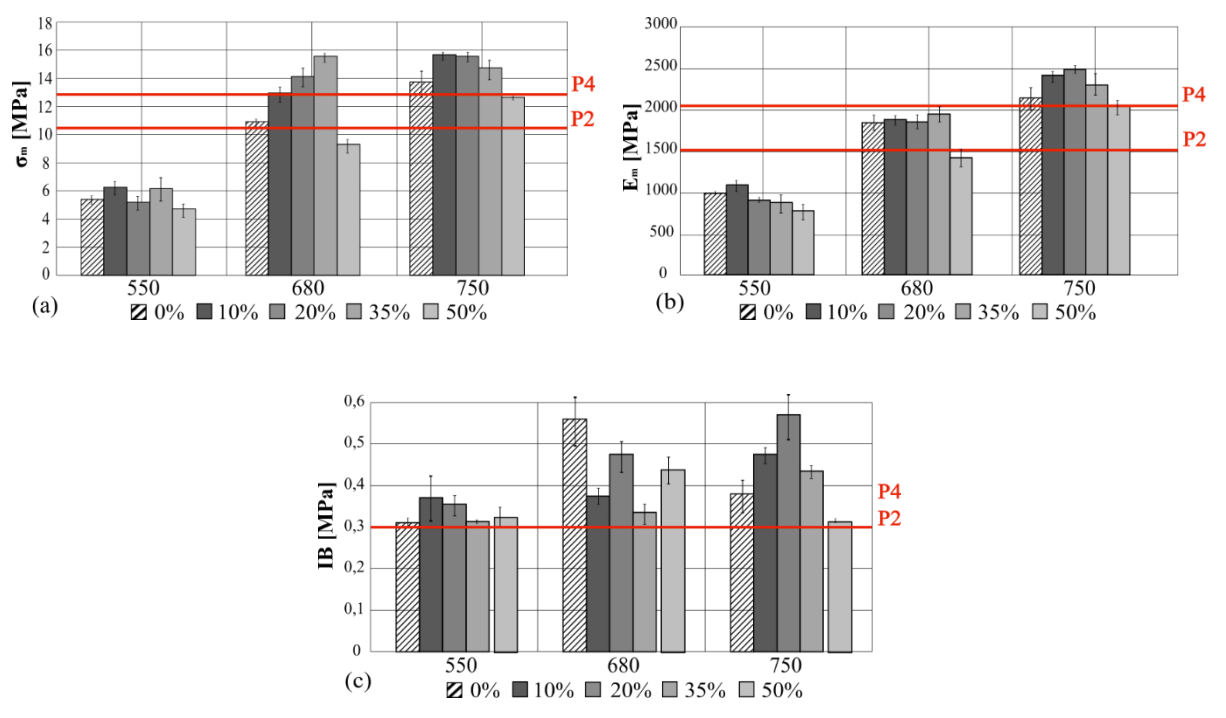


Figure 30. Comparison with normative limits for different types of particleboard panels for the following characteristics: (a) bending strength σ_m , (b) Modulus of elasticity E_m and (c) Internal bond (IB).

The threshold value for internal bond (IB) strength is set at 0.3 MPa, which applies to both P2 and P4 class particleboards, as illustrated in Figure 30 (c). Almost all specimens with densities of 680 kg/m³ and 750 kg/m³ exceed this limit.

Only the specimens with a density of 750 kg/m³ and the quantity of AD inside the core of 10%, 20% and 35% are suitable for the P4 class, considering also the standard deviation of the data.

In Table 20 the values of bending strength σ_m , Modulus of elasticity E_m and Internal bond (IB) obtained in this work were compared with those found in the literature regarding AD particleboard panels. Fernandez-Villena et al. [98] studied one-layer particleboards manufactured with a mixture of AD and wood. The resin that they used was urea formaldehyde, making it a very similar type of board compared to the one manufactured and characterized in the present study. Using 50% AD and 50% virgin wood, they obtained physical and mechanical values very similar to those obtained in the present study, as reported in Table 22.

The table reported below shows that the results obtained in this study are consistent with those from similar research both in mechanical and physical terms, which validates the work carried out here.

Table 22. Comparison of values of Modulus of rupture (MOR), Modulus of elasticity (MOE) and Internal bond (IB) of particleboard manufactured with Arundo donax or a mixture of Arundo donax and wood, found in literature and results obtained in this work.

Reference	Biomaterial	Binder	Density [kg/m³]	MOR [MPa]	MOE [MPa]	IB [MPa]
[16]	AD	Urea Formaldehyde	628-758	9.9-17.7	1468- 3026	0.258- 1.309
[96]	AD	Urea Formaldehyde	463-612	3.7-10-3	976-1362	\
[99]	AD	Phenol- Formaldehyde	\	\	1250- 3500	\
[34]	AD	Binderless	735-913	10.5-14.2	1378- 2052	0.58-1.12

[33]	AD	Non-modified starches	812-932	3.2-16.7	569-2521	0.04-0.4
[98]	AD and Wood	Urea Formaldehyde	631-850	8-19	900-2100	0.45-1.5
Present work	AD and recycled	Urea Formaldehyde	538-748	5.2-15.8	901-2471	0.31-0.57

This first Wave analyzed the physical and mechanical properties of a sandwich particleboard, consisting of three layers. The outer layers are made of recycled wood and urea formaldehyde, while the inner layer is composed of a mix of recycled wood and AD in varying quantities, along with urea formaldehyde. The particleboards were tested for thickness swelling, internal bond, surface soundness and three-point bending.

The conclusions achieved are reported below:

- 1. The study revealed a linear relationship between density and the bending properties such as bending strength σ_m and Modulus of elasticity E_m of the particleboards. Higher densities enhance the interconnection between the chips and improve adhesion between the resin and AD chips. Since AD has a smoother outer surface [108] compared to wood, achieving stable resin adhesion is more challenging at lower densities. However, increasing the compaction pressure enhances this bond.
- 2. It was observed that at low densities (550 kg/m³) there are no significant changes in mechanical properties with changing the amount of AD inside the core of the particleboard. This is due to a combination of two factors.
- 3. The optimal quantity of AD chips to be incorporated into the core of the particleboard, which results in the best mechanical performance, varies slightly with the density of the particleboard. Specifically, as the density increases, the ideal amount of AD for the bending properties decreases from 20 % to 35 % of the total chips in the inner layer. Across all examined densities, there was a significant decline in mechanical properties once the AD content reached 50%, indicating that beyond a certain threshold, additional AD leads to a reduction in mechanical properties, as mentioned in point 1.
- 4. Thickness swelling (TS) tests have shown that the addition of AD except at a density of 550 kg/m³, reduces particleboard TS and shows a positive effect of the material on the particleboard's water resistance. Since TS is primarily due to fine particle size found in the outer layers of the particleboard where no material changes were made (no AD chips added), the increase in water resistance that AD could provide would likely be greater if the material were also used in the outer layers.
- 5. The 750 kg/m³ density particleboards with AD content ranging from 10% to 35% (considering standard deviation) ensured a class transition from P2 to P4 meaning a change of intended use from non-structural to structural (The 0% AD content do not exceed the threshold Young's modulus E_m value of 2050 MPa, considering the standard deviation of the data).

4.3 Wave 2

During Wave 2, the study focused on the effect of the shape and size of AD particles used for the substitution of recycled wood on the mechanical properties of the particleboard.

In the literature, numerous studies focus on wood chips, but there is no consensus on how wood particle size affects the properties of the panel.

In the study by Flores et al. [96] it was shown that increasing the slenderness ratio (length/thickness) improves the MOE and MOR of particleboard. The best results were obtained using the 2 mm and 4 mm sieves, indicating that medium-sized particles produced the most favourable outcomes, while the largest particles (8 mm) had negative results. García Esteban et al. [109] reached the same conclusion defining an optimal slenderness ratio range between 90 and 125, which significantly influences the

mechanical properties of particleboard. Similar findings were reported by Semple and Smith [110], as well as by Arabi et al. [111].

Benthien et al. [112] observed an increase in the material's mechanical properties with larger wood particle sizes. The research highlights that, as particle size increases, there is a decrease in the total surface area of a particle sample of equal mass, leading to an increase in the surface-specific adhesive quantity and, consequently, improved board properties. Thus, the improvement in the mechanical properties of particleboard observed with increasing wood particle size is not linked to slenderness but rather to the presence of a greater amount of resin related to the surface area of the chips.

In the study conducted by [101], adding fine particles to the core of a particleboard, replacing coarse particles, did not result in any statistically significant changes in the mechanical characteristics of the particleboard. This finding contradicts the trend observed in previous studies.

4.3.1 Materials

Part of the recycled wood chips was replaced with AD chips only in the core of the particleboard, using the percentages of substitution of 20 % and 35 % that yielded the best results in Wave 1. The materials used, such as AD, recycled wood and resins were the same as those used in Wave 1, please refer to paragraph 4.2.1 for an exhaustive list.

Different particleboard panels were manufactured by varying the percentage of AD in the core layer and the particle size of AD chips. Table 23 includes all specimen types produced and the notation followed hereinafter.

<i>Table 23.</i>	Types	of particleboard	panels.
------------------	-------	------------------	---------

Nomenclature	AD	AD Fractions	AD Fractions retained on the sieves			
of the panel	[%]	0.50 mm	1.00 mm	2.00 mm	4.00 mm	
A0	0					
B20	20	50%	50%			
B35	35	50%	50%			
C20	20		100%			
C35	35		100%			
D20	20		50%	50%		
D35	35		50%	50%		
E20	20			100%		
E35	35			100%		
F20	20		33%	33%	33%	
F35	35		33%	33%	33%	

The preparation of the AD chip is the same as that followed in Wave 1, as detailed in Section 3.2.2. The particleboards were designed to have a density ranging between 680 kg/m³ and 750 kg/m³, which is the commonly used range of the company and has shown excellent results in Wave 1. The resin percentage type and particle size distribution of the recycled wood were kept constant and identical to those used by the company. Additionally, the external layers were not modified in this phase.

To understand the effect of the particle size and geometry on the physical-mechanical properties of particleboard the slenderness (length/thickness) and aspect ratio (length/width) of the chips are measured. According to the literature [107, 96, 113] optimal values for the slenderness ratio range between 90 and 12. The dimensions of the particles were measured using an optical microscope Olympus SZX10, followed by an analysis of the images using AutoCAD 2023 software.

4.3.2 Methods

The production process for the particleboard is the same as that followed in Wave 1, as is the particleboard structure (details in Section 3.2.2).

A particle size analysis was performed on AD and recycled wood particles from the core of the sandwich particleboard. A manual method was used to achieve a three-dimensional characterization of each particle by capturing two optical microscope images, which were then processed in AutoCAD. The first image measured the length and width of each particle, while the second image, taken from a side perspective, provided the thickness measurement. This method enabled essential three-dimensional characterization, particularly important for non-cylindrical particles like these, where the width is about three times the thickness. For each sieve fraction, 100 randomly selected particles of both recycled wood and AD were examined.

From these measurements, two dimensionless values were derived: the slenderness ratio (length/thickness) and the aspect ratio (length/width), which, as noted in various studies, affect the mechanical properties of particleboard [107, 113, 96].

For Wave 2, the same tests as Wave 1 were followed, with the addition of the water absorption test. The water absorption test followed the same methodological procedure as the swelling test, with the only difference being to monitor the specimen's weight instead of its thickness. Formula (9) was adapted replacing t with p (specimen weight).

$$G_p = \frac{p_2 - p_1}{p_1} 100 \tag{13}$$

where p_1 is the weight of the test piece before immersion expressed in grams, t_2 is the weight of the test piece after immersion, also expressed in grams.

In summary, Table 24 reports the performed tests, the number and dimensions of the specimens and the reference standard [102].

Table 24. Type of tests carried out, standard associated to each test, number and dimensions of the specimens required for the physical-mechanical tests.

Test	Normative	Number of Specimens	Dimensions of specimen [mm]
Swelling in Thickness	EN 317 (1993)	8	50 x 50 x 22
Water absorption	EN 317 (1993)	8	50 x 50 x 22
Surface soundness	EN 311 (2002)	8	50 x 50 x 22
Internal Bond	EN 319 (1993)	8	50 x 50 x 22
Three-point bending	EN 310 (1993)	6	300 x 50 x 22

The data were statistically analyzed using the ANOVA method (Analysis of Variance) to evaluate whether the means of the measured mechanical properties of the composite material were significantly different from each other. For each test, a probability (Pr) was calculated, and the difference between means is considered significant when the Pr is less than 0.05. The method was implemented using Minitab v.18 software [114].

4.3.3 Results

4.3.3.1 Geometric study of chips

The AD particles were shredded using a mechanical hammer shredder and then sieved to match the same particle size distribution as the recycled wood particles used in the particleboard core. Figure 31 shows the recycled wood particles within the board's core, while Figure 32 displays the AD chips across various particle size distributions. As can be seen from the figures below, the AD has a particle size distribution that includes an additional range compared to wood, specifically 4 < d < 8 mm. This is because the company does not use chips greater than 4 mm for the production of its particleboard.

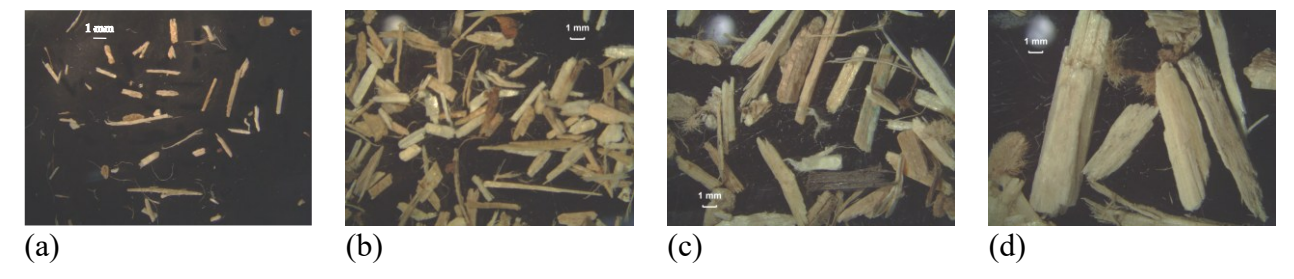


Figure 31. Size of particles of sieve-fractionated particles of wood recycled chips: (a) d < 0.5 mm; (b) between 0.5 < d < 1 mm; (c) between 1 < d < 2 mm; (d) between 2 < d < 4 mm.

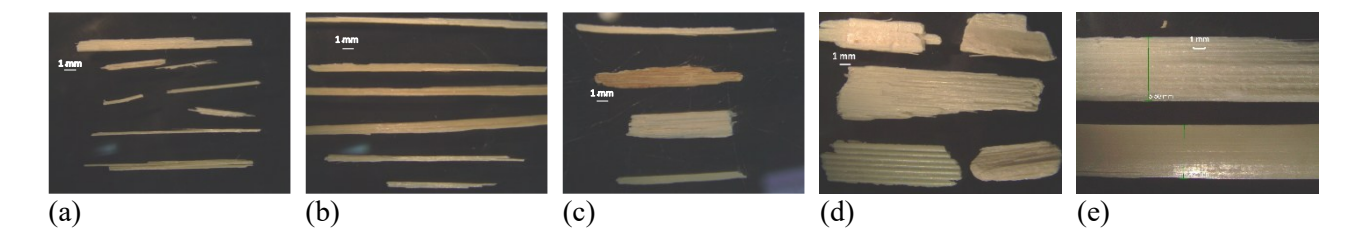


Figure 32. Size of particles of sieve-fractionated particles of Arundo donax chips: (a) d < 0.5 mm; (b) between 0.5 < d < 1 mm; (c) between 1 < d < 2 mm; (d) between 2 < d < 4 mm; (e) between 4 < d < 8 mm.

The mean values with their respective standard deviations for the slenderness ratio (length/thickness ratio) and aspect ratio (length/width ratio) for the recycled wood chips and AD are reported in Table 25.

Table 25. Average values and standard deviations for slenderness ratio (SR) and aspect ratio (AR), for Arundo donax and recycled wood.

Material	Sieve-fractionated Particle [mm]	Average length of the particles [mm]	SR	AR
	d < 0.5	5.54 (±2.1)	39.84 (±19.65)	12.85 (±6.34)
	0.5 < d < 1	9.75 (±4.4)	64.31 (±38.51)	20.74 (±12.42)
AD	1 < d < 2	$11.55 (\pm 6.6)$	65.04 (±58.13)	$20.98 \ (\pm 18.75)$
	2 < d < 4	24.31 (±14.9)	41.26 (±38.11)	13.31 (±12.29)
	4 < d < 8	27.47 (±18.46)	46.43 (±71.43)	14.98 (±23.04)
	d < 0.5	1.98 (±1.1)	18.97 (±12.80)	6.12 (±4.13)
Dagwalad wood	0.5 < d < 1	$3.27 (\pm 1.6)$	$16.46 (\pm 11.28)$	5.31 (±3.64)
Recycled wood	1 < d < 2	5.05 (±2.6)	$16.31\ (\pm 10.40)$	5.26 (±3.35)
	2 < d < 4	12.79 (±5.8)	14.92 (±7.53)	4.81 (±2.43)

Figures 33 and 34 illustrate the trends of the slenderness ratio (SR) and aspect ratio (AR) for AD and recycled wood, providing a better understanding of the results and their relationship with particle size.

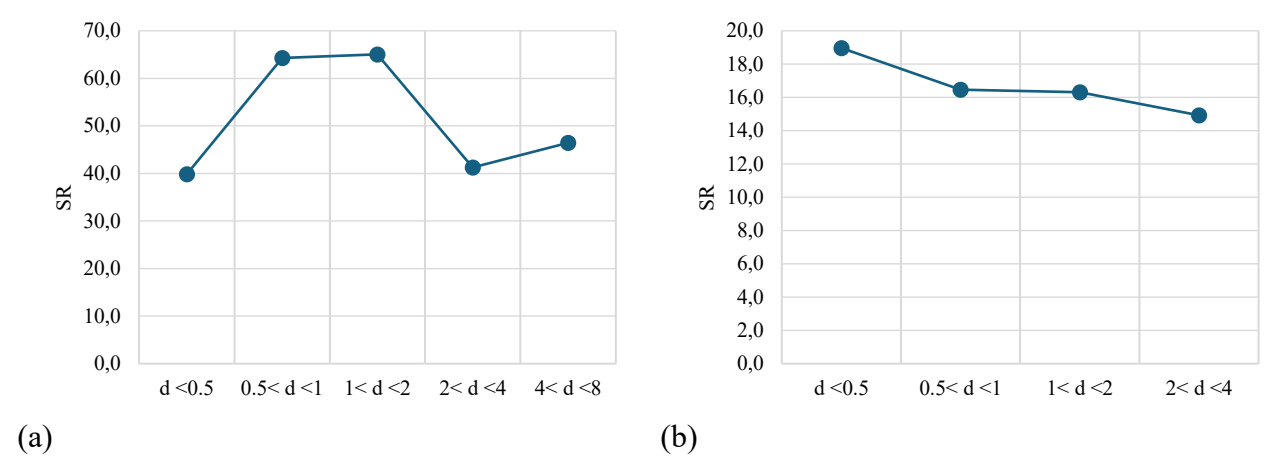


Figure 33. Trend of Slenderness Ratio (SR) with the granulometry for: (a) Arundo donax and (b) recycle wood.

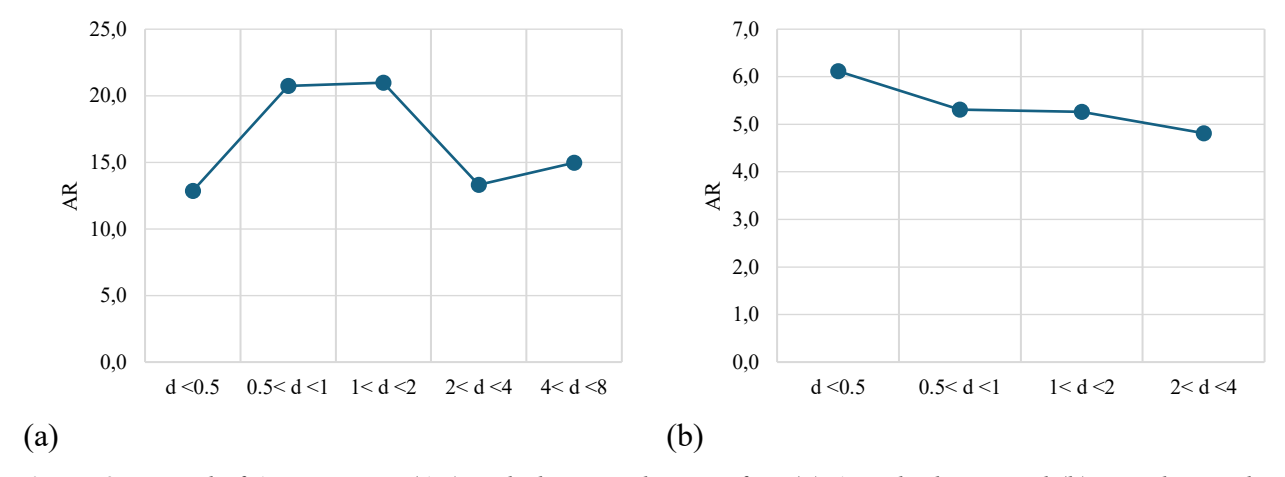


Figure 34. Trend of Aspect Ratio (AR) with the granulometry for: (a) Arundo donax and (b) recycle wood.

The first observation easily visible from Figures 33 and 34 is that the geometric characteristics of the particles of AD are much more spread compared to those of recycled wood, which shows homogeneity in the results. AD exhibits higher values of slenderness ratio (SR) and aspect ratio (AR) for intermediate particle sizes, specifically 0.5 < d < 1 and 1 < d < 2 with values almost double those of the other particle sizes.

Another important consideration is that the particles of AD are significantly more slender than those of wood. This was already easily verifiable through a visual inspection of the particles (Figures 31 and 32). The slenderness ratio (SR) for AD ranges from 39.84 to 64.31, while for wood it ranges from 14.92 to 18.97.

This data, which aligns with a portion of the existing literature [110, 111, 109, 96], confirms the increase in mechanical resistances observed in Wave 1 following the addition of AD. Higher values of SR and AR should correspond to greater values of MOR, MOE and IB. From this, it can be inferred that intermediate particle sizes of AD should ensure the best mechanical performance of the particleboard overall.

Once the mean and standard deviation of the SR and AR ratios were obtained for the various particle sizes of AD, it was decided to calculate the mean and standard deviation of SR and AR for the different combinations of AD particle sizes used to produce the various types of particleboard panels, as shown

in Table 23. The combined mean and combined standard deviation were subsequently calculated and are reported in Table 26.

Table 26. Average values and standard deviations for slenderness ratio (SR) and aspect ratio (AR) for the different particles of the AD used for the different types of particleboard.

Nomenclature	Fractions re	ractions retained on the sieves				AR
of the panel	0.50 mm	1.00 mm	2.00 mm	4.00 mm	– SR	AK
B20	50 %	50 %			65.19	21.03
B35	50 %	50 %			(± 49.28)	(± 15.90)
C20		100 %			66.08	21.13
C35		100 %			(± 58.09)	(± 18.74)
D20		50 %	50 %		53.67	17.31
D35		50 %	50 %		(± 49.13)	(± 15.85)
E20			100 %		41.26	13.31
E35			100 %		(± 38.11)	(± 12.29)
F20		33.3 %	33.3 %	33.3 %	51.25	16.53
F35		33.3 %	33.3 %	33.3 %	(± 57.53)	(± 18.56)

Figures 35 (a) and (b) show a graphical representation of the data reported in Table 26, of the slenderness ratio (SR) and aspect ratio (AR) of the different particleboards.

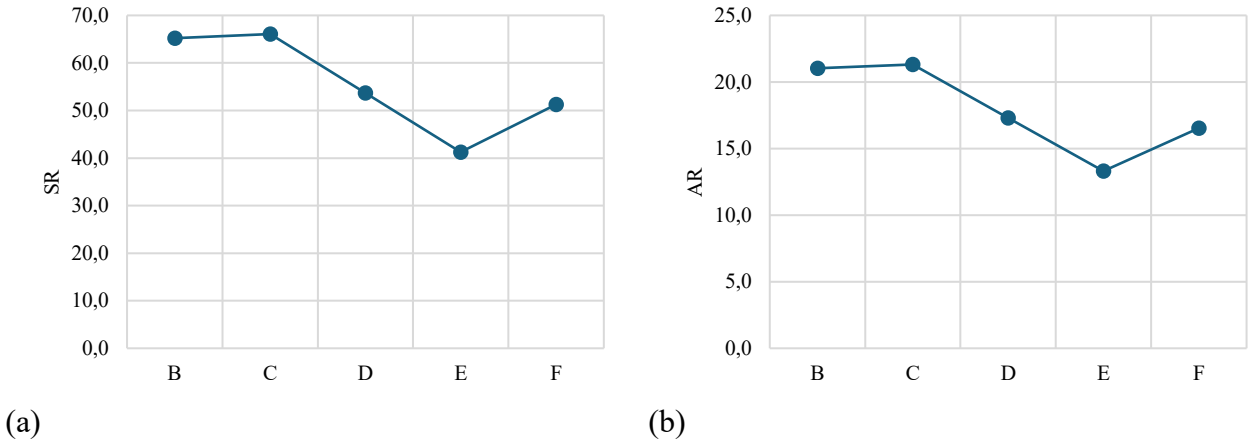


Figure 35. (a) Slenderness Ratio (SR) and (b Aspect Ratio (AR) AD for the different groups of particleboards.

The panels showing the best slenderness results in terms of AD are those belonging to types B and C.

4.3.3.2 Physical and mechanical properties

Table 27 reports the average and standard deviation of density, thickness swelling, water absorption, surface soundness and internal bond for the specimens.

Table 27. Average values and standard deviations for density, thickness swelling 2 h (TS 2 h), water absorption 2 h (WA 2 h), surface soundness and internal bond.

	Density [kg/m³]	TS 2 h [%]	WA 2 h [%]	Surface soundness [MPa]	IB [MPa]
A0	793.0 (± 18.03)	12.47 (± 1.43)	39.39 (± 3.68)	$1.06~(\pm~0.27)$	$0.45~(\pm~0.08)$
B20	$691.0\ (\pm\ 17.60)$	15.77 (± 1.61)	$62.52 (\pm 2.43)$	$0.45~(\pm~0.36)$	$0.16~(\pm~0.02)$
B35	691.0 (± 16.71)	13.37 (± 1.53)	59.10 (± 3.59)	$0.83~(\pm~0.03)$	$0.38 \ (\pm \ 0.10)$
C20	753.0 (\pm 22.47)	$12.04 (\pm 1.06)$	$46.48 \ (\pm \ 3.65)$	$1.23~(\pm~0.03)$	$0.48~(\pm~0.06)$
C35	$706.0 \ (\pm \ 19.38)$	11.94 (± 1.71)	$53.39 (\pm 7.90)$	$0.86~(\pm~0.26)$	$0.28~(\pm~0.10)$
D20	$665.0 \ (\pm\ 22.28)$	17.01 (± 3.65)	64.72 (± 12.41)	$0.87 (\pm 0.45)$	$0.30 \ (\pm \ 0.07)$
D35	781.0 (± 31.31)	$10.94 (\pm 0.66)$	$40.58 \ (\pm \ 4.48)$	$0.57 (\pm 0.12)$	$0.28 \ (\pm \ 0.05)$
E20	691.0 (± 25.98)	14.93 (± 1.69)	$68.57 (\pm 10.99)$	$0.15~(\pm~0.11)$	$0.14 (\pm 0.03)$
E35	746.0 (\pm 27.37)	13.21 (± 2.10)	$47.45~(\pm~4.95)$	$0.72~(\pm~0.33)$	$0.21~(\pm~0.07)$
F20	678.0 (± 17.94)	$12.17 (\pm 0.43)$	$60.60~(\pm~8.08)$	$0.64 (\pm 0.20)$	$0.22 (\pm 0.02)$
F35	684.0 (± 22.79)	14.28 (± 1.95)	55.97 (± 7.73)	$0.84~(\pm~0.26)$	$0.25~(\pm~0.03)$

For a better representation of the results reported in Table 36, the same data are presented in Figure 36 where the black dashed line indicates the value of A0, the reference specimen which corresponds to the panel without any modification.

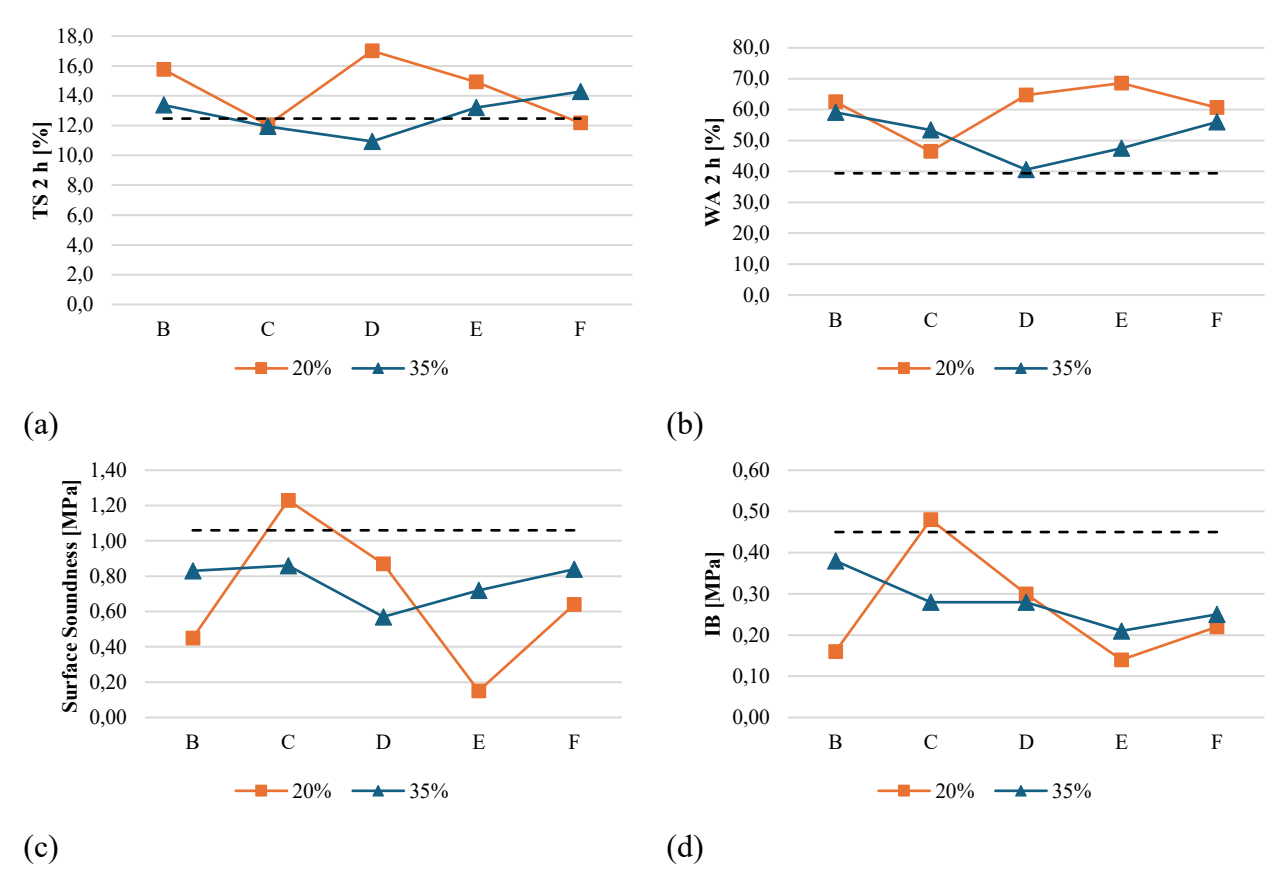


Figure 36. Trend of average values for (a) thickness swelling 2 h (TS 2 h), (b) water absorption 2 h (WA 2 h), (c) surface soundness and (d) Internal bond (IB), for 20 % (orange line) and 35 % (blue line) of AD content. The black dot line represents the value of the specific physical-mechanical property associated with the A0 specimen.

As can be observed from the graphs in Figure 36, no trend is evident with respect to the variation in the granulometry of AD chips in the core of the panel. This applies to all four properties studied. To confirm this the ANOVA (Analysis of Variance) method was employed. Box plots are reported in Figures 37 and 38 for the physical and mechanical properties: thickness swelling, water absorption, surface soundness and Internal bond (IB). On each box, the red line is set at the median value, while the bottom and top edges of the box indicate, respectively, the 25th and 75th percentiles; the black whiskers extend to the most extreme data points which are not considered outliers, while the outliers are plotted individually using a red cross marker.

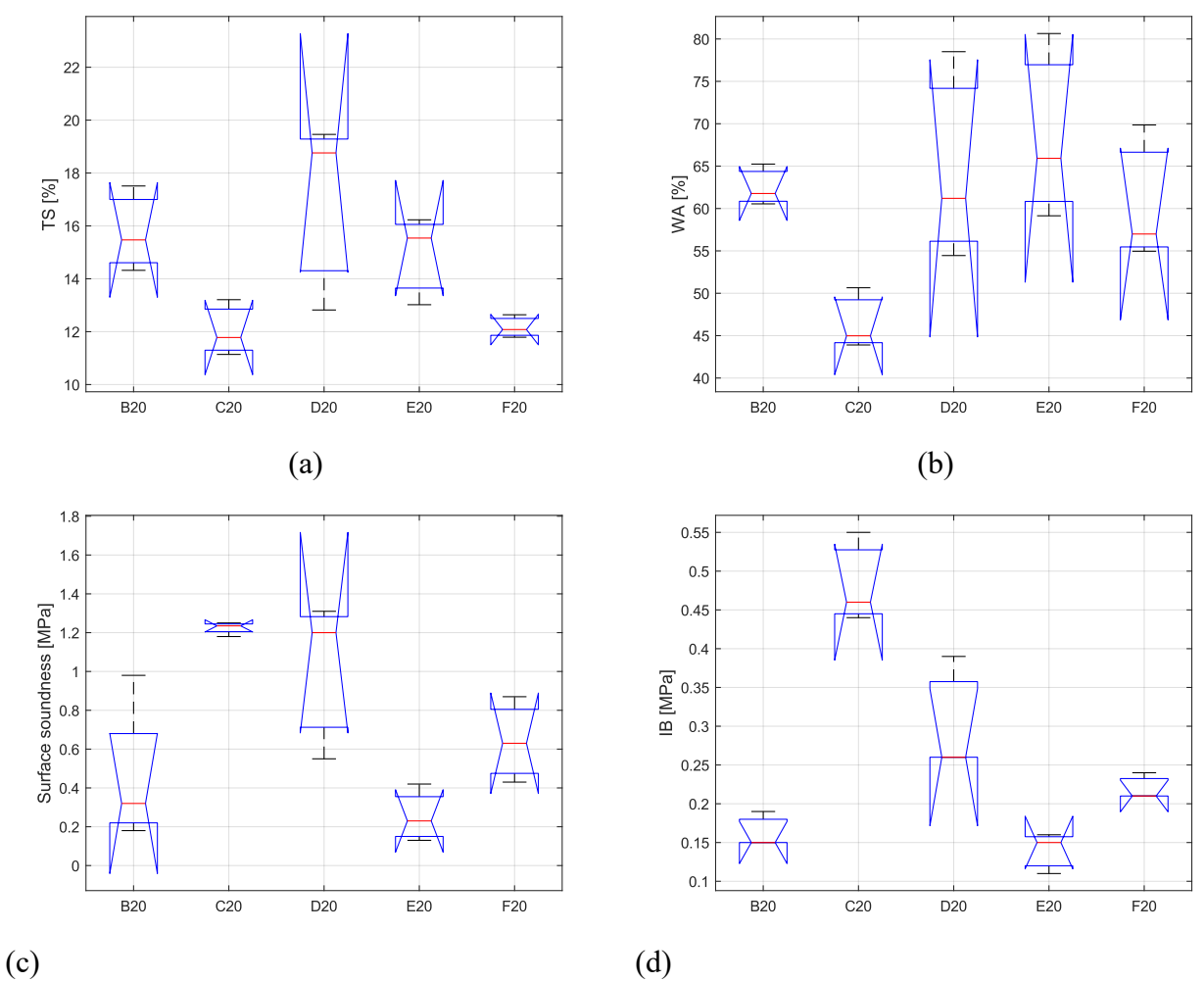


Figure 37. Box plots for the 20 % AD content, for physical and mechanical properties: (a) Thickness swelling 2 h; (b) Water absorption 2 h; (c) Surface soundness; (d) Internal bond.

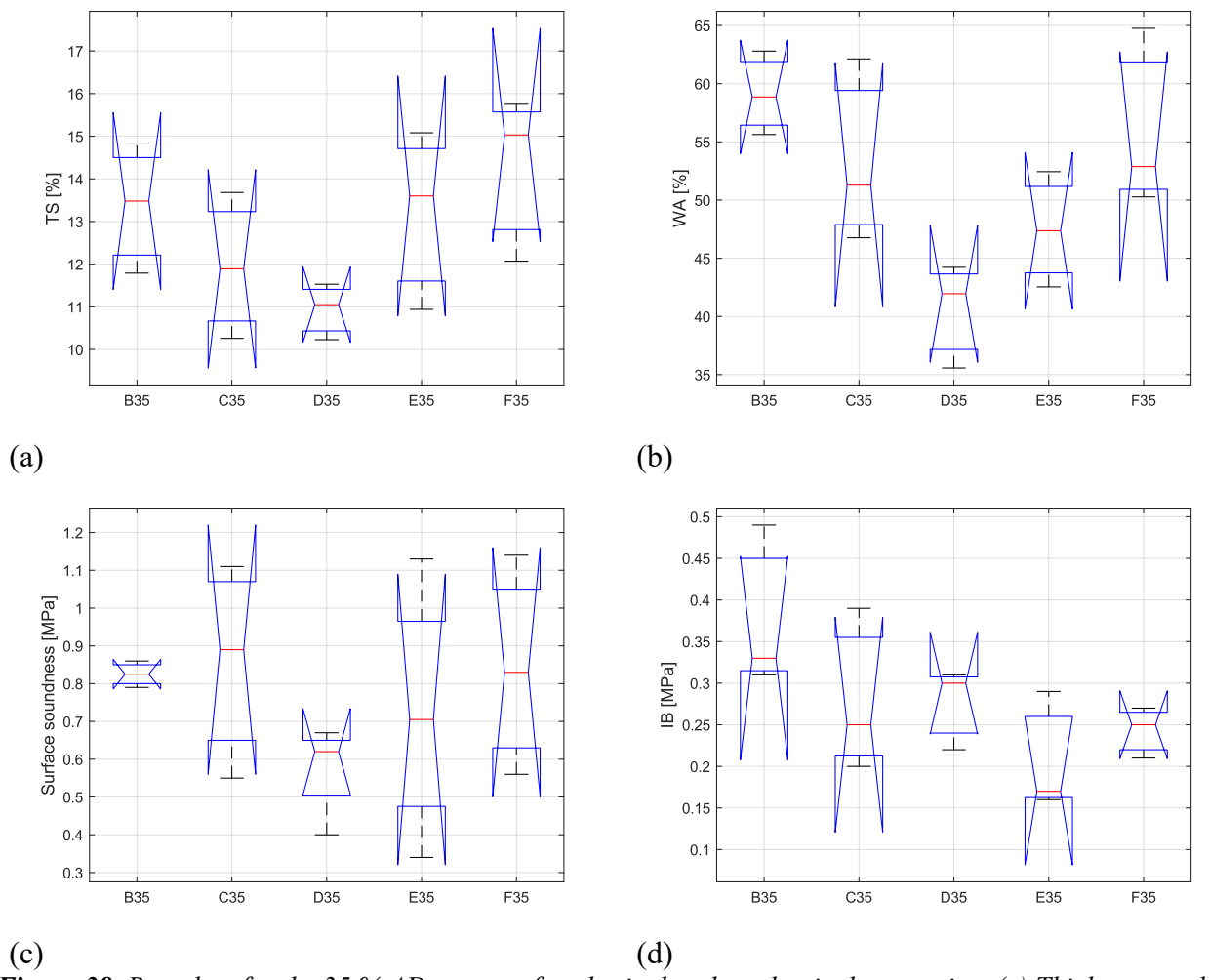


Figure 38. Box plots for the 35 % AD content, for physical and mechanical properties: (a) Thickness swelling 2 h; (b) Water absorption 2 h; (c) Surface soundness; (d) Internal bond.

Table 28 presents the outputs of the ANOVA test for the physical-mechanical properties under study. In the table:

- SS indicates the *Sum of Squares* between groups, representing the variability in the data due to differences between group means.
- **d.f.** indicates the *Degrees of Freedom* between groups.
- **MS** represents the *Mean Square* between groups.
- F is the ratio between the variability between groups and the variability within groups. The higher the F-value, the greater the variability between groups compared to within-group variability.
- **p** represents the probability of observing an F-value equal to or greater than the calculated value. If p is less than 0.05, it indicates that at least one group has a mean significantly different from the others.

Table 28. Test ANOVA for the results of the tests.

Quantity of AD [%]	Factor	Properties	SS	d.f.	MS	F	p
		TS 2 h [%]	58.51	4	14.628	3.64	0.04430
		WA 2 h [%]	847.88	4	211.971	2.95	0.07520
20	Granulometric size of AD	Surface soundness [MPa]	2.48	4	0.619	9.54	0.00060
	•	IB [MPa]	0.23	4	0.058	27.27	0.00002
		TS 2 h [%]	20.65	4	5.162	1.86	0.19470
	Granulometric size of AD	WA 2 h [%]	650.19	4	162.549	4.53	0.02410
35		Surface soundness [MPa]	0.22	4	0.055	1.07	0.40720
		IB [MPa]	0.05	4	0.012	2.14	0.14970

From Table 28 it can be observed that in the case of using 20 % of AD, there is a statistically significant difference between the groups of specimens studied, indicating that the granulometry of AD is an influential factor for these variables, particularly regarding surface soundness and internal bond. From Figure 37 the specimens showing the best performance in term of surface soundness and internal bond are those of C20, where the fraction retained on the 1 mm sieve was 100 % of the AD chips meaning the chips passed through the 2 mm sieve and were retained on the 1 mm sieve. Another series of specimens that performed well were the D20 specimens. However, no trend is observed in the properties as the granulometry of AD particles increases.

In the case of using 35 % AD, no statistically significant difference is observed between the groups of specimens studied, as seen in the table where the p-values are greater than 0.05 for all properties except for WA. Therefore, increasing the amount of AD results in a loss of its granulometry's influence on the panel properties.

4.3.3.3 Three-point bending test

Table 29 presents the mean values and standard deviations of the particleboard panels tested in the three-point bending test. In the post-processing phase, specimens whose density differed by \pm 10 % from the reference density (680 kg/m³) were not considered.

Table 29. Average values and standard deviations in brackets for the maximum load, bending strength σ_m , Modulus of elasticity E_m and the density for the different types of particleboards.

Particleboards	Maximum Load [N]	σ_m [MPa]	E _m [MPa]	Density [kg/m³]
A0	846.09 (± 118.92)	11.99 (± 1.78)	1752.13 (± 182.61)	683.37 (± 18.27)
B20	$844.67 \ (\pm \ 91.64)$	$14.72 \ (\pm \ 1.55)$	$1739.12 (\pm 146.77)$	732. 83 (± 19.35)
B35	$850.93~(\pm~80.94)$	$12.28 (\pm 1.06)$	$1617.63 \ (\pm \ 98.96)$	683.50 (± 16.45)
C20	759.34 (± 108.25)	$10.73~(\pm~1.34)$	$1536.62 (\pm 133.31)$	668. 49 (± 15.89)
C35	820.55 (± 131.53)	$13.80 \ (\pm \ 2.21)$	$2058.37 \ (\pm\ 287.88)$	666. 50 (\pm 14.67)
D20	$877.86 \ (\pm\ 101.25)$	12.91 (± 1.47)	$1602.86 \ (\pm\ 207.45)$	694.59 (± 18.34)
D35	$789.06 \ (\pm\ 76.80)$	$11.74 (\pm 1.35)$	$1521.37 \ (\pm\ 333.03)$	$707.38 \ (\pm \ 20.99)$
E20	984.64 (± 93.04)	$15.64 (\pm 1.38)$	2284.30 (± 198.61)	707.31 (± 18.62)

E35	$676.92 \ (\pm\ 282.85)$	$10.96 \ (\pm \ 0.85)$	$1485.51 \ (\pm \ 138.96)$	$667.42 \ (\pm \ 23.73)$
F20	$752.16 \ (\pm\ 52.58)$	$10.29~(\pm~0.72)$	$1431.02 \ (\pm \ 140.71)$	671.69 (± 17.54)
F35	$903.38 (\pm 84.45)$	$12.01 (\pm 1.10)$	1513.93 (± 115.38)	657.98 (± 14.65)

Figure 39 shows the trend of (a) Bending strength (σ_m) and (b) Modulus of elasticity (E_m) for the percentage of AD of 20 % (orange line) and 35 % (blue line), while the black dot line represents the value of the associated with the A0 specimen.

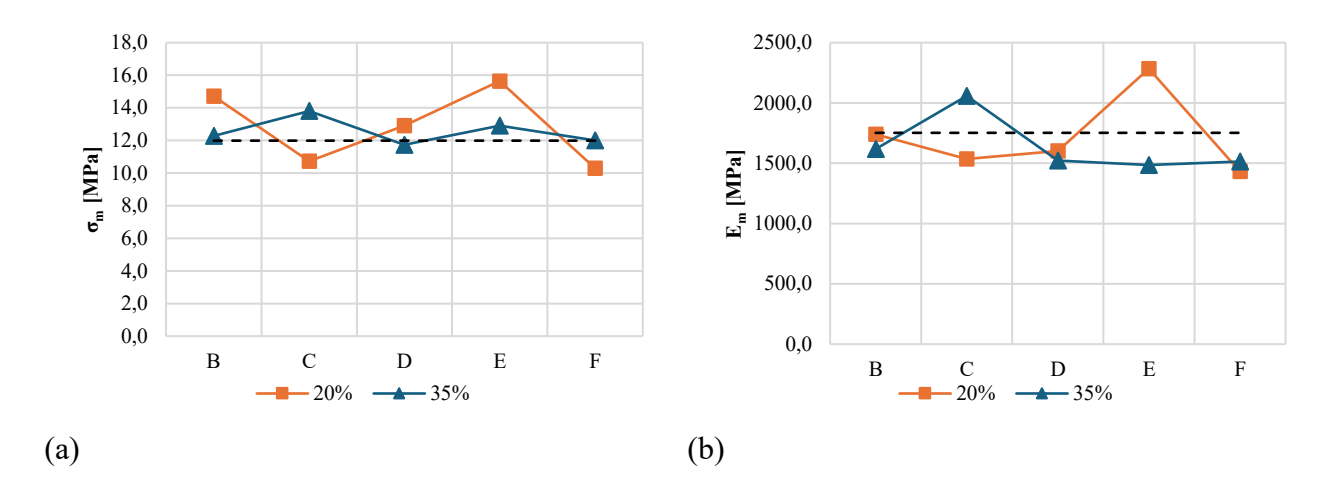


Figure 39. (a) Bending strength (σ_m) and (b) Modulus of elasticity (E_m) for 20 % (orange line) and 35 % (blue line) of Arundo donax content. The black dot line represents the value of the specific physical-mechanical property associated with the A0 specimen.

In Figures 39 (a) and (b) no trend is evident with respect to the variation in the granulometry of AD chips in the core of the panel. To confirm this the ANOVA (Analysis of Variance) method was employed.

Box plots are reported in Figures 40 and 41: (a) Bending strength (σ_m) ; (b) Modulus of elasticity (E_m) . On each box, the red line is set at the median value, while the bottom and top edges of the box indicate, respectively, the 25th and 75th percentiles; the black whiskers extend to the most extreme data points which are not considered outliers, while the outliers are plotted individually using a red cross marker.

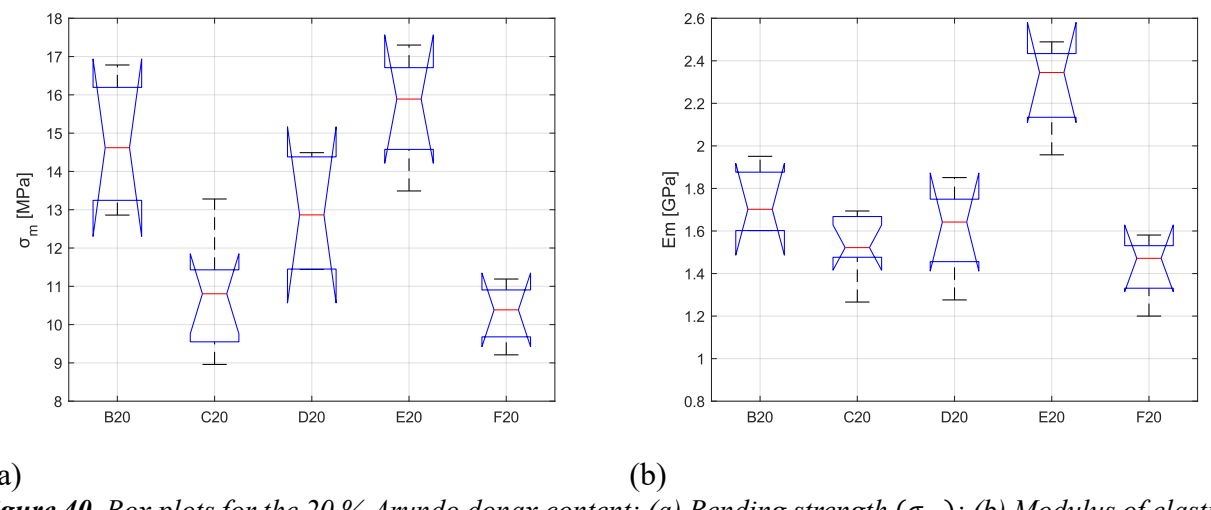


Figure 40. Box plots for the 20 % Arundo donax content: (a) Bending strength (σ_m) ; (b) Modulus of elasticity (E_m) .

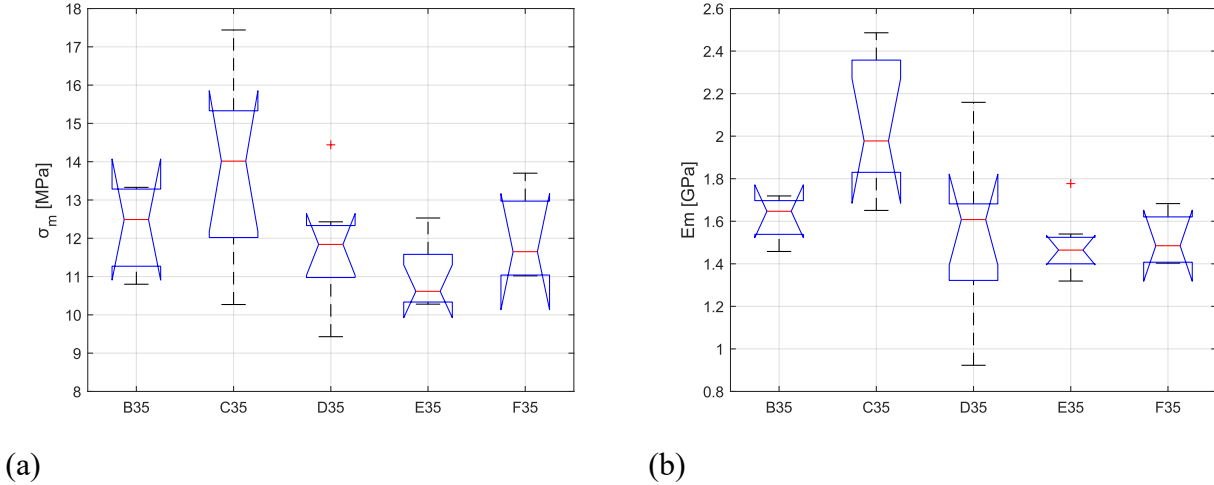


Figure 41. Box plots for the 35 % Arundo donax content: (a) Bending strength (σ_m) ; (b) Modulus of elasticity (E_m)

Table 30 presents the outputs of the ANOVA for the three-point bending test.

Table 30. Test ANOVA for the results of the tests.

Quantity of AD [%]	Factor	Properties	SS	d.f.	MS	F	p
20	Granulometric	σ _m [MPa]	104.57	4	26.141	11.73	0.00006
20	size of AD	E _m [GPa]	1.91	4	0.477	14.22	0.00002
35	Granulometric	σ _m [MPa]	33.66	4	8.415	3.23	0.02810
	size of AD	E _m [GPa]	1.73	4	0.433	6.34	0.00110

From the ANOVA test, results consistent with the previous tests are obtained: in the case of an AD content of 20%, a statistically significant difference is observed between the various groups. However, no trend is evident in relation to the variation in AD particle size within the core of the panel, the group of specimens that demonstrated the best performance includes those of type B20 and E20.

In the case of using 35 % AD, no statistically significant difference is observed between the groups of specimens studied in terms of Bending strength (σ_m).

4.3.4 Discussion

The objective of Wave 2 was to evaluate the influence of the granulometry of the AD chips added to the core of the panel on the physical-mechanical properties of the panels.

Following the granulometry analysis of the material, it was expected that the samples with a higher content of sieve-fractionated particles of AD between 0.5 and 1 mm and between 1 and 2 mm would exhibit the best performance in terms of bending strength (σ_m), modulus of elasticity (Em) and internal bond (IB) due to their higher values of slenderness ratio (SR) and aspect ratio (AR), by findings in the literature [110, 111, 109, 96].

In the case of adding 20% of AD, ANOVA analysis revealed a statistically significant variation in the mechanical properties based on granulometry; however, no trend or pattern was identified. For the addition of 35% AD the ANOVA analysis did not indicate significant variations between the different groups, and no trend could be defined in this case either.

In summary, the results of Wave 2 did not yield significant evidence, as the mechanical and physical properties of the panel showed no correlations, either direct or indirect, with chip size. This outcome, which diverges from the initial hypotheses based on the SR and AR parameters, suggests that other physical or chemical factors might play a predominant role.

The possible causes of this lack of correlation may lie in the complexity of the interactions between the panel components. Additionally, there could be effects related to chemical compatibility or the quality of the interface between the AD particles and the panel matrix.

In light of these results, further analysis is required, focusing on complementary variables such as density distribution, fibre orientation, and potential interactions between AD and other materials present in the core.

Finally, this study highlights the complexity of optimising composite materials and underscores the importance of an interdisciplinary approach that combines mechanical, chemical, and process analyses to achieve a deeper understanding of material performance.

4.4 Conclusions

This research, divided into three phases (Wave 1, Wave 2, and Wave 3), analysed the physical-mechanical properties of particleboards to understand the impact of adding AD particles in different percentages, layers of the particleboard, and varying sizes and shapes.

Wave 1 demonstrated the feasibility of producing particleboards containing a certain percentage of AD particles, replacing recycled wood in the core, not only maintaining but in some cases improving the mechanical properties of the original particleboard. The addition of AD to the core resulted in significant improvements in internal bond (IB) and bending strength (σ_m), especially for boards with a density of 750 kg/m³ and AD percentages ranging between 10% and 35%. These results highlighted:

- A linear relationship between the increase in particleboard density and improved mechanical
 properties, thanks to the enhanced interconnection between particles and better adhesion of
 the resin.
- The ability to reduce thickness swelling (TS) due to the addition of AD, suggesting better water resistance compared to recycled wood.
- The transition from P2 to P4 class in terms of mechanical performance for particleboards with a density of 750 kg/m³ and AD percentages between 10% and 35%, achieving structural standards without the need to increase resin content or board density. This maintained both production costs and the environmental footprint of the final product.

The incorporation of Arundo donax into the particleboard led to a significant improvement in both mechanical and physical properties, as extensively observed in Wave 1. In particular, the addition of AD resulted in an increase in bending strength and water resistance, up to a 35% content. Beyond this threshold, a sharp decline in performance was observed.

Another advantage of using AD as a substitute for wood is that it did not require any changes to the production process of the panel, thus avoiding modifications to the manufacturing chain that would have resulted in significant costs for the company. Furthermore, the processing methods for AD are not substantially different from those already used for recycled wood.

The use of a certain percentage of AD particles in the panel will allow the company to increase its production capacity by relying on a locally sourced raw material (km 0), with very low environmental and economic costs. In fact, one of the main drawbacks of recycled wood is its limited availability, which makes it difficult to scale up production without sourcing it from foreign markets—leading to increased economic costs and environmental impact due to transportation.

Despite theoretical assumptions suggesting a correlation between AD particle size in the core and the mechanical properties of the particleboard, the results of Wave 2 did not reveal clear trends or patterns. Specifically:

- ANOVA analysis showed statistically significant variations in the physical-mechanical properties of the particleboard with changes in the granulometry of AD particles in the core, but only in the case of a 20% AD addition. However, no consistent patterns or correlations were identified between AD particle size and board properties.
- Adding 35% AD did not result in significant variations in the physical-mechanical properties among the groups analysed.
- No direct or indirect correlations emerged between the size of AD particles and the physical-mechanical properties of the particleboard.

This outcome suggests that complex physical and chemical factors might outweigh the influence of particle size alone. For instance, the interface between AD particles and resin, as well as chemical compatibility, could play a critical role in determining the overall performance of the particleboard.

This research demonstrated the potential of AD as an alternative and sustainable material in particleboards, opening new opportunities for optimising composite materials. However, the results from Wave 2 emphasise the complexity of material interactions and the need for an interdisciplinary approach to better understand the mechanisms influencing the physical-mechanical properties of the boards.

Future phases of research, including the analyses planned in Wave 3, could provide crucial insights to further improve particleboard performance and broaden their applications. At the same time, they could contribute to environmental sustainability through the use of recycled and alternative materials.

A future step will be the analysis of the physical-mechanical properties of particleboards in which part of the recycled wood in the external layers will be replaced with AD, using the same replacement percentages applied in Wave 1.

The overall panel density will be 680 kg/m³. Two core types will be used for each AD replacement percentage:

- The first type, without modifications, will use the core typically produced by the company for this material.
- The second type will include AD, specifically using the composition that showed the best results in the previous two Waves.

No changes will be made to the type of resin or its percentage in the panel.

5. BINDERLESS PARTICLESBOARD

5.1 Introduction

The project stems from a collaboration between the University of Bologna and the company My.Fibers from Modena, a start-up focused on developing innovative, fully natural and renewable materials. It specialises in binder-free particleboard that is entirely natural, recyclable and compostable.

In the last decade, the sector of wood-based composites has faced two serious challenges: an increasing demand for roundwood in all wood consumption sectors (UNECE/FAO, 2019) and regulatory requirements to reduce the use of petroleum-based adhesives due to their hazardous emissions, like the use of urea-formaldehyde resin, commonly used in this sector. Despite the success in meeting industry benchmarks, formaldehyde emissions impacting the indoor air atmosphere continues to be a major concern.

To address this, new research on particleboards derived from lignocellulosic materials has focused on developing more sustainable alternatives to traditional wood-based particleboards bonded with synthetic resins. Such resins are often formaldehyde-based, a substance classified as carcinogenic and a significant environmental concern [115, 116, 117, 118].

The binderless particleboards which are free of synthetic adhesives, have emerged as a promising solution to address these issues. Many recent studies have focused on the use of renewable resources and agricultural waste to produce adhesive-free particleboards. These include materials such as hemp and wheat residues treated with steam explosion [118, 119], wine residues [116], brown algae [120], kenaf with potato starch [121] and a combination of rice straw and bagasse [122]. Thanks to their chemical compositions these materials can develop self-binding properties under the influence of heat and pressure. In addition to agricultural waste the use of bamboo processing residues treated through optimised fermentation with lactic acid bacteria has also been studied to improve the adhesive properties of lignocellulosic materials [123]. The natural components of bamboo such as lignin and hemicellulose degradation products play a fundamental role in the self-bonding mechanisms, making the resulting particleboards an interesting option for sustainable applications [123]. Likewise, *Arundo donax* has also been employed in the production of binderless particleboards [34] achieving MOR values of 14.2 N/mm², MOE of 2052.45 N/mm² and IB of 1.12 N/mm².

One of the most studied approaches to improving the properties of binderless particleboards is the pretreatment of natural fibres, such as steam explosion. This method involves exposing fibres to high-pressure steam followed by a sudden release of pressure, causing both mechanical and chemical breakdown of fibrous structures. This process results in partial depolymerisation of lignin and degradation of hemicellulose, making these chemical components more reactive and facilitating bond formation during hot pressing [117, 118, 119]. The steam explosion also increases the accessibility of fibre surfaces enhancing inter-fibre adhesion. Studies have demonstrated that this treatment yields particleboards with superior mechanical properties compared to traditional methods, thanks to the improved distribution of lignin as a natural binder and the increased density of chemical bonds formed.

Additionally, the use of natural additives such as starch or phytic acid, can enhance mechanical properties by increasing the self-binding strength of lignin and hemicellulose and improving the fire resistance of particleboards [121, 117]. A study optimising the processing parameters for the fabrication of binderless jute-based particleboards revealed that hemicellulose decomposition during thermal treatment generates degradation products such as simple sugars and furans, which contribute to the self-bonding of the particleboard [124]. The best results were obtained with a pressing

temperature of 220 °C for 6 minutes and a fine/coarse fibre ratio of 50:50 demonstrating superior thermal stability and improved mechanical properties [124].

A crucial factor is the influence of the density on the physical and mechanical properties of such particleboards. Recent studies have shown that higher density significantly enhances the mechanical performance and water resistance of binderless particleboards [125]. For instance, particleboards produced with sorghum residues have demonstrated good performance meeting European standards and making them suitable for general applications [125]. Another factor affecting the physical and mechanical properties of binderless particleboards is particle size. A study conducted by M. Chen et al. [126] found that smaller particle sizes and optimal production conditions (220 °C, 30 minutes, density of 1.0 g/cm³) achieved MOR values of 28 MPa, MOE of 5.3 GPa and IB of 2.74 MPa [126]. These developments demonstrate the potential of binderless particleboards as a sustainable and environmentally friendly alternative, reducing dependence on virgin timber and synthetic adhesives. The present study fits within this context by analysing the mechanical properties and water resistance of binderless particleboard based on pretreated hemp fibres and aggregates. However, the details of the production process remain confidential for industrial secrecy reasons.

The purpose of the collaboration project between the University of Bologna and the start-up My. Fibers are to study the physical and mechanical properties of an innovative panel, composed of an aggregate and hemp fibres pretreated with a revolutionary process, without any addition of chemical binders, the pretreated fibres were called by the company "Mytrill". This production process will not be detailed in this document for confidentiality reasons.

The studies and tests conducted are the same as those already performed and detailed in sections 4.2.3 and 4.3.2 namely: thickness swelling, water absorption, internal bond, surface soundness and three-point bending test. With the aim of defining a possible classification for this type of binderless particleboards according to EN 312 standard [76].

Regarding the aggregates added to the pretreated hemp fibres, five different types of aggregates will be used: flax, AD, bamboo, hemp shives (the stalk of the hemp plant) and digestate. All types of aggregates are eco-sustainable and recyclable.

The first four types of aggregates have a high fibre content which is expected to enhance the mechanical performance of the panel. Bamboo shavings, hemp shives and digestate are by-products of the agro-industrial sector.

Bamboo is well recognised for its rapid growth, high mechanical strength and excellent toughness, making it a popular choice for various applications, including furniture and structural materials [127]. However, significant amounts of bamboo waste are generated during its processing and production. R. Fu et al. [123] studied the use of bamboo particles to create self-bonded bamboo particleboards.

Hemp shives from the hemp plant have a high fibre content and exhibit excellent mechanical properties. However, in the hemp textile sector, they are often regarded as a by-product and waste material. After the extraction of bast fibers the hemp woody part, called shives or hurds, remains up to 75% of the stalk mass having a great potential to be used in particleboard production because of its chemical components being similar to woods [128]. The most productive hemp varieties can yield up to 15–20 t/ha of dry shives mass, with the estimated average availability of hemp shives in Europe reaching at least 700,000 t/year in 2018. According to Romanese [129] approximately two-thirds of industrial hemp shives in Europe are used as animal bedding, while the remaining one-third is utilised for insulation in construction and as garden mulch. Research has shown that hemp shives offer a viable alternative to spruce strands for reducing volatile organic compounds in bio-based materials [130]. Additionally, hemp shives have been identified as a suitable raw material for particleboard production using synthetic PMDI resin [131]. However, binderless boards made solely from hemp shives through thermoforming processes demonstrated very poor water resistance [132].

Digestate is a by-product of the anaerobic digestion of organic biomass and represents a key resource for the circular economy and the ecological valorisation of organic waste.

Digestate is divided into two fractions: a solid and a liquid. Both fractions are useful for improving soil quality and reducing the reliance on chemical fertilisers. Specifically, the solid fraction is rich in organic matter and can be used as a soil amendment or for compost production. The liquid fraction, on the other hand, contains a higher concentration of nutrients such as nitrogen, phosphorus and potassium, is often used as a liquid fertiliser for agriculture.

Current regulations impose specific limits on the amount of nitrogen that can be present in the soil to prevent eutrophication and water pollution. Once the nitrogen level reaches this limit, adding fertilizer or digestate is no longer permitted. In addition, the solid fraction is more challenging to use for soil fertilisation and is also less rich in nutrients.

This creates a major challenge in digestate management since there is an excess of solid fraction that cannot be used in fertilizing the soil.

When the solid digestate is not used in agriculture or for compost production, it can accumulate, posing the risk of environmental pollution, causing unpleasant odours or interfering with waste management. Additionally, its management can incur additional costs, particularly if disposal or treatment requires advanced technologies. For this reason, it is essential to develop sustainable solutions for the recycling and efficient use of solid digestate such as its valorisation to produce building materials or other eco-sustainable products.

5.2 Manufacture and Methods

Table 31 provides the chemical compositions of the various aggregates used.

The pretreated hemp fibres, hemp hurds, flax and bamboo were supplied by the company My.Fibers. The hemp fibres are extracted from the plant and separated from the hurds through mechanical grinding, followed by sieving to isolate medium-length fibres from shorter ones.

The hemp hurds, flax and bamboo undergo mechanical grinding and subsequent sieving to achieve a particle size of less than 2 mm.

The AD used was the same as that described in Chapter 4 (Paragraph 4.2.1). Its particle size distribution is consistent with that used for the other aggregates.

Table 31.	Chemical	of hemp.	flax.	hamboo	and Arundo donax.	

References	Material	Chemical composition [%]					
References	Material	Cellulose	Hemicelluloses	Lignin	Others		
[133]		67.0	16.1	3.3	3.6		
[134]	Haman	74.4	17.9	3.7	1.7		
[135]	Hemp	74.0	18.0	4.0	\		
[136]		76.1	12.3	5.7	4.9		
[137]	- Flax	76.2	9.4	9.1	5.3		
[138]		68.2-75.5	16.4-31.0	4.0-6.1	\		
[139]	Dambaa	47.2	23.9	25.4	0.5		
[140]	Bamboo	30.0-52.0	45.0-25.0	33.0-24.0	\		
[141]	Arundo donax	43.1	21.9	22.4	12.6		

All these materials were dried using an oven at a temperature of T = 85 °C until reaching a mass variation of less than 0.1% after 24 h in the oven [69].

The digestate was supplied by the agricultural company of Medicina (Bologna). The material used consisted of both liquid and solid phases, extracted from the plant before the separation of the two components.

Due to a non-disclosure agreement between the Start-Up and the University of Bologna, it is not possible to include in this document details regarding the production and preparation process. Several types of binderless particleboards were produced varying:

- the type of aggregate.
- the compaction pressure during the forming phase.
- the ratio between Mytrill and the aggregate.

Specifically, six different types of aggregates were used: Arundo donax, bamboo, hemp hurds, digestate and flax.

Three levels of forming pressure were applied: 0.2 MPa, 0.5 MPa and 1 MPa.

For all particleboard types, a Mytrill-to-aggregate ratio of 40/60 was used, except for particleboards with compaction pressures of 0.5 and 1 MPa with hemp hurds as the aggregate. In this case, two different Mytrill-to-aggregate ratios of 40/60 and 60/40 were selected to preliminarily evaluate how an increase in Mytrill content affects the product's characteristics.

The particleboards where the aggregate is digestate were produced only at the highest forming pressure, 1 MPa because technical issues arose during the forming phase at lower pressures.

For the particleboards in which the aggregate was the flax, it was decided to manufacture the board only with the 0.5 MPa level of forming pressure.

The particleboards, measuring 30 x 20 x 1.5 cm, were produced through a cold-pressing process using a pump with a dual function: removing excess water from the Mytrill and creating a vacuum in the mould to guarantee a better quality of the particleboards. After the forming process, the panel was cured in an oven for 1 hour at 100°C to remove excess moisture and allow Mytrill to exhibit its binding properties.

Table 32 collects all the produced binderless particleboards and their characteristics.

Table 32. Types of particleboard panels.

Nomenclature of	of the panel	Pressure [MPa]	Aggregate	Mytrill-to- aggregate ratio [%]
	A2	0.2	AD	
A	A5	0.5	AD	40-60
	A10	1	AD	
	B2	0.2		
В	B5	0.5	Bamboo	40-60
	B10	1		
	C2	0.2		
C	C5	0.5	Hemp hurds	40-60
	C10	1		
C/60	C/60-5	0.5	II 1	60-40
C/60	C/60-10	1	Hemp hurds	00-40
D	D10	1	Digestate	40-60
L	L5	0.5	Flax	40-60

The test conducted for this binderless particleboard follows the same procedure described in Sections 3.2.3 and 4.3.2. Table 33 presents the summary of the tests performed, the number and dimensions of the specimens and the corresponding reference standard [102].

Table 33. Type of tests carried out, standard associated to each test, number and dimensions of the specimens required for the physical-mechanical tests.

Test	Normative	Number of Specimens	Dimensions of specimen [mm]
Swelling in Thickness	EN 317 (1993)	8	50 x 50 x 22
Water absorption	EN 317 (1993)	8	50 x 50 x 22
Surface soundness	EN 311 (2002)	8	50 x 50 x 22
Internal Bond	EN 319 (1993)	8	50 x 50 x 22
Three-point bending	EN 310 (1993)	6	300 x 50 x 22

5.3 Results

5.3.1 Physical properties

Table 34 presents the average and standard deviation of density, thickness swelling (TS) and water absorption (WA) after 2 and 24 hours of immersion for all the specimens.

Table 34. Average values and standard deviations for density, thickness swelling (TS) and water absorption (WA) after 2 and 24 h of immersion.

	Density [kg/m3]	TS 2 h [%]	TS 24 h [%]	WA 2 h [%]	WA 24 h [%]
A2	359.0 (± 17.4)	13.3 (± 2.6)	14.8 (± 2.1)	202.0 (± 11.3)	212.8 (± 10.9)
B2	$379.0 \ (\pm \ 16.5)$	$16.0 \ (\pm \ 3.6)$	$18.6 \ (\pm \ 3.5)$	$183.5~(\pm~18.4)$	$197.4~(\pm~23.9)$
C2	$300.7 \ (\pm\ 22.6)$	$13.6 \ (\pm \ 2.5)$	$16.0 \ (\pm \ 2.3)$	$247.9 \ (\pm \ 2.1)$	266.6 (± 1.3)
A5	365.8 (± 13.7)	15.3 (± 1.44)	17.6 (± 2.14)	$183.9 (\pm 10.3)$	196.2 (± 9.3)
B5	$403.8 \ (\pm \ 10.4)$	$18.8 \ (\pm \ 3.25)$	$20.6 \ (\pm \ 5.0)$	$171.4 (\pm 13.8)$	$183.3~(\pm~19.8)$
C5	$272.8 \ (\pm \ 5.7)$	$12.5~(\pm~2.19)$	$15.1 (\pm 2.3)$	$257.7 (\pm 8.8)$	281.6 (± 11.0)
L5	$330.4 (\pm 4.6)$	$17.3 (\pm 1.9)$	$18.8 (\pm 1.3)$	$225.3 (\pm 7.9)$	$246.0 \ (\pm \ 10.4)$
C/60-5	$420.0 \ (\pm \ 14.2)$	$18.3~(\pm~0.4)$	$21.2 (\pm 0.56)$	$154.8 \ (\pm \ 3.2)$	171.2 (± 1.0)
A10	401.8 (± 13.4)	17.9 (± 1.1)	20.2 (± 1.0)	174.5 (± 7.3)	189.9 (± 5.2)
B10	432.6 (± 11.2)	$20.2 (\pm 2.0)$	22.5 (± 1.4)	$154.3~(\pm~12.2)$	$167.6 \ (\pm\ 15.4)$
C10	$322.7 (\pm 2.5)$	$18.9 (\pm 1.6)$	$20.1 (\pm 1.3)$	$222.0 \ (\pm \ 3.4)$	244.9 (± 7.7)
D10	$390.2 (\pm 21.3)$	$19.1 (\pm 3.8)$	$20.8 \ (\pm \ 4.1)$	$185.9 (\pm 20.5)$	208.9 (± 19.4)
C/60-10	599.5 (± 79.9)	22.3 (± 1.9)	$28.2 (\pm 2.5)$	129.8 (± 4.3)	142.5 (± 6.4)

To better illustrate the results presented in Table 34, the same data are shown in Figure 42 for the TS and Figure 43 for the WA.

Inspecting Figure 42, no significant differences in TS are observed among the specimens when varying the type of aggregate added, not even in the case of digestate (an aggregate with a completely different nature compared to the others).

Figure 43 shows that the specimens with hemp hurds as aggregates exhibit higher WA values at both 2 hours and 24 hours for all three forming pressure levels. Meanwhile, the specimens of type C/60, with a Mytrill-to-aggregate ratio of 60/40, show the lowest WA and the highest TS values at the same forming pressure.

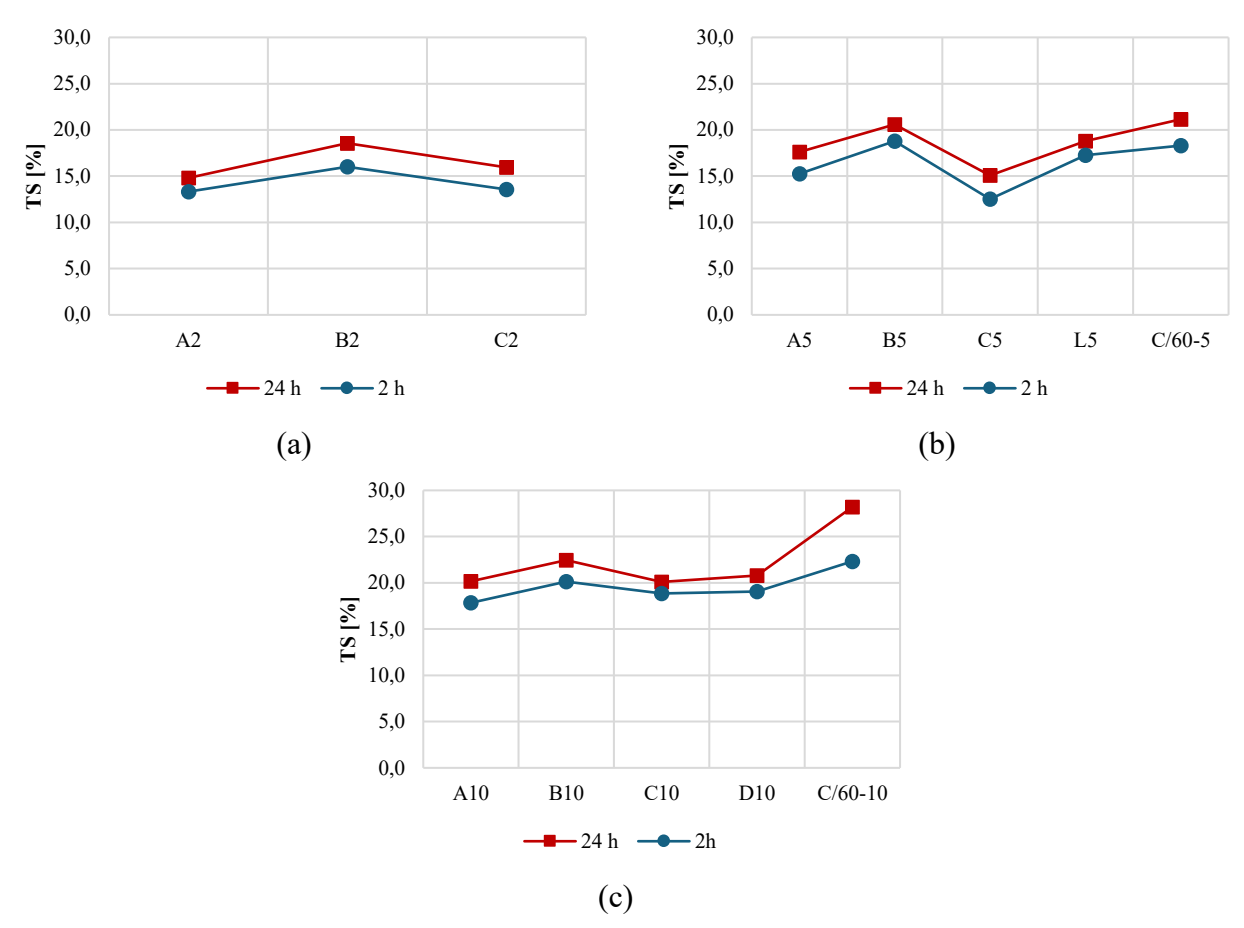
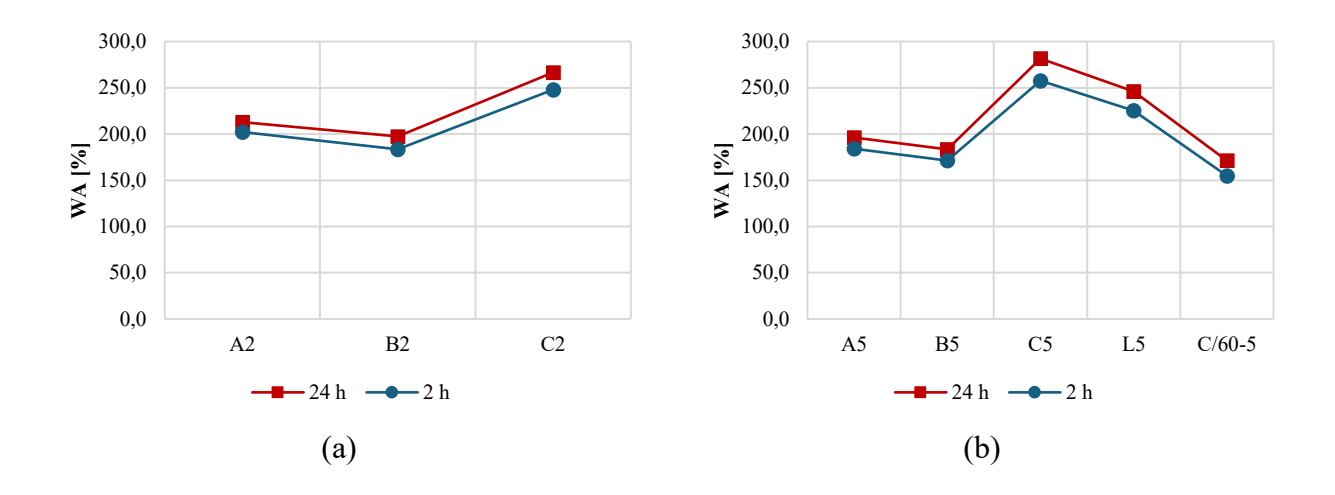


Figure 42. Trend of average values of thickness swelling 2 h (TS 2 h) and 24 h (TS 24 h) for the forming pressure of: (a) 0.2 MPa, (b) 0.5 MPa and (c) 1 MPa.



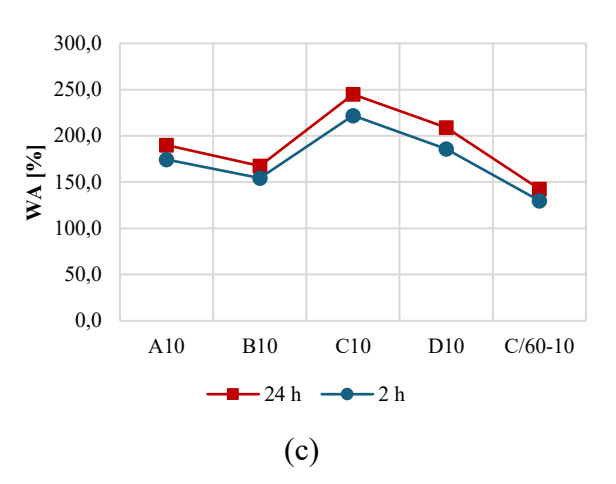


Figure 43. Trend of average values of water absorption 2 h (WA 2 h) and 24 h (WA 24 h) for the forming pressure of: (a) 0.2 MPa, (b) 0.5 MPa and (c) 1 MPa.

Figures 44 (a) and (b) present the TS and WA at 24 h values for the different pressures and aggregates. The red line represents the standard limits associated with the P4 class of particleboard [76].

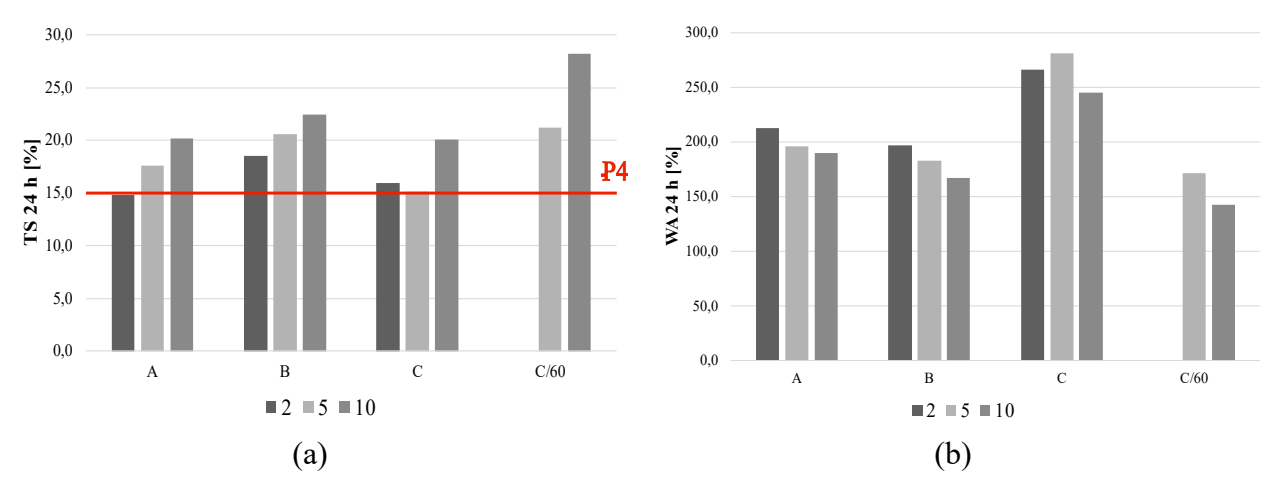


Figure 44. Comparison with normative limits for different types of particleboards for: (a) TS 24 h and (b) WA 24 h. The red line represents the standard limits associated with the P4 class.

In Figure 44 it can be clearly observed that increasing the forming pressure from 0.2 to 1 MPa results in a higher TS and lower WA. Since pressure is directly related to density, there is a direct proportionality between TS and density, while the relationships between density and WA, as well as between TS and WA are inversely proportional. In other words, the denser the panel, the greater the swelling of the particleboard and the lower the amount of water absorbed by the panel.

This is because particleboards with lower densities have a higher percentage of voids within their volume, which are filled with water upon immersion. This leads to an increase in the specimen's weight but not its volume.

In contrast, higher-density particleboards contain a greater quantity of fibres and aggregate particles within the same volume. When immersed in water these fibres and particles tend to saturate. The saturation of fibres does cause a substantial volumetric expansion, as reflected in the TS value.

Figure 44 (a) shows that almost all specimens exhibit values exceeding the maximum threshold specified by the standard. This indicates a sensitivity of this type of particleboard to the water. To ensure values below the maximum threshold specified by the standard, it will be necessary to apply

specific treatments to the external surface of the panels or to perform pre-treatments on their constituent elements.

5.3.2 Mechanical properties

5.3.2.1 Surface Soundness and Internal Bond

Figures 45 (a) and (b) reported the setup of the surface soundness test, while the setup of the internal bond tests was reported in Figure 45 (c).

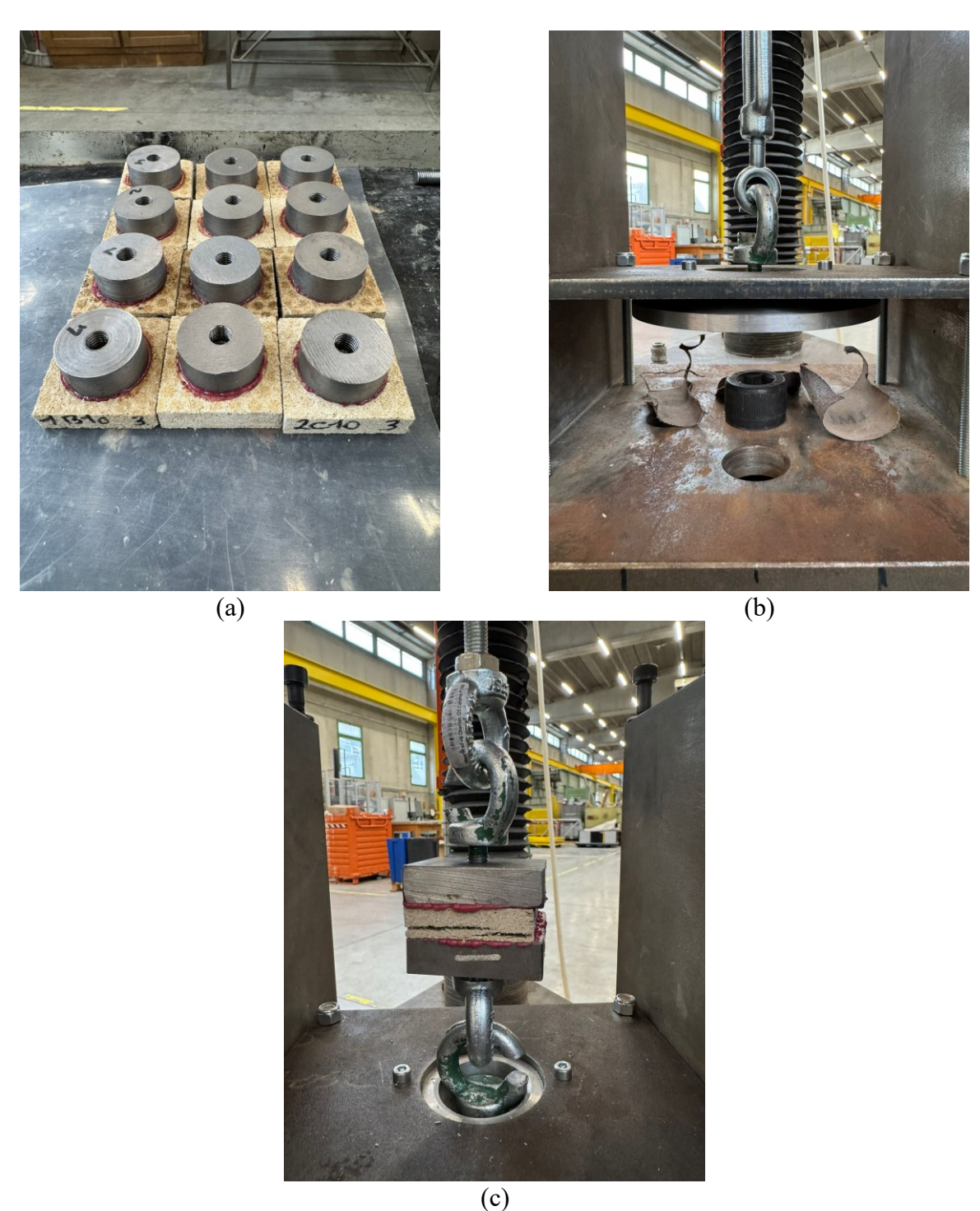


Figure 45. (a) Specimens setup; (b) Setup for the surface soundness test; (c) Setup for the internal bond test.

The mean values and standard deviations of the particleboard panels tested for the surface soundness and internal bond (IB) test were reported in Table 35.

Table 35. Average values and standard deviations for surface soundness and internal bond.

	Surface soundness [MPa]	IB [MPa]
A2	$0.23~(\pm~0.02)$	$0.19 \ (\pm \ 0.02)$
B2	$0.32~(\pm~0.04)$	$0.28~(\pm~0.02)$
C2	$0.28~(\pm~0.01)$	$0.30 \ (\pm \ 0.02)$
A5	$0.27~(\pm~0.07)$	$0.20~(\pm~0.05)$
B5	$0.33~(\pm~0.08)$	$0.26~(\pm~0.01)$
C5	$0.33 \ (\pm \ 0.10)$	$0.22~(\pm~0.01)$
L5	$0.32 \ (\pm \ 0.06)$	$0.24~(\pm~0.02)$
C/60-5	$0.46~(\pm~0.04)$	$0.42~(\pm~0.05)$
A10	$0.31 (\pm 0.06)$	$0.28~(\pm~0.04)$
B10	$0.23~(\pm~0.05)$	$0.30~(\pm~0.01)$
C10	$0.31~(\pm~0.04)$	$0.26~(\pm~0.01)$
D10	$0.31 \ (\pm \ 0.10)$	\
C/60-10	$0.64~(\pm~0.05)$	$0.52 (\pm 0.01)$

From the table above, it can be observed that the values of surface soundness and IB are almost independent of the type of aggregate used, as previously noted in Section 5.4.1.

For a better representation of the results reported in Table 33, the same data are presented in Figure 46. The red lines represent the standard limits associated with the P1 and P2 classes of particleboard [76].

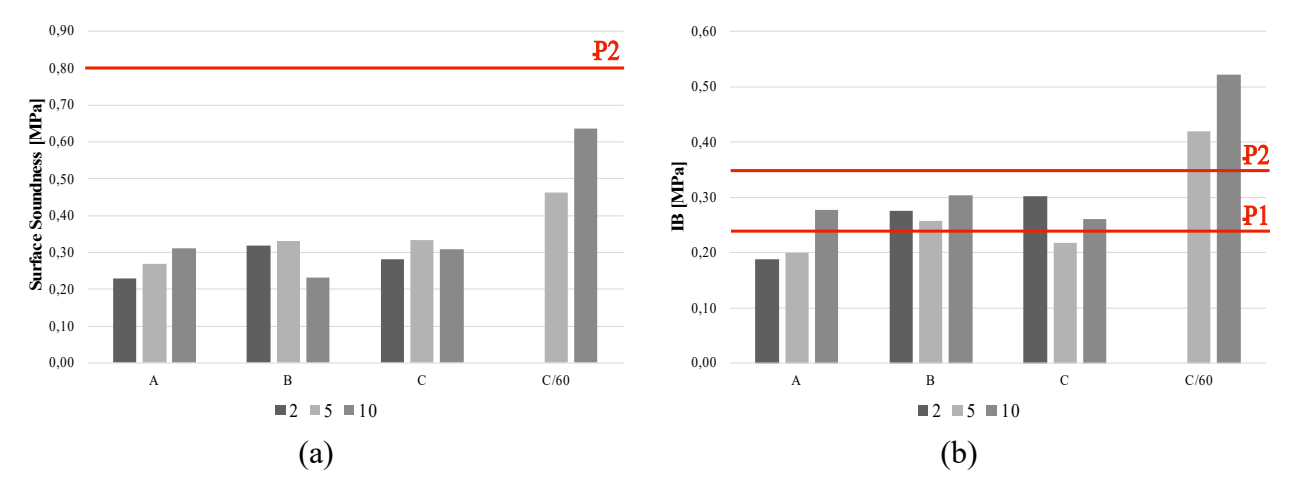


Figure 46. Comparison with normative limits for different types of particleboards for: (a) surface soundness test and (b) internal bond (IB). The red lines represent the standard limits associated with the P1 and P2 classes

The limit value associated with class P1 is not shown in Figure 46 (a), why it doesn't exist for this class of particleboard (general-purpose boards for use in dry conditions). None of the tested particleboards were able to meet the minimum Surface Soundness value specified by the standard.

Regarding the IB value (Figure 46 (b)), all particleboards manufactured using a pressing pressure of 1 MPa exceeded the minimum value for P1 classification. In the case of bamboo, this applies to all pressing pressures used.

The only particleboards capable of meeting the minimum IB value required for classification as P2 (boards for interior fitments, including furniture, for use in dry conditions) were the binderless particleboards of the C/60 type, manufactured using either a pressing pressure of 0.5 MPa or 1 MPa. This type of particleboard exhibits significantly higher IB and Surface Soundness values compared to the other cases, with increases of 86% and 48.5% respectively, for a pressing pressure of 0.5 MPa, and 86% and 124% respectively, for a pressing pressure of 1 MPa. This is partly due to the higher density of these panels, which is 22.4% higher for a pressing pressure of 0.5 MPa and 55% higher for a pressing pressure of 1 MPa compared to the particleboards with the same pressing pressure. The higher percentage of Mytrill (pre-treated hemp fibre) may ensure better adhesion and, consequently, higher mechanical strength.

Figure 47 provides optical microscope images of the fracture surfaces of the specimens tested for the IB test, for a pressing pressure of 1 MPa and various types of aggregates.

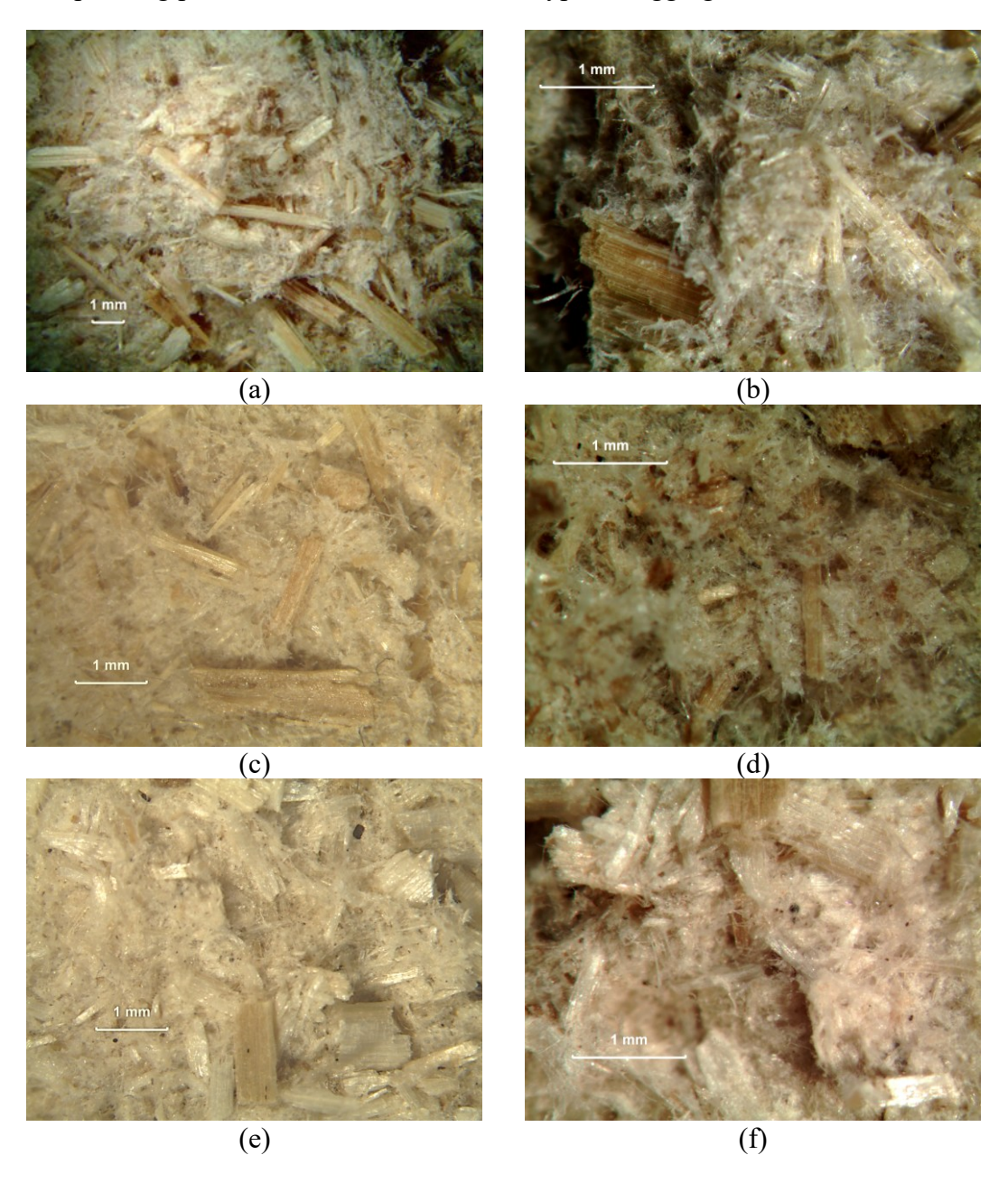




Figure 47. Optical microscope images of the fracture surfaces after the IB test, for the specimens with a pressing pressure of 1 MPa and the different types of aggregates: (a)-(b) Arundo donax; (c)-(d) Bamboo; (e)-(f) Hemp; (g)-(h) Hemp with a ratio of matrix/aggregate of 60/40.

From the images shown in Figure 47, it can be observed that the hemp fibres subjected to the pretreatment process appear to be very short.

Moreover, in traditional particleboards, such as those tested and studied in Chapter 4, the binder formed only a thin imperceptible film on the external surface of the wood chips that made up the panel structure, with stresses being transmitted mutually through contact and friction between them. In contrast, in this case, the binder, Mytrill, completely encloses the aggregate material chips preventing mutual contact between them.

5.3.2.2 Three-point bending

Figure 48 reported the setup of the three-point bending test.

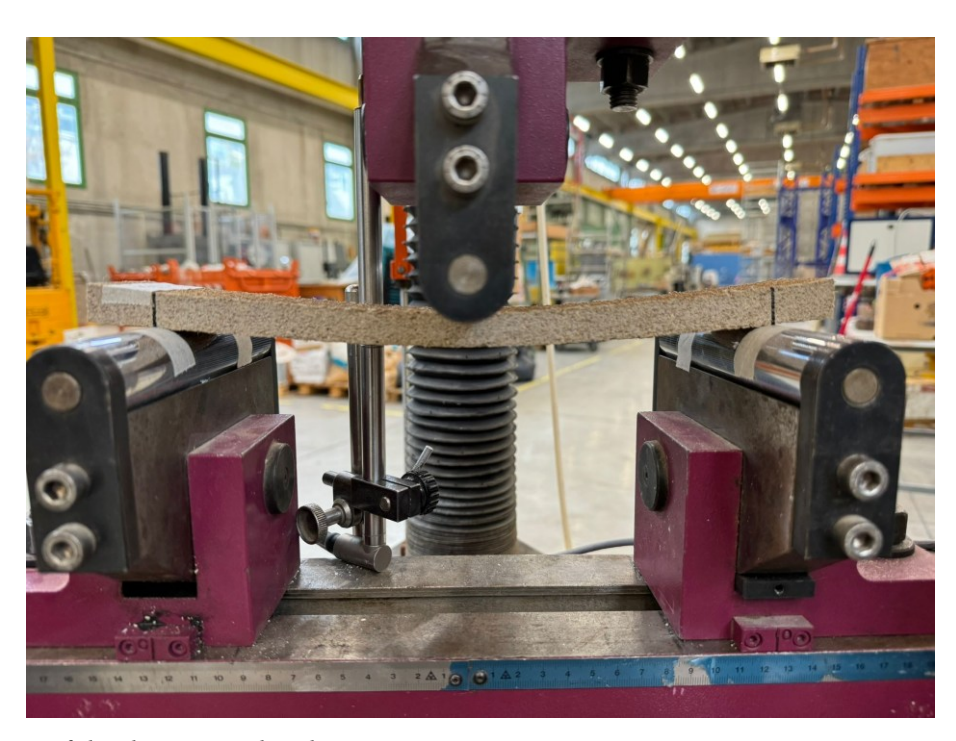


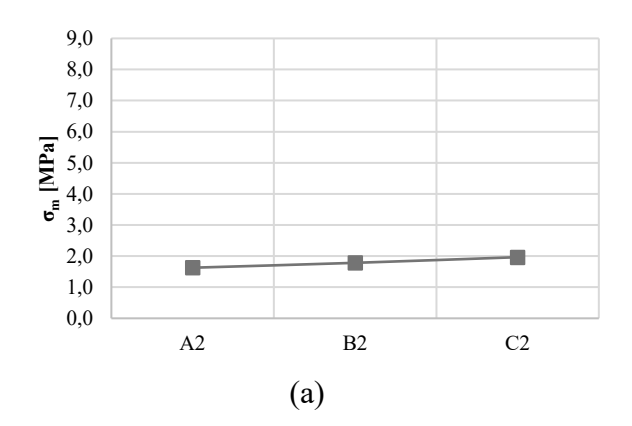
Figure 48. Setup of the three-point bending test

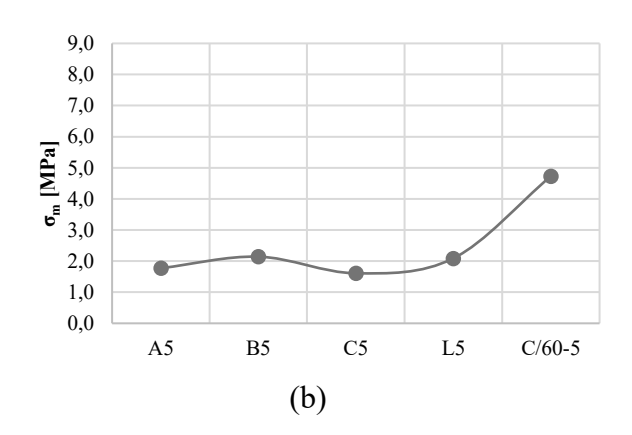
Table 36 presents the mean values and standard deviations of the binderless particleboard panels tested in the three-point bending test.

Table 36. Average values and standard deviations in brackets for the maximum load, bending strength σ_m , Modulus of elasticity E_m and the density for the different types of particleboards.

Particleboards	Maximum Load [N]	σ_m [MPa]	E _m [MPa]	Density [kg/m³]
A2	44.4 (± 1.1)	$1.63~(\pm~0.04)$	189.52 (± 12.34)	359.0 (± 17.4)
B2	47.6 (± 15.6)	$1.78~(\pm~0.29)$	$246.33 \ (\pm\ 15.75)$	379.0 (± 16.5)
C2	$60.44~(\pm~48.94)$	$1.97~(\pm~0.35)$	262.78 (± 48.94)	300.7 (± 22.6)
A5	51.4 (± 7.9)	$1.77 (\pm 0.23)$	224.01 (± 51.24)	365.8 (± 13.7)
B5	$56.4 (\pm 4.0)$	$2.14 (\pm 0.26)$	$293.18\ (\pm\ 52.83)$	403.8 (± 10.4)
C5	62.11 (± 7.04)	$1.61~(\pm~0.20)$	$175.59 (\pm 18.51)$	272.8 (± 5.7)
L5	54.33 (± 5.33)	$2.09 (\pm 0.20)$	$283.36 \ (\pm\ 36.04)$	330.4 (± 4.6)
C/60-5	98.73 (± 6.75)	$4.73~(\pm~0.30)$	510.88 (± 17.18)	420.0 (± 14.2)
A10	65.0 (± 9.1)	2.48 (± 0.12)	305.69 (± 27.03)	401.8 (± 13.4)
B10	52.2 (± 10.2)	$2.64 (\pm 0.16)$	$208.90 \ (\pm\ 34.16)$	432.6 (± 11.2)
C10	58.77 (± 4.94)	$2.08~(\pm~0.20)$	$271.51\ (\pm\ 32.82)$	322.7 (± 2.5)
D10	39.10 (± 15.86)	$1.89 \ (\pm \ 0.97)$	256.94 (± 118.64)	390.2 (± 21.3)
C/60-10	156.65 (± 122.41)	$8.09 (\pm 0.70)$	926.26 (± 117.14)	599.5 (± 79.9)

Figure 49 shows the trend of Bending strength (σ_m), while Figure 50 shows the trend of Modulus of elasticity (E_m), for the different forming pressures.





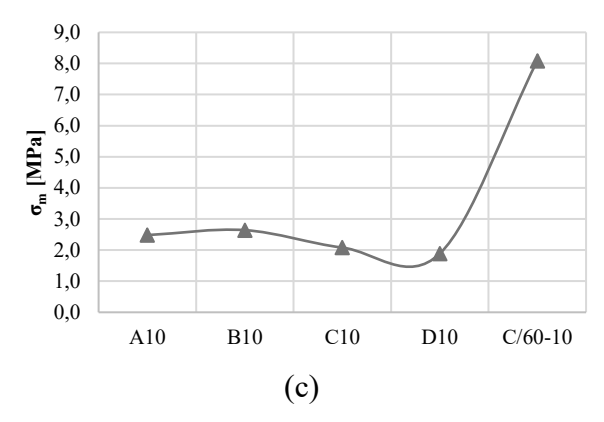


Figure 49. Bending strength (σ_m) for different values of forming pressure: (a) 0.2 MPa, (b) 0.5 MPa and (c) 1 MPa.

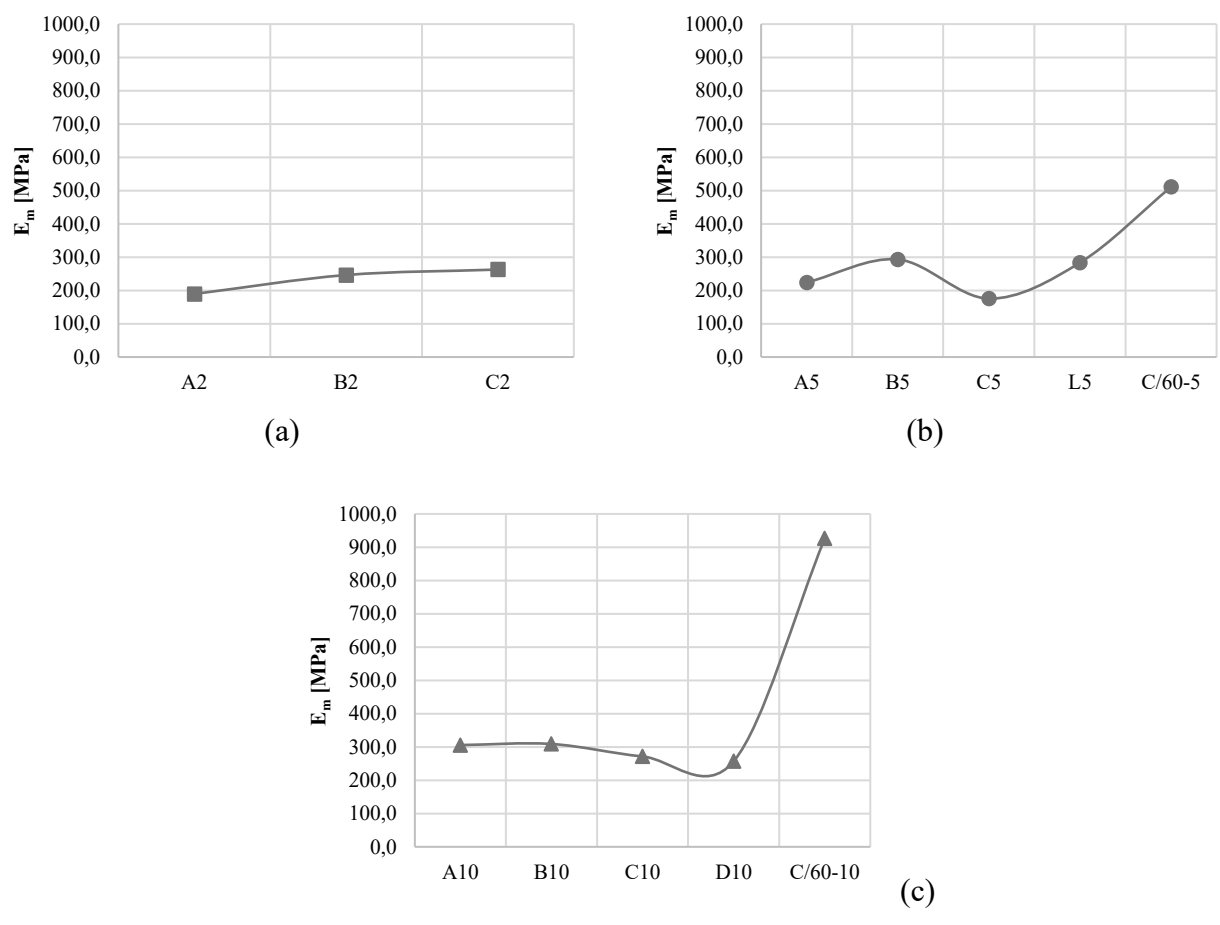


Figure 50. Modulus of elasticity (E_m) for different values of forming pressure: (a) 0.2 MPa, (b) 0.5 MPa and (c) 1 MPa.

Figures 49 and 50 illustrate that the flexural mechanical properties of particleboards are almost independent of the type of aggregate used, as previously observed in earlier sections for other physical and mechanical properties analyzed. The only particleboards that deviate from the others are those of the C/60 type, which exhibit significantly higher flexural mechanical performance compared to other types. They show an increase in bending strength (σ_m) of 156.7 % for a pressing pressure of 0.5 MPa, and 236.8 % for a pressing pressure of 1 MPa. This is consistent with the results obtained in Section 5.4.2.1.

Figure 51 (a) presents the Bending strength (σ_m) values, while Figure 51 (b) shows the Modulus of elasticity (E_m) values, for the different pressures and aggregates. The red lines represent the standard limits associated with the P1 and P2 classes of particleboard [76].

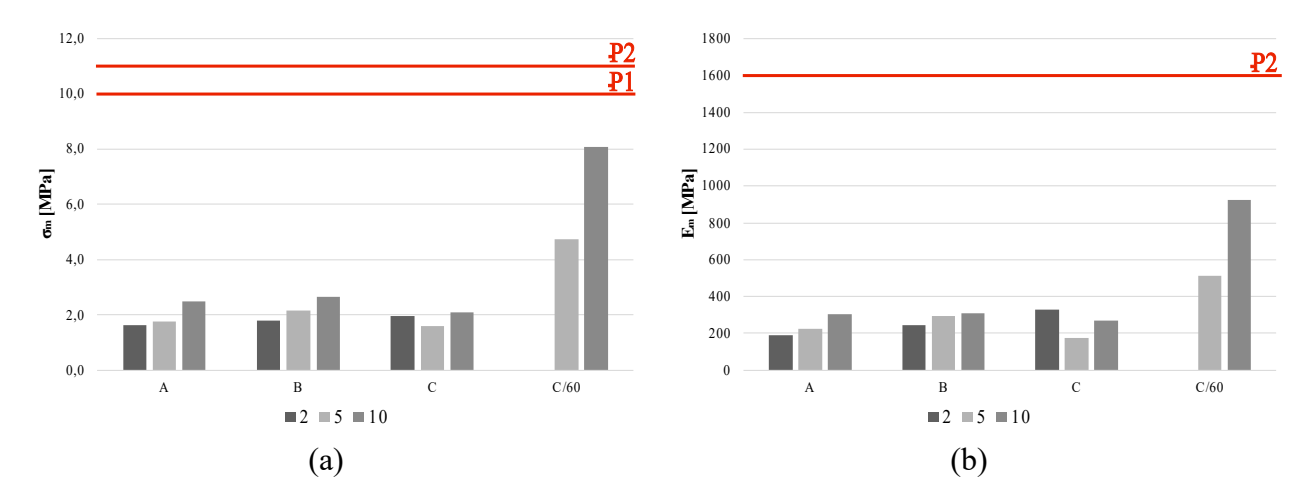


Figure 51. Comparison with normative limits for different types of particleboards for: (a) Bending strength (σ_m) and (b) Modulus of elasticity (E_m) . The red lines represent the standard limits associated with the P1 and P2 classes.

In Figure 51 (b), the limit value associated with class P1 is not shown because it doesn't exist for this particleboard classification.

The same considerations discussed in the previous section regarding the results for surface soundness and IB properties also apply here.

5.4 Conclusion

The study conducted allowed the evaluation of the physical and mechanical properties of innovative binderless particleboard made from pre-treated hemp fibres, free of synthetic binders and natural aggregate, with the aim of evaluating their classification according to the EN 312 standard and contributing to the development of sustainable and eco-friendly materials.

From the water resistance tests, it was found that swelling (TS) and water absorption (WA) properties are primarily influenced by the density of the panels rather than the type of aggregate used. Panels with higher density exhibited greater sensitivity to water in terms of TS, while panels with lower density absorbed a higher quantity of water. However, almost all samples exceeded the maximum thresholds established by the standard, highlighting the need for surface treatments or pre-treatments of the constituent elements to enhance their performance.

The Surface Soundness and Internal Bond tests revealed that the C/60-type panels, particularly those pressed at 0.5 MPa and 1 MPa showed significantly superior performance compared to other types of particleboards. This result is attributed to the elevated percentage of Mytrill (pre-treated hemp fibres), which ensures higher density and more effective adhesion.

From the optical microscope investigations, it emerged that, unlike traditional particleboards, in this case, the binder (Mytrill) completely encases the chips of the aggregate material preventing direct contact between them.

The flexural tests confirmed that mechanical properties are almost independent of the type of aggregate. The particleboards with a high percentage of Mytrill showed higher bending strength and modulus with respect to the others. The best performance is achieved with higher densities.

In Table 37 the results obtained for C10 and C/60-10 particleboards are comparable with those reported in the literature for binderless particleboards and with the results from experimental investigations on particleboards studied in Chapter 4, with densities ranging between 550 kg/m³ and 600 kg/m³. The results obtained in this study are consistent with those from similar research, which validates the work carried out here.

Table 37. Comparison of Modulus of rupture (MOR), Modulus of elasticity (MOE), Internal bond (IB), TS 24 h and WA 24 h of binderless particleboards found in literature, those obtained in Chapter 4 for the density 550-600 kg/m³ and results obtained in this Chapter.

Reference	Biomaterial	Density [kg/m ³]	MOR [MPa]	MOE [MPa]	IB [MPa]	TS 24 h [%]	WA 24 h [%]
[126]	Broussonetia papyrifera	800	7-12	1240- 1806	0.21- 0.45	31-73	\
[34]	AD	883	14.2	1903	0.75	53	\
[116]	Winery by-products	833-875	2.2-4.0	\	0.25- 0.66	45-116	\
[121]	Kenaf	800	11.4	1540	\	241	444
[119]	Hemp Shives and Wheat Straw	800	15.5	2750	0.64	4	53
[142]	Bamboo	1000-1150	9-13	1500- 2000	0.2-0.8	20-40	\
Charter 4	AD and recycled wood	561-626	4.8-6.6	774-1130	0.15- 0.28	10.2-15.8	77-84
C10	Pre-treated hemp & hemp hurds	323	2.1	272	0.26	20.1	244
C/60-10	Pre-treated hemp & hemp hurds	600	8.1	926	0.52	28.2	142

In conclusion, the results demonstrate that C/60 panels made from pre-treated hemp fibres and subjected to the highest forming pressures represent a promising solution for the development of fully natural and high-performance materials. However, further investigations are needed to optimize the physical-mechanical properties and ensure greater compliance with regulatory requirements, particularly regarding the role of density, fibre saturation and potential surface treatments.

6. Conclusions

This thesis explored the use of natural and sustainable materials across three distinct projects: sandwich panels with a honeycomb core, particleboards with recycled wood, and binderless panels made from pre-treated hemp fibres. The central thread running through all these projects has been the use of Arundo donax, a plant that due to its rapid growth and ability to thrive in less fertile environments, offers a sustainable alternative to traditional raw materials. The decision to focus on this plant was driven by the urgent need to transition towards more sustainable practices in construction, particularly in the context of reducing dependence on non-renewable resources and minimizing the environmental footprint of building materials.

The results highlight the innovative potential of these materials in terms of both mechanical performance and environmental sustainability, offering a practical perspective for industrial applications and a significant reduction in ecological impact.

Specifically, regarding the honeycomb panels, the feasibility of using Arundo donax rings in the core of a sandwich panel has been demonstrated. It was shown that surface abrasion treatment of the lateral sides of the Arundo donax rings significantly improves the mechanical properties of the panel. This treatment enhances the adhesion between the resin, used to bond the rings together and to the skins forming the panel, and the Arundo donax rings, thereby increasing the stiffness, shear strength, and flexural resistance of the panel. The FE models developed for the three-point bending test confirmed the effectiveness of these treatments, accurately representing the panel's linear and non-linear mechanical behaviour.

The research on particleboard, with recycled wood and Arundo donax, showed the possible integration of Arundo donax into particleboards to enhance their mechanical properties and water resistance, enabling the particleboards to achieve P4 classification without increasing density or resin content. The results highlighted a linear relationship between density and mechanical performance, as well as the positive role of Arundo donax in reducing thickness swelling (TS). However, the granulometric analysis conducted in Wave 2 did not yield significant results, suggesting that other physical and chemical factors may have a predominant influence. Future investigations planned for Wave 3 aim to further optimize particleboard composition and expand potential applications.

The last part of the thesis showed particleboard, based on hemp fibres produced without synthetic binders, using a matrix based on pre-treated hemp fibres (Mytrill). The panels demonstrated promising performance, although further optimization is required to fully comply with regulatory standards. The density and the percentage content of Mytrill relative to the aggregate proved to be the key factors influencing the physical and mechanical properties of the panel. Various types of aggregates were tested, but it was found that the panel's properties were entirely independent of the nature and origin of the aggregates. The results represent a significant step towards the development of entirely natural panels, although further research is needed to enhance water resistance and mechanical properties.

The thesis involved collaborations between academic institutions and industrial partners and has contributed to a deeper understanding of how construction materials that meet the growing demand for environmental responsibility can be produced. These diverse collaborations not only explored the technical characteristics and performance of some innovative particleboards but also emphasized the importance of integrating eco-consciousness into material design and construction processes.

As we look ahead, AD-based materials, particularly in the form of particleboards, hold substantial promise. Continued research and optimization will be key to unlocking their full potential, allowing them to play a pivotal role in the sustainable construction practices of tomorrow.

A list of possible future steps can be traced for each project.

Specifically for the honeycomb panels, an important step will be the replacement of epoxy resins with bio-based alternatives, such as Polylactic Acid (PLA) or polyhydroxyalkanoates (PHA), making honeycomb panels a fully eco-friendly solution for the construction industry.

For the particleboards, the use of Arundo donax in the outer layers of particleboards could improve the physical-mechanical properties and water resistance with a significant reduction in ecological footprint.

Finally, the performance of the binderless particle boards could be improved by increasing the density, the percentage content of Mytrill, and the granulometry of hemp fibres on the physical-mechanical behaviour of the material.

Appendix A

Introduction

Referring to the previous chapter, an alternative to the use of flax fiber was evaluated, as well as a possible different production process for the manufacturing of the skins. The objectives were to reduce the environmental impact and production costs of the material.

The increased awareness about environmental impact has resulted in a reduction of synthetic-based elements in composite material reinforcement [143]. As a result, the incorporation of cellulosic fibres such as flax, hemp, kenaf, Juta and sisal has gained significant attention in recent years [144, 145]. These fibres can be harvested from the stem, leaves, or seeds of certain plants. Hemp, flax, kenaf, and jute fibres are extracted from the plant stem, while sisal fibres are extracted from the plant leaves, and cotton fibres are also extracted from the seeds [146].

Natural fibres are themselves a composite material, as they are made up of fibres, microfibrils, and a matrix. The matrix consists of two components: hemicellulose (a low-molecular-weight polysaccharide of irregular composition, made up of different sugars) and lignin (a heavy and complex organic polymer composed of various phenolic compounds). The microfibrils are composed of cellulose chains that exhibit a varying degree of crystallinity (crystallinity index) and a certain twist angle, which is the angle they form with their longitudinal axis. The three main components of natural fibres are cellulose, hemicellulose, and lignin.

The strength and stiffness of fibres depend on their cellulose content, crystallinity index, and microfibrillar angle. Another important factor influencing the physical-mechanical properties of fibres is their diameter; as the diameter increases, the ultimate tensile strength and elastic modulus significantly decrease. The strength of natural fibres follows Griffith's theory [147], developed for brittle materials, where the main idea is that the strength of the material depends on the size of microscopic defects within the material. In this perspective, an increase in fibre diameter raises the likelihood of critical defects, leading to a higher probability of premature material failure [148, 149, 150].

The individual fibres are grouped into bundles, held together by lignin and pectin. These bundles exhibit mechanical strength characteristics inferior to those associated with the individual fibres.

The utilization of natural fibers in place of synthetic alternatives provides several clear benefits, such as reduced economic and environmental costs [52], low density [53], easy availability and favorable thermal and acoustic insulation properties, along with adequate strength and stiffness [151, 152].

The advantage associated with natural fibres is ensuring their increasing utilization. A recent survey revealed that the use of natural fibres in the automotive sector has doubled, rising from 9,600 tonnes in 1999 to 19,000 tonnes in 2005. Flax fibres hold the largest market share, accounting for 65% of the total. This trend can also be observed in fibre-reinforced composite materials. The use of natural fibres as reinforcements in composite materials within this sector has seen a 100% increase, from 15,000 tonnes in 1999 to 30,000 tonnes in 2005 [153].

However, certain limitations exist, including weak adhesion between the fibers and the resin matrix, limited thermal stability, degradation, hydrophilic tendencies leading to potential dimensional instability, degradation of mechanical properties at temperatures exceeding 180°-200°C, and significant variability in performance due to the organic nature of the materials [154].

Jute, Kenaf, and Sisal fibres were discarded as they are cultivated and produced in non-EU countries, particularly in Southeast Asia, Africa, or South American countries, which would increase both economic and environmental costs due to transportation.

Cotton fibre was excluded as cotton cultivation requires the highest water input, thus having the greatest environmental impact.

Hemp fiber was chosen as reinforcement material not only for its good mechanical properties but also for its lower price compared to other fibres like flax one. Moreover, our country has historically been a major producer and cultivator of hemp fibre. Hemp has a long history in the Italian peninsula, where its fibres were used to make fabrics, ropes, and highly durable lines for the naval industry. In Italy, around 80,000 hectares of land were dedicated to hemp cultivation in 1910.

There are also macroeconomic reasons, as nowadays France is the largest producer and cultivator of flax fibre, making the country a leader in the sector, which is not the case for hemp.

The hemp fibres were used in the form of fabric, it was used consisted of bidirectional woven, equal fibres aligned along the warp and the weft directions. The woven fabric was chosen because it is easy to laminate compared to short fibres or fibre bundles and facilitates the manufacturing process, thus speeding up the production process.

In composite materials, the matrix is typically composed of thermoplastic or thermosetting resins. Thermoplastic resins present several advantages, such as low processing costs, design flexibility, and ease of molding complex parts. However, their use requires high processing temperatures, which must be controlled to prevent the thermal degradation of natural fibers. An alternative is epoxy resin, a thermosetting resin, which is widely used due to its excellent mechanical properties for composites [154, 155]. Natural fiber composites made with thermosetting resins are highly resistant to solvents, tough, and resistant to creep. To facilitate production and optimize reinforcement structures, textile preforms are commonly used [156, 157].

To significantly reduce energy costs, i.e. the economic and environmental costs of the finished product, the production of the composites was a cold pressing process, without heat input, by using a specific thermosetting resin that cures at room temperature, different types of composites were produced, adjusting variables such as mold pressure, layer orientation, and the amount of resin used. The goal is to identify the production process that yields the best mechanical properties for the composite. The composites underwent tensile testing with varying fabric ply orientations. The mechanical properties of the tensile tests have been studied according to the ASTM D3039 standard [158].

The goal is to produce, characterize, and optimize a fiber-composite material reinforced with hemp fibers to be used as the skin for the previously studied honeycomb panel. Other potential applications for this material could include: the construction field, for example as a skin for panels made of agriculture waste or other natural crops [87], to reinforce wooden structural elements such as beams or columns [159].

Materials

Hemp fibres provided by Linificio e Canapificio Nazionale were utilized as reinforcement in the form of Satin Balance bidirectional woven fabric, consisting of 100% hemp fibres, with the specifications detailed in Table 38.

Table 38. Physical properties of the hemp woven fabric used.

Woven thickness	1,6 mm
Woven Warp Density	6.5 yarns/cm
Woven Weft Density	6.0 yarns/cm
Woven Density per unit area	350 g/m^2
Twist level	39 turns/m
Hemp fibre Density	1.48 g/cm^3
Tenacity at break of the yarns before weaving	24 cN/Tex [155]
Tenacity at break of the yarns after weaving	17 cN/Tex [155]

Longitudinal tensile strength of the fibres (σ_f)	429 ± 10,2 MPa [160]
Longitudinal modulus of elasticity of fibre before weaving	
at strain between 0.0% and 0.1%	62 GPa [155]
at strain between 0.3% and 0.5%	36 GPa [155]
Longitudinal modulus of elasticity of fiber after weaving	
at strain between 0.0% and 0.1%	68 GPa [155]
at strain between 0.3% and 0.5%	29 GPa [155]

In Figure 52 it is possible to observe the hemp fabric and the single hemp yard.

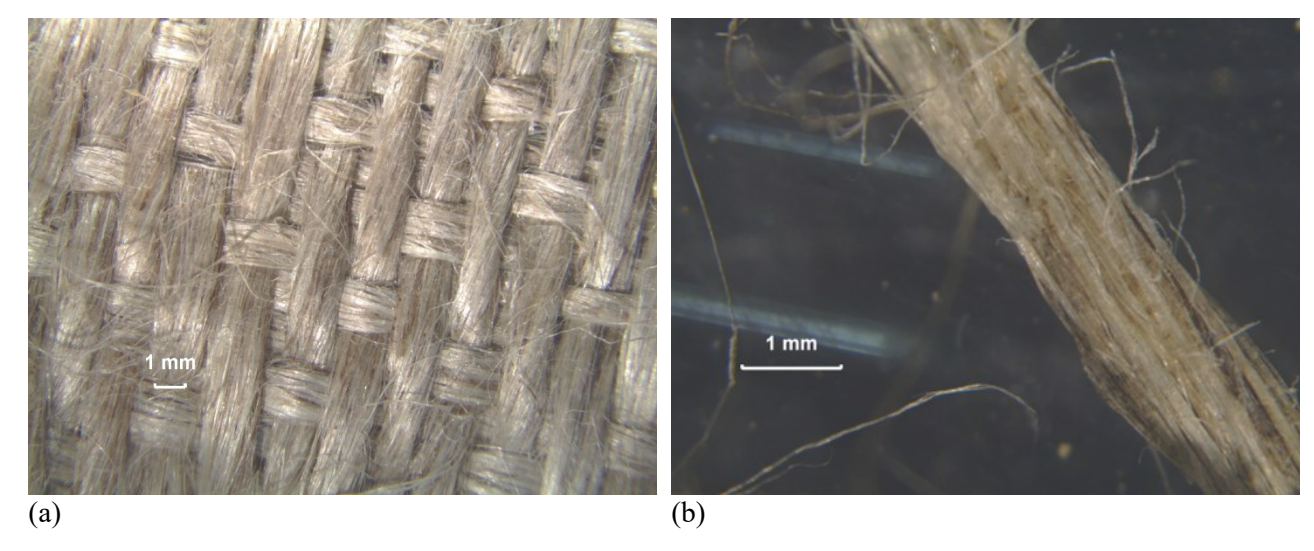


Figure 52. Microscopic images: (a) hemp woven fabric and (b) single hemp fiber.

The epoxy resin used was SX10 EVO, provided by Mike Compositi, which can harden at room temperature. It exhibits the following mechanical properties: tensile strength ranging from 55 to 65 MPa, Young's modulus of 2800 to 3300 MPa and maximum tensile deformation of 2-3% at failure.

Manufacture and Methods

The composite plies were manually laminated and then manufactured by the moulding at room temperature, at approximately 25°C. Working at room temperature in addition to reducing the production cost, avoids the degradation of natural fibres [154]. Before the lamination, the fabrics were cut to the dimensions of 200×300 mm, then were conditioned at a constant temperature of 23°C and 65% relative humidity (RH) for at least 24 hours before the composite manufacturing, in a climate chamber [155, 161]. The resin was mixed with the hardener, following the dosage indicated by the manufacturer (Mike Compositi-Mates Italy), i.e., 100:26 by weight. For the fabric impregnation process, the recommendations provided by the resin manufacturer were followed. The two plies were posed on a square steel mould with dimensions $300 \times 300 \times 10$ mm covered with a detached fabric of the type of ELA $20~\mu$ used to prevent the matrix from sticking to the metal plate and were hand layed-up, impregned manually with the epoxy resin. On top of it, a layer of Peelply PP105R100 fabric was placed (and then eliminated) to guarantee a better elimination of air bubbles trapped in the fabric and improve the matrix outflow from the specimen during the pressing phase.

Lastly, above the peel-ply was put a release fabric ELA 20 μ . Figure 53 illustrates each stage of this process. After completing the manual impregnation of the composites, they were formed using cold molding with the Metro Com machine (Comazzi, Novara, Italy) under various configurations, with no additional heat applied throughout production. This approach lowered energy consumption, though it did increase processing time. The mold includes an edge opening, allowing excess resin to flow out. The composite dimensions are $200 \times 300 \times 2$ mm.

Two composite series (detailed in Table 39) were created, based on the orientation of the hemp fabric, to assess bidirectional performance. These series were further divided into four groups (labeled A, B, C, and D) to reflect different production methods used for the composite material. The variables considered were the matrix quantity, the molding pressure, and the application time (as shown in Table 40). In Table 40, the Load/Duration ratio indicates the pressure exerted by the press on the composite and the duration of this applied pressure.

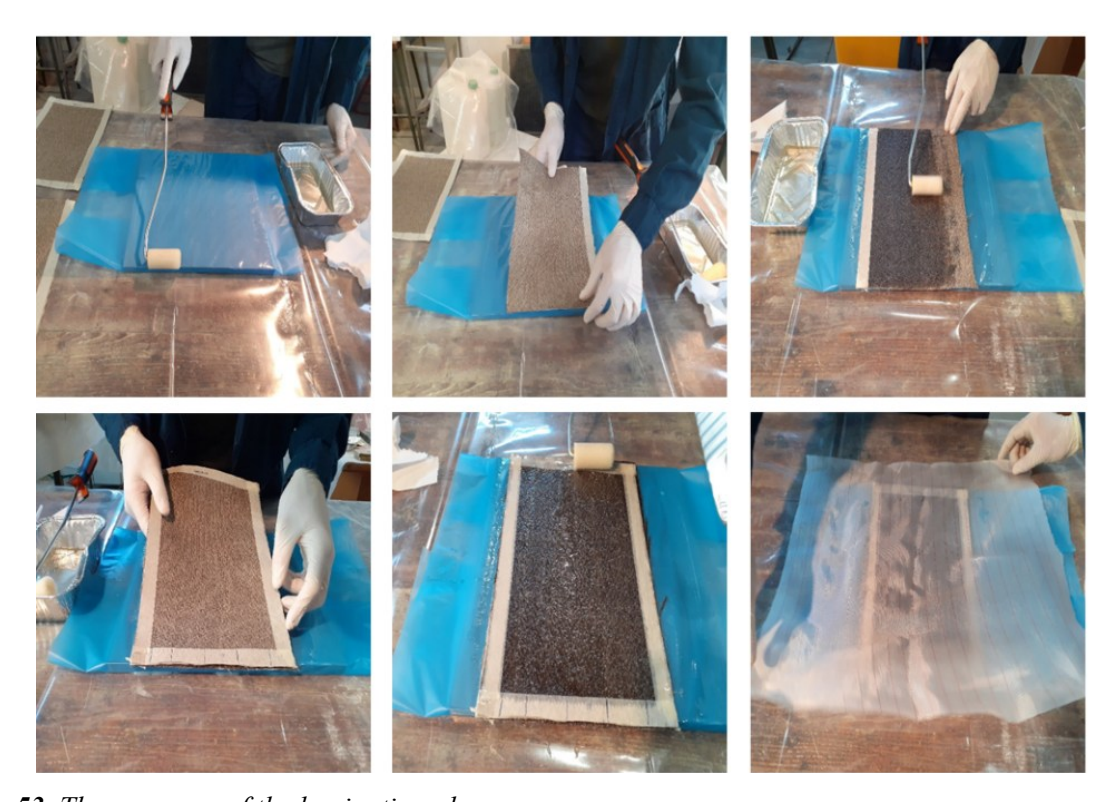


Figure 53. The sequence of the lamination phases.

Table 39. Differences between the two series.

Series	1	2
Characteristics	Two plies were stacked with the same orientation, the weft direction parallel to the test direction.	Two plies were stacked orthogonal to each other.

Table 40. Four groups of composites. The amount of liquid matrix, used during the impregnation process, is reported as the ratio of the mass of the resin to the mass of fibers, both expressed in grams.

Groups	Load /Duration	Quantity of liquid resin [g] /fiber [g]
A	20000 N/1h + 600 N/5h	200/100
В	600 N/6h	200/100
C	20000 N/1h + 600 N/5h	300/100
D	4000 N/1h + 600 N/5h	200/100

The moulding process followed for the composites of groups A, C and D were similar. The composites of groups A and C were subjected to a Load of 20000 N, as made in [155], while the composite of group D was subjected to a Load of 4000 N. After one hour the composites plate of groups A, C and

D were loaded with a load of 600 N for 5 hours. The composite plates of group B followed a different moulding process they were loaded for 6 hours with a load of 600 N. All the processes were carried out at an ambient temperature of 25°C.

Following the manufacturing, the composite plates were conditioned at a constant temperature of 23° C and 50% RH, for at least four weeks to reach the moisture content equilibrium [155, 161]. After that period all the composite plates were cut into five specimens, that will be used for the tensile tests, the dimensions of the specimens were $250 \times 25 \times 2$ mm, according to ASTM D 3039/D 3039M - 00 [158].

The online mechanical test conducted was the tensile test, for the mechanical characterization of the material.

The tensile tests were carried out using a Galdabini press machine. This test permitted us to determine the tensile strength of the composite. To prevent failure in the anchoring, as suggested by ASTM D3039 [158], the extremity of the specimens was reinforced with tabs having a thickness of 1 mm at each side, the material of the tabs was carbon fibre composite. The dimensions of the tabs are 60 × 25 × 1 mm, compliant with the standard [158]. The tensile test was performed in displacement control with a speed of 2mm/min as indicated by the USA standard D3039 [158]. The strain data acquisition was made with Digital Image Correlation (DIC) reported in Figure 54. The use of this technology requires the preparation of the specimens to create a texture, so the specimens were painted black, with a pattern of white dots. The samples were kept in the machine and tensile forces were enforced until the failure of the material. Elongation, breaking strength, ultimate tensile strength and Young modulus of the composites were recovered.



Figure 54. On the left, is the Galdabini Machine used for the tensile test. On the right, are the Digital Image Correlation instruments.

The data were statistically analyzed using the ANOVA method (Analysis of Variance) to evaluate whether the means of the measured mechanical properties of the composite material were significantly different from each other. For each test, a probability (Pr) was calculated, and the difference between means is considered significant when the Pr is less than 0.05. The method was implemented using Minitab v.18 software [114].

The microstructural analysis of the rupture surface of the specimens after the tensile test was carried out using a Scanning Electron Microscope (SEM).

Test Results

First, the results of the investigation into the components of the various composites are presented, specifically the percentage of matrix, fibers, and voids within the composites.

Figures 55 (a) and (b) show the percentages by volume and mass of the constituent of the composites.

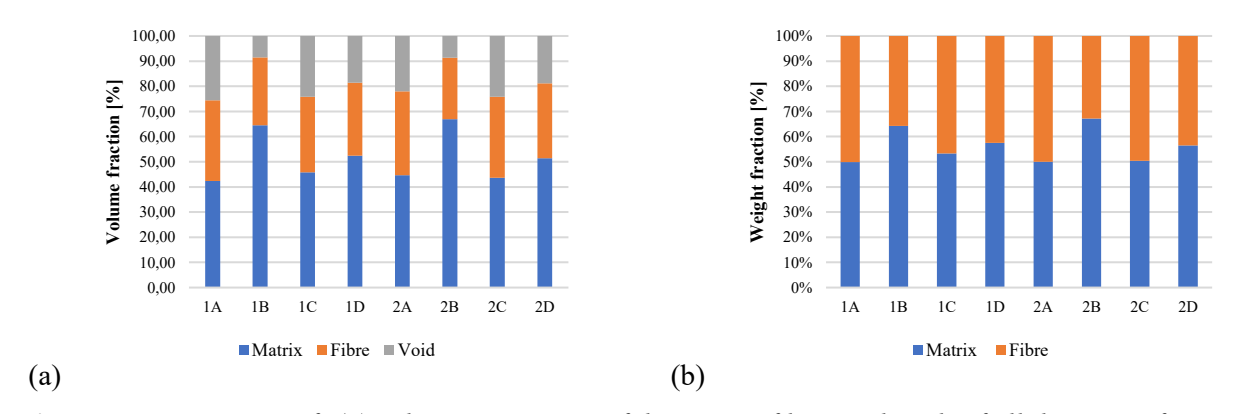


Figure 55. Histograms of: (a) volume percentage of the matrix, fibres and voids of all the types of composites and (b) weight percentage of the matrix and fibres.

It was noted that with an increase in the molding load, the fiber and void volume fractions rise from 25% and 10% to 33% and 24%, respectively, while the matrix volume fraction decreases from 65% to 43%. This suggests inadequate fiber impregnation by the resin, likely due to its high viscosity when used at room temperature. The applied load is directly related to the volume of voids and fibers in the composite and inversely related to the matrix volume.

Once the initial experimental phase related to the material composition was completed, the tensile testing phase on the specimens began.

The tension tests show elastic-brittle behaviour for all the different types of composites. Figure 56 (a) shows the stress-strain curve of specimen 1A1, in which it is possible to see the elastic-brittle behaviour, the stress-strain curves associated with the other specimens will not be reported as they have the same trend.

In Figure 56 (b) it is possible to observe a decrease in the stiffness of the material up to 0.5% of deformation, so a non-linear behavior, after this value the material assumes a linear behaviour up to the brittle failure.

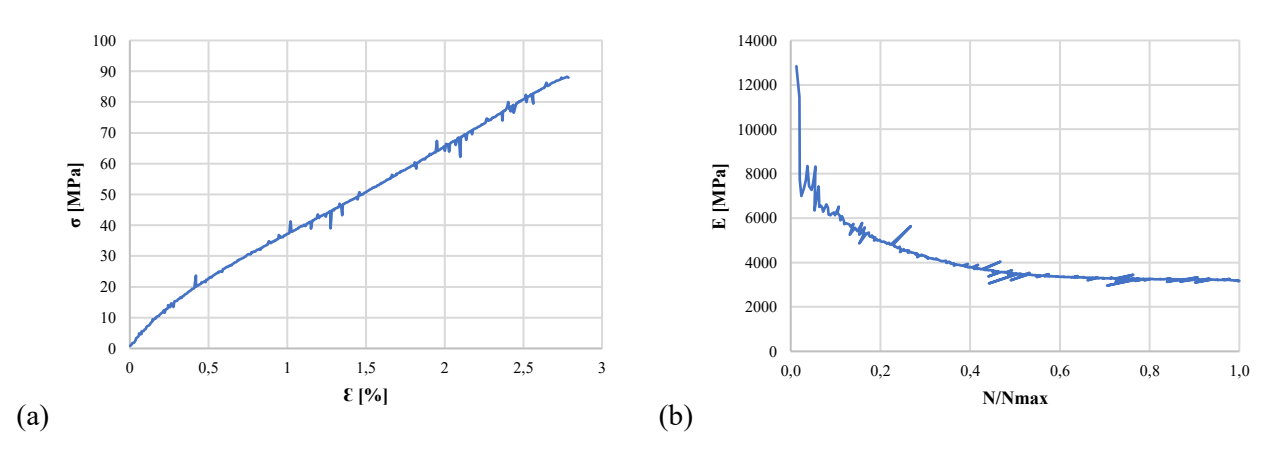


Figure 56. (a) Stress-Strain in the longitudinal direction and (b) Elastic modulus- N/N_{max} for the generic samples 1A1.

The elastic module E shows a peak during the initial phase of loading, with values similar to Young's modulus of the hemp fibres, and then a rapid decrease occurs till $0.1~N/N_{max}$, where N is the tensile load applied to the specimens. The decrease continues less rapidly up to $0.6~of~N/N_{max}$, from this point

E reached almost a constant value until the failure. The loss of stiffness between 0.1 and 0.6 of N/N_{max} is 50-60%, this is due to multiple factors:

1) Detachment between individual fibers and the matrix, or between yarns and the matrix, occurs due to weak adhesion between the materials, a typical issue in composites with natural fibers. This phenomenon is visible in the SEM images in Figure 57, showing the fracture surfaces of specimens 1A1, 1B2, 2B4, 1C3, and 2C5, which serve as representatives for each composite type.

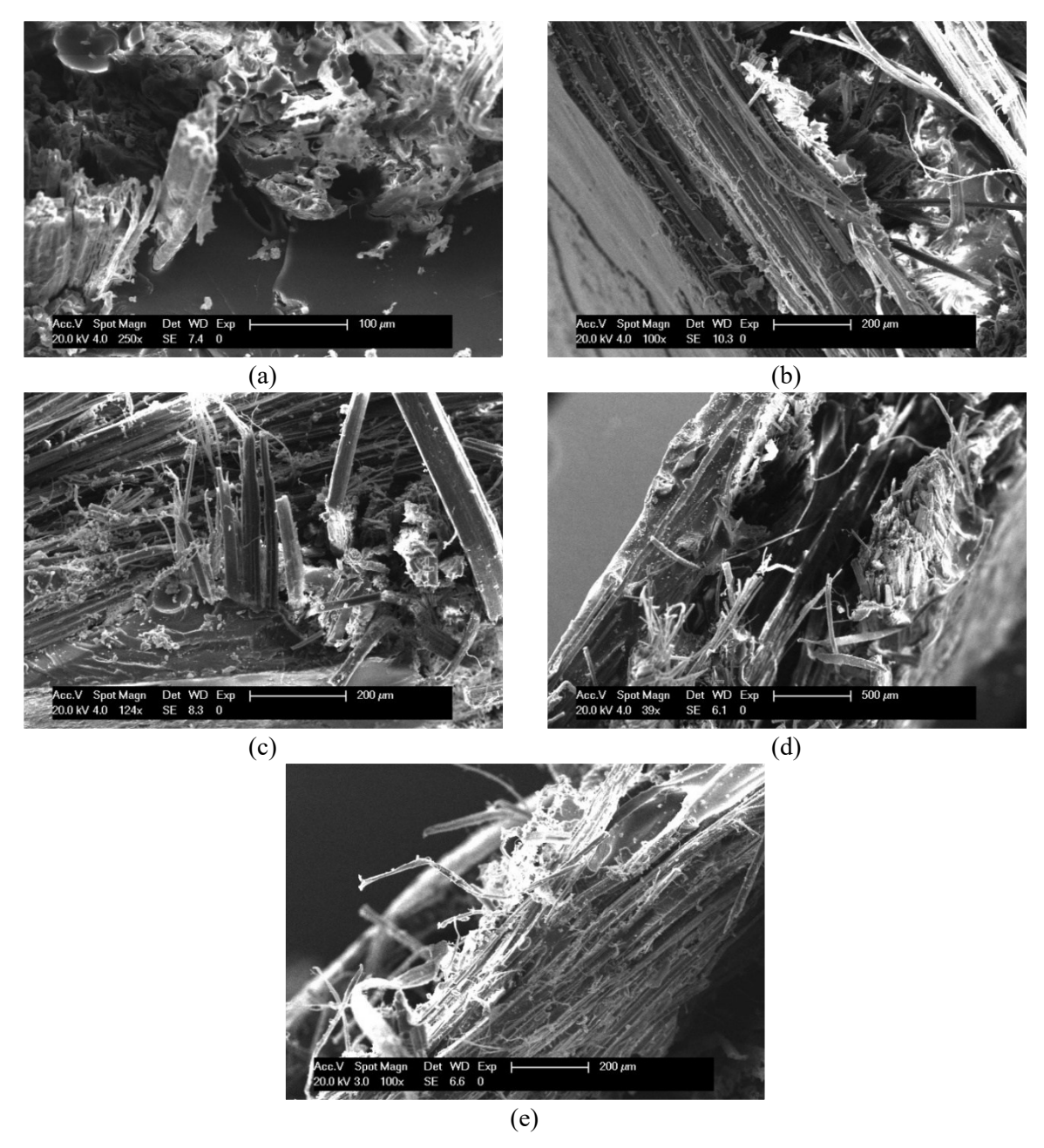


Figure 57. Images obtained from the Scanning Electron Microscope (SEM) for the fracture surfaces of some of the specimens tested with tension test: (a) are reported the specimens 1A1; (b) are reported the specimens 1B2; (c) are reported the specimens 2B4; (d) are reported the specimens 1C3; (e) are reported the specimens 2C5.

2) Fraying of the threads of the fabric, caused by incorrect impregnation of the fabric, is probably caused by the cold moulding process, which proves the fact that the resin has a high viscosity.

This phenomenon can be seen in Figures 58 and 57 (c), which display SEM images of the fracture surfaces for specimens 1A2 and 1B2. The images reveal several detached fiber bundles, along with a reduced torsion angle, resulting in elongation and a loss of stiffness in the composite material.

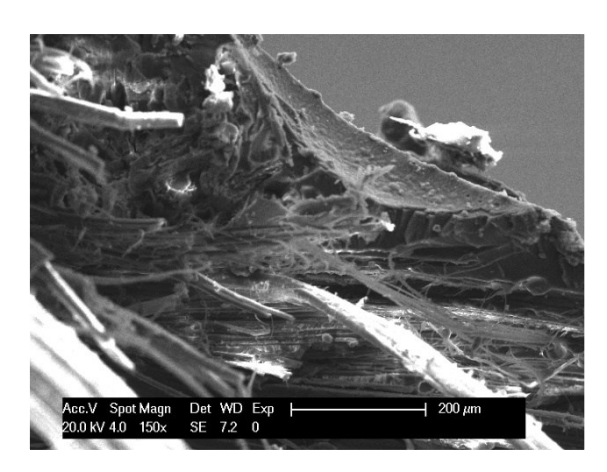


Figure 58. Images obtained from the Scanning Electron Microscope (SEM) for the fracture surfaces of the specimens 1A2 tested with tension test.

3) Voids were observed in the composite structure. SEM analysis showed that in composites produced with higher pressure, like composites A and C, the resin had difficulty penetrating, leading to a few voids within the composite, as illustrated in Figures 57 (d) and 58. In contrast, composites made with lower pressure, such as those in group B, contain a larger number of small voids, as shown in Figures 59 and 57 (c). This may be attributed to the lower compaction pressure during material formation, along with the absence of vacuum treatment in the composite process.

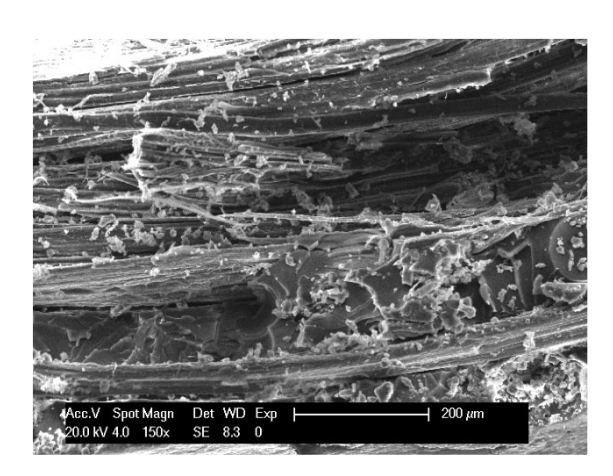


Figure 59. Images obtained from the Scanning Electron Microscope (SEM) for the fracture surfaces of the specimens 1B2 tested with tension test.

No significant differences were noted between Series 1 and Series 2 using the SEM.

The density of the composites changes between 0.95-1.15 g/cm3, the maximum density is associated with the samples of group B, while the lower density is related to the samples of group A. There is no difference in density between the two series, indicating that this value depends only on the manufacturing and lamination process of the composite as expected.

Table 41 reports the average and standard deviation of the mechanical characteristics of the different composite materials studied.

Table 41. Average and standard deviation, in brackets, of displacement, maximum load, strain in longitudinal and transverse direction, tensile strength, Coeff. of Poisson, Young modulus at 0.1 of N/N_{max} , Young modulus at 0.6 of N/N_{max} , for all the composites.

Spec	cimen	Displacement	Force	$\epsilon_{ m L}$	ε _T	σ	Coeff.	E (0.1	E (0.6
Serie	Group	[mm]	[N]	[%]	[%]	[MPa]	Poisson	N/Nmax) [GPa]	N/N_{max}) [GPa]
1	A	3.9	3770.2	2.75	-0.64	86.6	0.23	6.04	3.34
		(± 0.2)	(± 199)	(± 0.1)	(± 0.1)	(± 3)	(± 0.04)	(± 0.31)	(± 0.07)
	В	3.6	4554.7	2.54	-0.16	88.3	0.06	6.52	4.31
		(± 0.1)	(± 149)	(± 0.1)	(± 0.1)	(± 3)	(± 0.01)	$(\pm \ 0.85)$	(± 0.52)
	C	3.9	3781.2	2.70	-0.23	81.2	$0.08~(\pm$	4.84	3.31
		(± 0.1)	(± 93)	(± 0.3)	(± 0.1)	(± 3)	0.02)	(± 0.16)	(± 0.15)
	D	3.6	3871.3	2.55	-0.28	80.3	0.11	7.18	3.66
		(± 0.1)	(± 109)	(± 0.1)	(± 0.1)	(± 4)	(± 0.01)	$(\pm \ 0.44)$	(± 0.15)
2	A	3.6	3671.6	2.72	-0.74	88.4	0.27	7.23	3.70
		(± 0.1)	(± 122)	(± 0.1)	(± 0.1)	(± 4)	(± 0.03)	(± 0.32)	(± 0.17)
	В	3.4	4269.1	2.51	-0.37	75.1	0.15	5.58	3.81
		(± 0.2)	(± 188)	(± 0.1)	(± 0.1)	(± 3)	(± 0.03)	(± 0.34)	(± 0.11)
	C	3.6	3813.3	2.49	-0.55	88.4	0.22	7.18	3.88
		(± 0.1)	(± 104)	(± 0.1)	(± 0.1)	(± 2)	(± 0.02)	(± 0.18)	(± 0.09)
	D	3.6	3953.4	2.51	-0.46	84.2	0.18	6.53	3.86
		$(\pm \ 0.1)$	(± 96)	(± 0.1)	(± 0.1)	(± 1)	(± 0.02)	(± 0.72)	(± 0.12)

The groups exhibiting the highest longitudinal and transversal deformations are those with the greatest percentage of voids, namely group A and group C, while group B, with the lowest void percentage, shows the least deformation in both directions.

Regarding tensile stress, no significant difference is observed between the groups. Series 1 samples demonstrate tensile stress values 2% to 8% lower than Series 2, likely due to the slightly higher warp density of 6.5 yarns/cm compared to the weft density of 6.0 yarns/cm, reflecting a minor imbalance in the woven fabric's bidirectionality. Since Series 1 samples have both hemp fabric layers aligned with the weft direction, they display slightly lower mechanical properties compared to Series 2, where one layer aligns with the warp direction.

Additionally, Series 1 has an average transversal deformation lower than that of Series 2 (ranging from 13% to 58%), possibly due to improved interlocking between the two fabric layers.

The results indicate that compaction pressure did not significantly affect the mechanical properties of the composite. Therefore, the composite in group B best meets the initial objectives: minimizing the environmental and economic impact of the production process and the final product without compromising its mechanical properties. Group B composites maintain the same mechanical characteristics as others but require a lower compaction load in production, resulting in reduced energy consumption and lower environmental and economic costs.

To better understand the data reported in Table 39 box plots are reported in Figure 60 for all the types of composites for the main mechanical properties: σ , coefficient of Poisson, E at 0.1 N/N_{max} and E at 0.6 N/N_{max}. On each box, the red line is set at the median value, while the bottom and top edges of the box indicate, respectively, the 25th and 75th percentiles; the black whiskers extend to the most extreme data points which are not considered outliers, while the outliers are plotted individually using a red cross marker.

Box plots in Figure 60 (a), show that for groups A and C (groups characterized by high forming pressure), the specimens from series 2 exhibit higher $E_{0.1}$ values compared to those from series 1. Conversely, for the specimens from groups B and D, where the compaction pressure during forming was low, the opposite trend is observed.

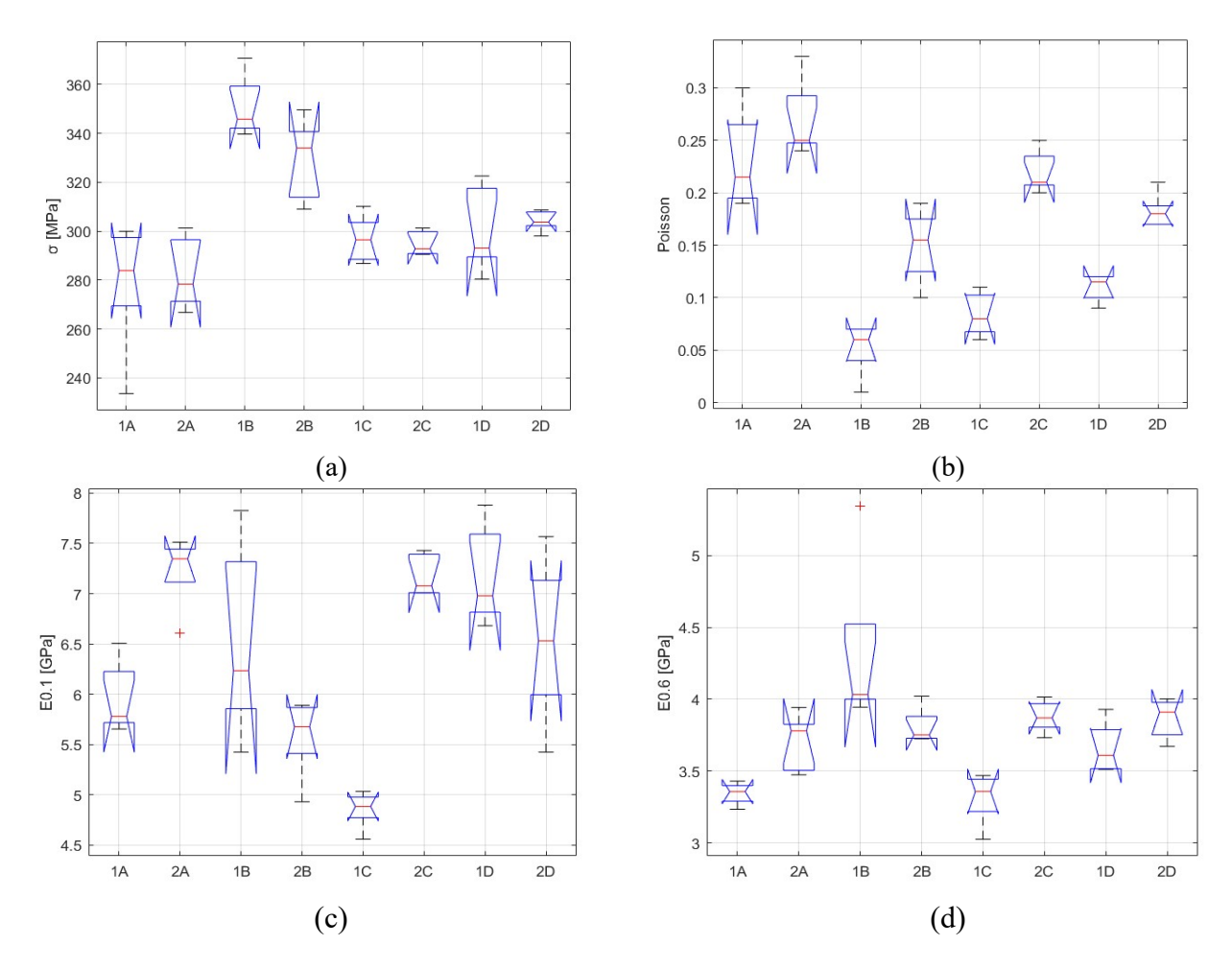


Figure 60. Box plots of the mechanical properties for all the tested species: (a) Strength σ ; (b) coefficient of Poisson; (c) Elastic modulus E for 0.1 N/N_{max}; (d) Elastic modulus E for 0.6 N/N_{max}.

As can be seen from Table 42 there is no statistically significant variation in the tensile strength of the material between the two series. Regarding the groups, the only one whose specimens show statistically significant differences compared to the others is group B, with its tensile strength values being higher than the others.

In Table 43 it is evident that there is a difference between the specimens of series 1 and those of series 2, except those belonging to group A. Specifically, the specimens from series 2 exhibit higher Poisson ratios than those from series 1. This means that the specimens from series 2 undergo greater transverse deformations compared to those from series 1, given the same longitudinal deformation. Additionally, group A has a p-value lower than 0.05 compared to the other groups, indicating that the specimens from this group exhibit greater deformations.

Tables 44 and 45 do not show a clear difference among the groups in terms of Young modulus.

Table 42. P-values for σ . Values lower than 0.05 are indicated in bold.

	2A	1B	2B	1C	2C	1D	2D
1A	1.000	0.000	0.000	0.585	0.704	0.326	0.172
2A		0.000	0.001	0.819	0.901	0.561	0.344
1B			0.328	0.000	0.000	0.000	0.001
2B				0.033	0.021	0.090	0.188
1C					1.000	1.000	0.992
2C						0.998	0.973
1D							1.000

Table 43. P-values for Poisson coefficient. Values lower than 0.05 are indicated in bold.

	2A	1B	2B	1C	2C	1D	2D
1A	0.467	0.000	0.011	0.000	0.999	0.000	0.251
2A		0.003	0.000	0.000	0.156	0.000	0.001
1B			0.001	0.662	0.000	0.094	0.000
2B				0.038	0.023	0.532	0.722
1C					0.000	0.878	0.000
2C						0.000	0.457
1D							0.018

Table 44. P-values for $E_{0.1}$. Values lower than 0.05 are indicated in bold.

	2A	1B	2B	1C	2C	1D	2D
1A	0.014	0.708	0.950	0.047	0.021	0.021	0.686
2A		0.444	0.001	0.000	1.000	1.000	0.465
1B			0.137	0.001	0.542	0.544	1.000
2B				0.403	0.001	0.001	0.128
1C					0.000	0.000	0.001
2C						1.000	0.564
1D							0.566

Table 45. P-values for $E_{0.6}$. Values lower than 0.05 are indicated in bold.

	2A	1B	2B	1C	2C	1D	2D
1A	0.441	0.000	0.143	1.000	0.061	0.580	0.073
2A		0.011	0.996	0.271	0.945	1.000	0.963
1B			0.060	0.000	0.149	0.006	0.126
2B				0.067	1.000	0.979	1.000
1C					0.025	0.394	0.030
2C						0.866	1.000
1D							0.899

Table 46 shows the fiber and resin used, the manufactured process, the tensile strength, and elastic modulus of different composites made in other research found in the literature, as well as the data of the composite relating to series 1 group B, chosen as representative of all those manufactured in the present study.

Few papers describe a manufacturing process similar to the one used in this research where there is no heat transfer in the press mould. Sivasankar et al. [162] have created a composite consisting of 50 % hemp fiber and 50 % Abaca fiber, in the form of a unidirectional fabric, and an epoxy resin. The composite was made using a hand rolling and cold moulding process; tensile tests showed an average composite tensile stress of 48.5 MPa. Shebaz Ahmed et al. [163] have created a composite of hemp and flax fiber, in the form of a unidirectional epoxy matrix fabric, whose tensile stress was found to

be equal to 46.1 MPa. In both cases, the tensile stress associated with fibre-reinforced composites is lower than those obtained in this research.

Higher values of strength can be obtained with the hot moulding process. In the research of Corbin et. al. [155], hemp fiber and epoxy resins are hot moulded at 130 °C at a pressure of 3 bar for 1 h. This process guarantees a complete impregnation of the hemp fiber fabric due to the fluidity of the resin as confirmed by the low value, 0.5 % - 3 %, of the percentage (by volume) of voids, much lower than the percentage of voids found in this paper. The tensile stress of the composite in [155] was equal to 100 MPa for the direction parallel to the warp and 200 MPa for that parallel to the weft, while Young's modulus was equal to 12 GPa along the warp and 16 GPa along the weft direction. Lower mechanical performances are shown when natural adhesives like PLA [164, 165] and cashew nutshell liquid are used, due to the lower mechanical properties of the resin itself. The design of the mechanical characteristics should depend on the field of application of the material.

Table 46. Values of tensile stress and Young's modulus for composites manufactured in different research found in literature and data of the composite relating to series 1 group B, manufactured in this research.

Authors	Fiber	Matrix	Production process	Tensile strength [MPa]	Young's modulus E [MPa]
Samples 1B	Hemp fiber bi- directional fabric	Epoxy Resin	Cold moulding	88	4318
[162]	Unidirectional, Abaca and Hemp fiber	Epoxy Resin	Cold moulding	49	/
[163]	Unidirectional woven fabric of hemp and flax fiber	Epoxy Resin	Cold moulding	46	/
[155]	Hemp unidirectional woven fabric	Epoxy resin	Hot moulding at 130°C	90-210	11000- 20000
[164]	Non-woven hemp fiber	PLA	Hot moulding at 170°C	41	5600
[165]	Short hemp fiber	Polypropylene	Hot moulding at 200 °C	25	/
[166]	Non-woven fiber hemp	Cashew nutshell liquid	Moulding	29	7200

Discussion

Some conclusions can be drawn:

- The Young's modulus value, measured from 0.6 N/Nmax until failure, ranges between 3.3 and 4.4 GPa. This value is 8% to 30% higher than the modulus of the epoxy resin alone, attributed to the reinforcement provided by the hemp fibers in the composite, which thereby enhances the mechanical properties of the resin.
- The presence of hemp fibres increased the maximum tensile stress of the matrix by 23% to 64%, depending on the groups.
- The groups showing the highest longitudinal and transverse deformations are those with the highest percentage of voids, namely group A and group C. In contrast, group B, which has the lowest void percentage, exhibits the least longitudinal and transverse deformations. This is correlated with a higher stiffness value in the composite of group B compared to groups A and C.
- It has been observed that as the press load increases, the percentage (by volume) of fibres and voids increases, while the percentage (by volume) of the matrix decreases. This indicates a low impregnation of the fibres by the matrix, as observed in Figures 57 (c) 58 where the fabric

is less impregnated compared with the fabric of the composite shown in Figure 59. This can be attributed to the high viscosity of the resin caused by a production process without heat transfer. The high viscosity of the resin did not ensure an optimal impregnation of the woven fabric, trapping air bubbles during the manufacturing. Even using high pressures for the moulding process led to only a reduction of the present resin in the composite, without reducing the void volume. This is because the resin is unable to penetrate the internal layers of the fabric, remaining exclusively on the external part of the same, impregnating only the external fibers of the fabric and not the internal ones. This creates an external surface that prevents the air bubbles from escaping, even under high pressures. This applies both to the fabric as a whole and to the fiber bundles that make up the fabric, where only the external fibers of the bundle are impregnated by the resin, while the internal fibers are not.

• The tensile stress of the composites was found to be independent of the press load. This is partly due to the factors discussed previously and the lamination process used. A hand lamination process was applied without any vacuum or specialized high-temperature autoclave treatment. Such treatments would have significantly reduced the volume of voids and excess matrix in the composite.

Acknowledgment

The work for this PhD thesis has been one of the most challenging endeavours of my life, as it represents the culmination of an academic journey where one chooses to push themselves to the limit. I sincerely thank my supervisor, Prof. Luisa Molari, first and foremost for giving me the opportunity to engage with the world of research. I am deeply grateful for her guidance throughout my research journey and for her invaluable advice. Thank you for dedicating part of your time not only to reading and discussing with me the drafts of my thesis and the various scientific articles I authored but also for supporting the other projects carried out during my PhD program.

A special thanks go to my co-supervisors: Prof. Vincent Placet, who supported me during my external research period with his team at the University of Besançon, France, and Prof. Stefania Manzi, without whose support it would not have been possible for me to conduct the fundamental experimental campaigns. To both of you, my heartfelt gratitude for your time and assistance in writing this thesis.

I am also deeply indebted to the technical staff of the LISG laboratory at DICAM. In particular, I would like to extend my sincere thanks to Mario Marcolongo and Roberto Bianchi for their help in the practical execution of the experimental tests included in my thesis projects. Without their assistance, these tests would not have been possible.

A special mention goes to Mattia Ferrante and Giulia Conidi for the time and effort they dedicated to the success of the particleboard panel project, as well as to Pierluigi Zambelli, whose coordination was essential for the project's inception.

I would also like to express my immense gratitude to my colleagues, Eleonora Cintura, Letizia Crociati, and Leo Amaral, who, over these three years, never ceased to encourage and support me, showing their unwavering appreciation and kindness.

Lastly, I want to thank my parents, without whom I would not have been able to embark on this research journey.

References

- [1] J. Jiang, B. Ye and J. Liu, «Research on the peak of CO₂ emissions in the developing world: Current progress and future prospect», *Applied Energy*, vol. 235, pp. 186-203, 2019.
- [2] U. Al-mulali and C. N. B. Che Sab, «The impact of energy consumption and CO₂ emission on the economic and financial development in 19 selected countries», *Renewable and Sustainable Energy Reviews*, vol. 16, n. 7, pp. 4365-4369, 2012.
- [3] S. Di Fazio and L. Lamberto, «Construction Design Systems for Sustainable Farm Bulding. A case study in Calabria, Italy», in XVIIth World Congress of the International Commission of Agricultural and Biosystems Engineering (CIGR), Québec City, Canada, 2010.
- [4] M. Maraldi, L. Molari, N. Regazzi and G. Molari, «Analysis of the parameters affecting the mechanical behaviour of straw bales under compression», *Biosystems Engineering*, vol. 160, pp. 179-193, 2017.
- [5] M. Maraldi, L. Molari, N. Regazzi and G. Molari, «Method for the characterisation of the mechanical behaviour of straw bales», *Biosystems Engineering*, vol. 151, pp. 141-151, 2016.
- [6] L. Molari, F. S. Coppolino and J. J. García, «Arundo donax: A widespread plant with great potential as sustainable structural material», Construction and Building Materials, vol. 268, n. 1349, 2021.
- [7] E. A. Nurdiah, «The Potential of Bamboo as Building Material in Organic Shaped Buildings», *Procedia Social and Behavioral Sciences*, vol. 216, pp. 30-38, 2016.
- [8] L. Balaguer, «Las plantas invasoras: el reflejo de una sociedad crispada o una amenaza científicamente contrastada?», *Historia Natural*, n. 5, pp. 32-41, 2004.
- [9] O. Polunin and A. J. Huxley, Flowers of the Mediterranean, Londra: Chatto and Windus xii, 1965.
- [10] F. J. Andreu-Rodríguez, A. Perez-Espinosa, M. D. Pérez-Murcia, R. Moral, E. Agulló, M. Ferrández-Villena, M. T. Ferrández-García and M. A. Bustamante, «Near infrared reflectance spectroscopy (NIRS) for the assessment of biomass production and C sequestration by *Arundo donax L*. in salt-affected environments», *Agricultural Water Management*, vol. 183, pp. 94-100, 2017.
- [11] F. Zanetti, E. Alexopoulou, D. Scordia, W. Zegada-Lizarazu, M. Christou, G. Testa, S. L. Cosentino and A. Monti, «Long-Term Yields of Switchgrass, Giant Reed, and Miscanthus in the Mediterranean Basin», *BioEnergy Research*, vol. 8, n. 4, pp. 1492-1499, 2015.
- [12] R. Pilu, A. Manca and M. Landoni, «Arundo donax as an energy crop: pros and cons of the utilization of this perennial plant», Environmental Science, Agricultural and Food Sciences, vol. 58, n. 1, 2013.
- [13] S. Cosentino and V. Copani, «Canna comune per la destinazione energetica. Il punto sulla propagazione agamica negli ambienti del Meridione d'italia», Progetto di ricerca SUSCACE e FAESI, 2012.
- [14] K. J. Niklas, «Modes of Mechanical Failure of Hollow, Septate Stems», vol. 81, n. 1, pp. 11-21, 1998.
- [15] A. A. Shatalov and H. Pereira, «Influence of stem morphology on pulp and paper properties of *Arundo donax L.* reed», *Industrial Crops and Products*, vol. 15, pp. 77-83, 2002.
- [16] T. García-Ortuño, J. Andréu-Rodríguez, M. T. Ferrández-García, M. Ferrández-Villena and C. E. Ferrández-García, «Evaluation of the physical and mechanical properties of particleboard made from giant reed (*Arundo donax L.*)», *BioResources*, vol. 6, n. 1, pp. 477-486, 2011.

- [17] S. Greco, L. Molari, G. Valdrè and J. J. Garcia, «Multilevel analysis of six species of Phyllostachys bamboo and *Arundo donax*: preliminary survey on Italian grown stands», *Wood Science and Technology*, vol. 58, n. 3, p. 1025–1049, 2024.
- [18] H. C. Spatz, H. Beismann, F. Brückert, A. Emanns and T. Speck, «Biomechanics of the giant reed *Arundo donax*», *Philosophical Transactions of the Royal Society B*, vol. 352, n. 1349, pp. 1-10, 1997.
- [19] S. Abrantes, M. E. Amaral, A. P. Costa, A. A. Shatalov and A. P. Duarte, «Evaluation of giant reed as a raw-material for paper production», *Appita Journal*, vol. 60, n. 5, pp. 410-415, 2007.
- [20] A. A. Shatalov and H. Pereira, «Xylose production from giant reed (*Arundo donax L.*): Modeling and optimization of dilute acid hydrolysis», *Carbohydrate Polymers*, vol. 87, n. 1, pp. 210-217, 2012.
- [21] M. J. Ahmed, «Potential of *Arundo donax L*. stems as renewable precursors for activated carbons and utilization for wastewater treatments: Review», *Journal of the Taiwan Institute of Chemical Engineers*, vol. 63, pp. 336-343, 2016.
- [22] M. Pelegrín, J. A. Sáez-Tovar, J. Andreu-Rodríguez, M. D. Pérez-Murcia, E. Martínez-Sabater, F. C. Marhuenda-Egea, A. Pérez-Espinosa, M. A. Bustamante, E. Agulló, A. Vico, C. Paredes and R. Moral, «Composting of the invasive species *Arundo donax* with sewage and agri-food sludge: Agronomic, economic and environmental aspects», *Waste Management*, vol. 78, pp. 730-740, 2018.
- [23] M. Borin, A. C. Barbera, M. Milani, G. Molari, S. M. Zimbone and A. Toscano, «Biomass production and N balance of giant reed (*Arundo donax L*.) under high water and N input in Mediterranean environments», *European Journal of Agronomy*, vol. 51, n. 10, pp. 117-119, 2013.
- [24] L. Corno, R. Pilu and F. Adani, «*Arundo donax L.*: A non-food crop for bioenergy and biocompound production», *Biotechnology Advances*, vol. 32, n. 8, pp. 1535-1549, 2014.
- [25] D. Scordia, S. L. Cosentino, J. W. Lee and T. W. Jeffries, «Bioconversion of giant reed (*Arundo donax L*.) hemicellulose hydrolysate to ethanol by Scheffersomyces stipitis CBS6054», *Biomass and Bioenergy*, vol. 39, pp. 296-305, 2012.
- [26] G. Ragaglini, F. Dragoni, M. Simone and E. Bonari, «Suitability of giant reed (*Arundo donax L.*) for anaerobic digestion: effect of harvest time and frequency on the biomethane yield potential», *Bioresource Technology*, vol. 152, pp. 107-115, 2014.
- [27] M. Martínez-Sanz, E. Erboz, C. Fontes and A. López-Rubio, «Valorization of *Arundo donax* for the production of high performance lignocellulosic films», *Carbohydrate Polymers*, vol. 199, pp. 276-285, 2018.
- [28] T. Scalici, V. Fiore and A. Valenza, «Effect of plasma treatment on the properties of *Arundo Donax L*. leaf fibres and its bio-based epoxy composites: A preliminary study», *Composites Part B: Engineering*, vol. 94, pp. 167-175, 2016.
- [29] C. E. Ferrandez-Garcia, T. García-Ortuño, J. Andreu, M. Ferrández-Villena and M. T. Ferrández García, «Mechanical Properties of a Cement Mortar Reinforced with *Arundo donax L.* Reeds», in *Proc. of the Second Intl. Conf. on Advances In Civil, Structural and Environmental Engineering- ACSEE 2014.*, Zurich, Switzerland, 2014.
- [30] F. Gini and F. Piva, «"Fibre naturali e sostenibilità". L'utilizzo delle fibre di canna plaustre per una tecnologia innovativa nel riedificamento del Centro d'incontro per anziani di via Vipacco.», Tesi di laurea, presso il Politecnico di Torino, Torino, 2019.
- [31] B. Brunetti, «Baraccas: esempi antichi di architettura in canna palustre», *Architetturaecosostenibile.it*, Wednesday Gennuary 2015.

- [32] E. Cintura, P. Faria, L. Molari, L. Barbaresi, D. D'Orazio and L. Nunes, «Characterization of an *Arundo donax*-based composite: A solution to improve indoor comfort», *Industrial Crops and Products*, vol. 208, 2024.
- [33] C. E. Ferrandez-Garcia, J. Andreu, M. T. F. García and T. García-Ortuño, «Panels made from giant reed bonded with non-modified starches», *BioResources*, vol. 7, n. 4, 2012.
- [34] M. Ferrandez-Villena, C. E. Ferrandez-Garcia, T. Garcia-Ortuño, A. Ferrandez-Garcia and M. T. Ferrandez-Garcia, «The Influence of Processing and Particle Size on Binderless Particleboards Made from *Arundo donax L*. Rhizome», *Polymers*, vol. 12, n. 3, 2020.
- [35] E. Ceotto, C. Vasmara, R. Marchetti, S. Cianchetta and S. Galle, «Biomass and methane yield of giant reed (*Arundo donax L.*) as affected by single and double annual harvest», *GCB Bioenergy: Bioproducts for a Sustainable Bioeconomy*, vol. 13, n. 3, pp. 393-407, 2021.
- [36] E. Alexopoulou, F. Zanetti, D. Scordia, W. Zegada-Lizarazu, M. Christou, G. Testa, S. L. Cosentino and A. Monti, «Long-Term Yields of Switchgrass, Giant Reed, and Miscanthus in the Mediterranean Basin», *BioEnergy Research*, vol. 8, n. 4, p. 1492–1499, 2015.
- [37] T. Danelli, A. Sepulcri, G. Masetti, F. Colombo, S. Sangiorgio, E. Cassani, S. Anelli, F. Adani and R. Pilu, «*Arundo donax L.* Biomass Production in a Polluted Area: Effects of Two Harvest Timings on Heavy Metals Uptake», *Applied Sciences*, vol. 11, n. 3, 2021.
- [38] S. Kausar, Q. Mahmood, I. A. Raja, A. Khan, S. Sultan, M. A. Gilani and S. Shujaat, «Potential of *Arundo donax* to treat chromium contamination», *Ecological Engineering*, vol. 42, pp. 256-259, 2012.
- [39] B. Barbosa, S. Boléo, S. Sidella, J. Costa, M. P. Duarte, B. Mendes, S. Cosentino and A. L. Fernando, «Phytoremediation of Heavy Metal-Contaminated Soils Using the Perennial Energy Crops Miscanthus spp. and *Arundo donax L.*», *BioEnergy Research*, vol. 8, n. 4, pp. 1500-1511, 2015.
- [40] N. Fiorentino, V. Ventorino, C. Rocco, V. Cenvinzo, D. Agrelli, L. Gioia, I. Di Mola, P. Adamo, O. Pepe and M. Fagnano, «Giant reed growth and effects on soil biological fertility in assisted phytoremediation of an industrial polluted soil», *Science of The Total Environment*, vol. 575, pp. 1375-1383, 2017.
- [41] G. Mavrogianopoulos, V. Vogli and S. Kyritsis, «Use of wastewater as a nutrient solution in a closed gravel hydroponic culture of giant reed (*Arundo donax*)», *Bioresource Technology*, vol. 82, n. 2, pp. 103-107, 2002.
- [42] A. Joseph, «Liquid water lake under ice in Mars's southern hemisphere—Possibility of subsurface biosphere and life», *Water Worlds in the Solar System*, pp. 453-522, 2023.
- [43] J. Lange, A. von der Heyden and S. Grimm, «Sandwich panels in buildings: Core, structure and design», in *The Seventh International Conference on Structural Engineering, Mechanics and Computation*, Cape Town, 2019.
- [44] B. V. Ramnath, K. Klagarraja and C. Elanchezhian, «Review on Sandwich Composite and their Applications», *Materials Today: Proceedings*, vol. 16, n. 2, pp. 859-864, 2019.
- [45] L. B. L. Gato, S. L. M. Ribeiro Filho, T. H. Panzera, M. L. P. Tonatto, A. L. Christoforo and F. Scarpa, «Sandwich Structures Made of Discarded Bottle Caps Core and Hybrid Glass Fibre Composite Skins», *Applied Composite Materials*, vol. 28, n. 1, p. 1427–1449, 2021.
- [46] P. R. Oliveira, M. May, S. Kilchert, L. Á. de Oliveira, T. H. Panzera, V. Placet, F. Scarpa and S. Hiermaier, «Eco-friendly panels made of autoclaved flax composites and upcycled bottle caps core: experimental and numerical analysis», *Composites Part C: Open Access*, vol. 4, 2021.

- [47] S. Antony, A. Cherouat and G. Montay, «Fabrication and Characterization of Hemp Fibre Based 3D Printed Honeycomb Sandwich Structure by FDM Process», *Applied Composite Materials*, vol. 27, n. 9, p. 935–953, 2020.
- [48] F. Napolitano, J. C. dos Santos, R. J. da Silva, G. G. Braga, R. T. S. Freire and T. H. Panzera, «Sandwich panels made of aluminium skins and gapped-bamboo ring core», *Journal of the Brazilian Society of Mechanical Sciences and Engineering*, vol. 45, n. 5, 2023.
- [49] S. Darzi, H. Karampour, H. Baillères, B. P. Gilbert and D. Fernando, «Load bearing sandwich timber walls with plywood faces and bamboo core», *Structures*, p. 2437–2450, 2020.
- [50] Y. Fu and P. Sadeghian, «Bio-Based Sandwich Beams made of Paper Honeycomb Cores and Flax FRP Facings: Flexural and Shear Characteristics», *Structures*, vol. 54, n. 1, pp. 446-460, 2023.
- [51] L. A. de Oliveira, G. Luiza, C. Coura, M. L. Passaiatonatto, T. H. Panzera, V. Placet and F. Scarpa, «A novel sandwich panel made of prepreg flax skins and bamboo core», *Composites Part C Open Access*, 2020.
- [52] D. B. Dittenber and G. Hota, «Critical review of recent publications on use of natural composites in infrastructure», *Composites Part A Applied Science and Manufacturing*, vol. 43, n. 8, p. 1419–1429, 2012.
- [53] A. Stamboulis, C. Baillie and T. Peijs, «Effects of environmental conditions on mechanical and physical properties of flax fibers», *Composites Part A Applied Science and Manufacturing*, vol. 32, n. 8, pp. 1105-1115, 2001.
- [54] S. H. Aziz and M. P. Ansell, «The effect of alkalization and fibre alignment on the mechanical and thermal properties of kenaf and hemp bast fibre composites. Part 1. Polyester resin matrix», *Composites Science and Technology*, vol. 64, n. 9, pp. 1219-1230, 2004.
- [55] L. Yan, N. Chouw and K. Jayaraman, «Flax fibre and its composites A review», *Composites Part B Engineering*, vol. 56, pp. 296-317, 2013.
- [56] V. Fiore, L. Calabrese, G. Di Bella, T. Scalici, G. Galtieri, A. Valenza and E. Proverbio, «Effects of aging in salt spray conditions on flax and flax/basalt reinforced composites: Wettability and dynamic mechanical properties», *Composites Part B Engineering*, vol. 93, n. 11, 2016.
- [57] G. Cicala, G. Cristaldi, G. Recca and A. Latteri, «Composites Based on Natural Fibre Fabrics», *Woven Fabric Engineering*, vol. 379, n. 28, 2010.
- [58] I. Pillin, A. Kervoelen, A. Bourmaud, J. Goimard, N. Montrelay and C. Baley, «Could oleaginous flax fibers be used as reinforcement for polymers?», *Industrial Crops and Products*, vol. 34, n. 3, pp. 1556-1563, 2011.
- [59] H. Ku, H. Wang, N. Pattarachaiyakoop and M. Trada, «A review on the tensile properties of natural fiber reinforced polymer composites», *Composites Part B: Engineering*, vol. 42, n. 4, pp. 856-873, 2011.
- [60] C. Baley, A. Bourmaud and P. Davies, «Eighty years of composites reinforced by flax fibres: A historical review», *Composites Part A: Applied Science and Manufacturing*, vol. 144, 2021.
- [61] A. P. More, «Flax fiber-based polymer composites: a review», *Advanced Composites and Hybrid Materials*, vol. 5, pp. 1-20, 2022.
- [62] L. CoDyre, K. Mak and A. Fam, «Flexural and axial behaviour of sandwich panels with biobased flax fibre-reinforced polymer skins and various foam core densities», *Journal of Sandwich Structures & Materials*, vol. 20, n. 5, 2018.
- [63] Y. Fu and P. Sadeghian, «Flexural and shear characteristics of bio-based sandwich beams made of hollow and foam-filled paper honeycomb cores and flax fiber composite skins», *Thin-Walled Structures*, vol. 153, 2020.

- [64] L. Á. Oliveira, G. L. C. Coura, M. L. P. Tonatto, T. H. Panzera, V. Placet and F. Scarpa, «A novel sandwich panel made of prepreg flax skins and bamboo core», *Composites Part C: Open Access*, vol. 3, 2020.
- [65] K. Uehara and M. Sakurai, «Bonding strength of adhesives and surface roughness of joined parts», *Journal of Materials Processing Technology*, vol. 127, n. 2, pp. 178-181, 2002.
- [66] K. R. Ramakrishnan, E. Sarlin, M. Kanerva and M. Hokka, «Experimental study of adhesively bonded natural fibre composite steel hybrid laminates», *Composites Part C: Open Access*, vol. 5, 2021.
- [67] A. Badami, M. L. Raffa, O. Klinkova, R. Rizzoni, T. D. S. Botelho and G. Zambelis, «Surface roughness influence on the behaviour of biocomposite adhesive joints», *International Journal of Mechanical Sciences*, vol. 283, n. 1, 2024.
- [68] M. Linke and R. Lammering, «On the calibration of the cohesive strength for cohesive zone models in finite element analyses», *Theoretical and Applied Fracture Mechanics*, vol. 124, 2023.
- [69] E. Cintura, P. Faria, M. Duarte and L. Nunes, «Bio-Wastes as Aggregates for Eco-Efficient Boards and Panels: Screening Tests of Physical Properties and Bio-Susceptibility», *Infrastructures*, vol. 7, n. 3, 2022.
- [70] T. Cadu, M. Berges, O. Sicot, V. Person, B. Piezel, L. Van Schoors, V. Placet, S. Corn, R. Léger, L. Divet, P. Ienny and S. Fontaine, «What are the key parameters to produce a high-grade bio-based composite? Application to flax/epoxy UD laminates produced by thermocompression», *Composites Part B: Engineering*, vol. 150, pp. 36-46, 2018.
- [71] ASTM, «C 393-00: Standard Test Method for Flexural Properties of Sandwich Constructions», 2000.
- [72] H. G. Allen, Analysis and Design of Structural Sandwich Panels, Oxford, 1969.
- [73] B. Sala, X. Gabrion, F. Trivaudey, V. Guicheret-Retel and V. Placet, «Influence of the stress level and hygrothermal conditions on the creep/recovery behaviour of high-grade flax and hemp fibre reinforced GreenPoxy matrix composites», *Composites Part A: Applied Science and Manufacturing*, vol. 141, 2021.
- [74] A. Demir, H. Ozturk, K. Edip, M. Stojmanovska and A. Bogdanović, «Effect of viscosity parameter on the numerical simulation of reinforced concrete deep beam behavior», *The Online Journal of Science and Technology*, vol. 3, n. 8, 2018.
- [75] A. E. Al-Snafi, «Iraqi Medicinal Plants with Antibacterial Effect-A Review», *OSR Journal Of Pharmacy*, vol. 9, n. 8, pp. 22-103, 2019.
- [76] EN 312, «Particleboards Specifications», European Committee for Standardization (CEN), Brussels, Belgium, 2010.
- [77] P. Potapov, M. C. Hansen, A. Pickens, A. Hernandez-serna, A. Tyukavina, S. Turubonova, V. Zalles, X. Li, A. Khan, F. Stolle, N. Harris, X. P. Song, A. Baggett, I. Kommareddy and A. Kommareddy, «The Global 2000-2020 Land Cover and Land Use Change Dataset Derived From the Landsat Archive: First Results», *Front Remote Sensing*, vol. 3, pp. 1-22, 2022.
- [78] M. Hansen, P. V. Potapov, R. Moore, H. Hancher, S. A. Turubanova, A. Tyukavina, D. Thau, S. V. Stehman, S. J. Goetz, L. T. R, A. Kommareddy, E. A, L. Chini, C. O. Justice and J. R. Townshend, «High-Resolution Global Maps of 21st-Century Forest Cover Change», *Science*, vol. 324, n. 6160, pp. 850-854, 2013.
- [79] R. J. Keenan, G. A. Reams, F. Achard, J. V. De Freitas, A. Grainger and E. Lindquist, «Dynamics of global forest area: Results from the FAO Global Forest Resources Assessment 2015», *Forest Ecology and Magement*, vol. 352, pp. 9-20, 2015.

- [80] L. R. V. Zeppetello, L. A. Parsons, J. T. Spector, R. L. Naylor, D. S. Battisti, Y. J. Masuda and N. H. Wolff, «Large scale tropical deforestation drives extreme warming Lucas», *Environ Res Lett*, vol. 15, n. 8, pp. 1-7, 2020.
- [81] X. Xu, X. Zhang, W. Riley, Y. Xue, C. A. Nobre, T. E. Lovejoy and G. Jia, «Deforestation triggering irreversible transition in Amazon hydrological cycle», *Environ Res Lett*, vol. 17, n. 3, 2022.
- [82] Ministero degli Affati Esteri e della Cooperazione, «Statistiche relative all'intersacmbio commerciale italiano nel settore del LEGNO (esclusi i mobili)», 2023.
- [83] L. Jiménez and I. Sanchez, «Residuos agrícolas para la obtención de pastas celulósicas en Espana», *Ingeniería Química*, n. 248, pp. 125-131, 1989.
- [84] R. Jiménez, G. Herruzo and T. C. Alcántara, «Posibilidades de aprovechamiento de los residuos lignocelulósicos», *Ingeniería química*, n. 254, pp. 191-197, 1990.
- [85] L. D. Nguyen, J. Luedtke, M. Nopens and A. Krause, «Production of wood-based panel from recycled wood resource: a literature review», *European Journal of Wood and Wood Products*, vol. 81, n. 3, pp. 1-14, 2023.
- [86] F. C. Bergeron, «Assessment of the coherence or the Swiss waste wood management», *Resources Conservation and Recycling*, vol. 91, pp. 62-70, 2014.
- [87] E. Cintura, P. Faria, L. Molari, L. Barbaresi, D. D'Orazio and L. Nunes, «A feasible re-use of an agro-industrial by-product: Hazelnut shells as high mass bio-agregates in building composites:hygrothermal, acoustic, and mechanical performace.», *Submitted to Journal of Cleaner Production*, vol. 434, 2024.
- [88] M. V. Scatolino, A. d. O. Costa, J. B. Guimarães Júnior, T. d. P. Protásio, R. F. Mendes and L. M. Mendes, «Eucalyptus wood and coffee parchment for particleboard production: Physical and mechanical properties», *Ciência e Agrotecnologia*, vol. 41, n. 2, p. 139–146, 2017.
- [89] J. P. Jimenez Jr, M. N. Acda, R. Razal, W. P. Abasolo, H. Hernandez and A. R. Elepaño, «Effect Tobacco Stalk Additive Particle Size on the Bond Strength and Formaldehyde Emission of Urea Formaldehyde Bonded Plywood», *The Philippine journal of science*, vol. 149, n. 2, pp. 333-342, 2020.
- [90] C. Guler, Y. Copur and C. Tascioglu, «The manufacture of particleboards using mixture of peanut hull (Arachis hypoqaea L.) and European Black pine (Pinus nigra Arnold) wood chips», *Bioresource Technology*, vol. 99, n. 8, pp. 2893-2897, 2008.
- [91] H. Pirayesh, P. Moradpour and S. Sepahvand, «Particleboard from wood particles and sycamore leaves: Physico-mechanical properties», *Engineering in Agriculture, Environment and Food*, vol. 8, n. 1, pp. 38-43, 2015.
- [92] H. S. Yang, D. J. Kim and H. J. Kim, «Rice straw—wood particle composite for sound absorbing wooden construction materials», *Bioresource Technology*, vol. 86, n. 2, pp. 117-121, 2003.
- [93] M. Staňková and T. Pipíška, «The Use of Recycled Wood as a Factor in Production Efficiency of Manufacturers in 4 Countries», *Croatian journal of forest engineering*, vol. 45, n. 2, 2024.
- [94] J. Iždinský, Z. Vidholdová and L. Reinprecht, «Particleboards from Recycled Wood», *Forests*, vol. 11, n. 11, 2020.
- [95] D. C. Lima, R. R. de Melo, A. S. Pimenta, T. D. Pedrosa, M. J. C. de Souza and E. C. de Souza, «Physical–mechanical properties of wood panel composites produced with Qualea sp. sawdust and recycled polypropylene», *Environmental Science and Pollution Research*, vol. 27, p. 4858–4865, 2020.
- [96] J. A. Flores-Yepes, J. J. Pastor, A. Martinez-Gabarron, J. Gimeno, I. Rodríguez-Guisado and M. J. Frutos, «*Arundo donax* chipboard based on urea-formaldehyde resin using under 4 mm

- particles size meets the standard criteria for indoor use», *Industrial Crops and Products*, vol. 34, n. 3, pp. 1538-1542, 2011.
- [97] M. Nazerian and V. Moazami, «Bending Strength of Sandwich-Type Particleboard Manufactured from Giant Reed (*Arundo donax*)», *Forest Products Journal*, vol. 65, n. 5, pp. 292-300, 2015.
- [98] M. Ferrandez-Villena, A. Ferrandez-Garcia, T. Garcia-Ortuño, C. E. Ferrandez-Garcia and M. T. Ferrandez Garcia, «Properties of Wood Particleboards Containing Giant Reed (*Arundo donax L.*) Particles», *Sustainability*, vol. 12, n. 24, 2020.
- [99] J. A. Flores-Yepes, J. J. Pastor, J. Gimeno, I. Rodriguez-Guisado and M. J. Frutos-Fernandez, «Full recovery of *Arundo donax* particleboard from swelling test without waterproofing additives», *BioResources*, vol. 7, n. 4, pp. 5222-5235, 2012.
- [100] L. Nunes, C. Eleonora, J. L. Parracha, B. Fernandes, V. Silva and P. Faria, «Cement-Bonded Particleboards with Banana Pseudostem Waste: Physical Performance and Bio-Susceptibility», *Infrastractures*, vol. 6, n. 6, 2021.
- [101] E. K. Sackey, K. E. Semple, S. W. Oh and G. D. Smith, «Improving core bond strength of particleboard through particle size redistribution», *Wood and Fiber Science*, vol. 40, n. 2, pp. 214-224, 2008.
- [102] EN 326-1, «Wood-based panels Sampling, cutting and inspection- Part 1», European Committee for Standardization (CEN), Brussels, Belgium, 1994.
- [103] EN 317, «Particleboards and fibreboards-Determination of swelling in thickness after immersion in water», European Committee for Standardization (CEN), Brussels, Belgium, 1993.
- [104] EN 311, «Wood-based panels-Surface soundness-Test method», European Committee for Standardization (CEN), Brussels, Belgium, 2002.
- [105] EN 319, «Particleboards and fibreboards-Determination of tensile strength perpendicular to the plane of the board», European Committee for Standardization (CEN), Brussels, Belgium, 1993.
- [106] EN 310, «Wood-based panels-Determination of modulus of elasticity in bending and of bending strength», European Committee for Standardization (CEN), Brussels, Belgium, 1993.
- [107] M. Arabi, A. R. Haftkhani and R. Pourbaba, «Investigating the Effect of Particle Slenderness Ratio on Optimizing the Mechanical Properties of Particleboard Using the Response Surface Method», *Bioresources*, vol. 18, n. 2, pp. 2800-2814, 2023.
- [108] A. E. Al-Snafi, «The constituents and biological effects of *Arundo donax* A review», *International Journal of Phytopharmacy Research*, vol. 6, n. 1, pp. 34-40, 2015.
- [109] L. Garcia Esteban, A. Guindeo Casasùs, C. Peraza Oramas and P. Palacios de Palacios, LA Madera y su Tecnologia, 2002.
- [110] K. E. Semple and G. D. Smith, «Prediction of internal bond strength in particleboard from screw withdrawal resistance models», *Wood and Fiber Science*, vol. 38, n. 2, pp. 256-267, 2006.
- [111] M. Arabi, M. Faezipour and H. Gholizadeh, «Reducing resin content and board density without adversely affecting the mechanical properties of particleboard through controlling particle size», *Journal of Forestry Research*, vol. 22, n. 4, p. 659–664, 2011.
- [112] J. T. Benthien, J. Sieburg-Rockel, N. Engehausen, G. Koch and J. Luedtke, «Analysis of Adhesive Distribution over Particles According to Their Size and Potential Savings from Particle Surface Determination», *Fibers*, vol. 11, n. 10, 2022.

- [113] E. Sackey and G. D. Smith, «Empirical distribution models for slenderness and aspect ratios of core particles of particulate wood composites», *Wood and Fiber Science*, vol. 41, n. 3, pp. 255-266, 2009.
- [114] «https://www.mathworks.com/help/stats/one-way-anova.html.».
- [115] F. Vitrone, D. Ramos, F. Ferrando and J. Salvadó, «Binderless fiberboards for sustainable construction. Materials, production methods and applications», *Journal of Building Engineering*, vol. 44, 2021.
- [116] R. A. Fernandes, S. Lopes, N. Ferreira, J. Santos, J. M. Martins and L. H. Carvalho, «Binderless particleboards obtained 100% from winery by-products for the packaging industry», *Frontiers in Food Science and Technology*, vol. 4, 2024.
- [117] K. Antoun, A. Besserer, R. El Hage, C. Segovia, R. Sonnier and N. Brosse, «Environmentally-friendly, binder-free, non-flammable particleboard with enhanced properties», *Industrial Crops and Products*, vol. 222, n. 1, 2024.
- [118] R. Tupciauskas, J. Rizhikovs, M. Andzs and O. Bikovens, «Influence of Manufacturing Conditions on Binder-Less Boards from Steam-Exploded Hemp Shives and Wheat Straw», *Materials*, vol. 15, n. 9, 2022.
- [119] R. Tupciauskas, J. Rizhikovs, P. Brazdausks, V. Fridrihsone and M. Andzs, «Influence of steam explosion pre-treatment conditions on binder-less boards from hemp shives and wheat straw», *Industrial Crops and Products*, vol. 170, 2021.
- [120] J. Bauta, G. Vaca-Medina, C. D. Raynaud, V. Simon, V. Vandenbossche and A. Rouilly, «Development of a Binderless Particleboard from Brown Seaweed Sargassum spp.», *Materials*, vol. 17, n. 3, 2024.
- [121] W. N. A. W. Nadhari, M. Danish, S. N. A. B. Abdullah, A. M. Alanazi, N. A. Karim and A. Mustapha, «Effect of potato starch on surface characteristics, mechanical, physical, and chemical binding mechanism of kenaf binderless particleboard», *Industrial Crops and Products*, vol. 212, 2024.
- [122] M. A. Jamaludin, S. A. Bahari, M. N. Zakaria and N. S. Saipolbahri, «Influence of Rice Straw, Bagasse, and their Combination on the Properties of Binderless Particleboard», *Wood Science and Technology*, vol. 48, n. 1, pp. 22-31, 2020.
- [123] R. Fu, M. Guan, G. Wang, L. Pan and Y. Li, «Optimised fermentation of bamboo waste using three types lactic acid bacteria and forming mechanism of binderless particleboard», *Industrial Crops and Products*, vol. 196, 2023.
- [124] I. P. Nitu, M. N. Islam, M. Ashaduzzaman, M. K. Amin and M. I. Shams, «Optimization of processing parameters for the manufacturing of jute stick binderless particleboard», *Journal of Wood Science*, vol. 66, n. 65, 2020.
- [125] A. Ferrandez-Garcia, M. T. Ferrandez-Garcia, T. Garcia-Ortuño and M. Ferrandez-Villena, «Influence of the Density in Binderless Particleboards Made from Sorghum», *Agronomy*, vol. 12, n. 6, 2022.
- [126] M. Chen, S. Zheng, J. Wu and J. Xu, «Study on preparation of high-performance binderless board from Broussonetia papyrifera», *Journal of Wood Science*, vol. 69, n. 17, 2023.
- [127] Z. Lou, Q. Wang, W. Sun, Y. Zhao, X. Wang, X. Liu and Y. Li, «Bamboo flattening technique: a literature and patent review», *European Journal of Wood and Wood Products*, vol. 79, n. 5, pp. 1035-1048, 2021.
- [128] A. Paze, P. Brazdausks, J. Rizikovs, M. Puke, R. Tupciauskas, M. Andzs, K. Meile and N. Vedernikovs, «Changes in the Polysaccharide Complex of Lignocellulose after Catalytic Hydrothermal Pre-Treatment Process of Hemp (Cannabis Sativa L.) Shives», in 23rd European Biomass Conference and Exhibition, Vienna, Austria, 2015.

- [129] L. Romanese, «The Future for Hemp: What Is at Stake?», 2019.
- [130] T. Adamová, J. Hradecký and M. Prajer, «VOC Emissions from Spruce Strands and Hemp Shive: In Search for a Low Emission Raw Material for Bio-Based Construction Materials», *Materials*, vol. 12, n. 12, 2019.
- [131] S. Sam-Brew and G. D. Smith, «Flax shive and hemp hurd residues as alternative raw material for particleboard production», *BioResources*, vol. 12, n. 3, pp. 5715-5735, 2017.
- [132] A. Almusawi, R. Lachat, K. Atcholi and S. Gomes, «Proposal of manufacturing and characterization test of binderless hemp shive composite», *International Biodeterioration & Biodegradation*, vol. 115, pp. 302-307, 2016.
- [133] C. Jarman, Plant Fibre Processing, London: Intermediate Technology Publications, 1998.
- [134] S. Kalia, B. S. Kaith and I. Kaur, «Pretreatments of Natural Fibers and their Application as Reinforcing Material in Polymer Composites A Review», *Polymer Engineering and Science*, vol. 49, n. 7, pp. 1253 1272, 2009.
- [135] J. Bolton, «The Potential of Plant Fibres as Crops for Industrial Use», *Outlook on Agriculture*, vol. 24, n. 2, 1995.
- [136] M. M. Kostic, B. Pejic and P. Skundric, «Quality of chemically modified hemp fibers», *Bioresource Technology*, vol. 99, n. 1, pp. 94-99, 2008.
- [137] R. El Hage, R. C. Martins, C. Brendlé, D. Lafon-Pham and R. Sonnier, «Enhancing Insight into Photochemical Weathering of Flax and Miscanthus: Exploring Diverse Chemical Compositions and Composite Materials», *Molecules*, vol. 29, n. 16, 2024.
- [138] B. Romanowska, W. Różańska and M. Zimniewska, «The Influence of the Chemical Composition of Flax and Hemp Fibers on the Value of Surface Free Energy», *Materials*, vol. 17, n. 5, 2024.
- [139] Y. Y. Bai, L. P. Xiao, Z. J. Shi and R. C. Sun, «Structural Variation of Bamboo Lignin before and after Ethanol Organosolv Pretreatment», *International Journal of Molecular Sciences*, vol. 14, n. 11, p. 21394–21413, 2013.
- [140] M. I. Maulana, M. Marwanto, D. S. Nawawi, S. Nikmatin, F. Febrianto and N. Kim, «Chemical components content of seven Indonesian bamboo species», in *IOP Conference Series Materials Science and Engineering*, 2020.
- [141] D. Ramos, N. E. El Mansouri, F. Ferrando and J. Salvadó, «All-lignocellulosic Fiberboard from Steam Exploded Arundo Donax L.», *Molecules*, vol. 23, n. 9, 2018.
- [142] M. Guan, R. Fu, C. Yong, Y. Li and X. Xu, «Properties of binderless bamboo particleboards derived from biologically fermented bamboo green residues», *Waste Management*, vol. 151, pp. 195-204, 2022.
- [143] S. D. Malingam, N. L. Feng, A. A. Kamarolzaman, H. T. Yi and A. F. Ab Ghani, «Mechanical Characterisation of Woven Kenaf Fabric as Reinforcement for Composite Materials», *Journal of Natural Fibers*, vol. 18, no. 5, pp. 653-663, 2021.
- [144] A. Bourmaud, J. Beaugrand, D. U. Shah, V. Placet and C. Baley, «Towards the design of high-performance plant fibre composites», *Progress in Materials Science*, vol. 97, no. 3, pp. 347-408, 2018.
- [145] A. Del Masto, F. Trivaudey, V. Guicheret-Retel, V. Placet and L. Boubakar, «Investigation of the possible origins of the differences in mechanical properties of hemp and flax fibres: A numerical study based on sensitivity analysis», *Composites Part A: Applied Science and Manufacturing*, vol. 124, 2019.
- [146] W. Brouwer, «Natural fiber composite: where can flax compete with glass?», *Sampe Journal*, vol. 36, n. 6, pp. 18-23, 2000.

- [147] A. A. Griffith, «The phenomena of rupture and flow in solids», *Philosophical Transactions of the Royal Society A*, vol. 23, 1921.
- [148] A. Bourmaud, C. Morvan and C. Baley, «Importance of fiber preparation to optimize the surface and mechanical properties of unitary flax fiber», *Industrial Crops and Products*, vol. 32, n. 2, pp. 662-667, 2010.
- [149] A. Duval, A. Bourmaud, L. Augier and C. Baley, «Influence of the sampling area of the stem on the mechanical properties of hemp fibers», *Materials Letters*, vol. 64, n. 4, pp. 797-800, 2011.
- [150] A. S. Virk, W. Hall and J. Summerscales, «Multiple Data Set (MDS) weak-link scaling analysis of jute fibres», *Composites Part A*, vol. 40, n. 11, pp. 1764-1771, 2009.
- [151] G. Thangavel, S. Mohanty and S. K. Nayak, «A review of the recent developments in biocomposites based on natural fibres and their application perspectives», *Composites Part A: Applied Science and Manufacturing*, vol. 77, pp. 1-25, 2015.
- [152] J. Bachmann, C. Hidalgo and S. Bricout, «Environmental analysis of innovative sustainable composites with potential use in aviation sector life cycle assessment review», *Science China Technological Sciences*, vol. 60, no. 9, pp. 1301-1317, 2017.
- [153] A. Shahzad, «Hemp fiber and its composite A review», *Journal of composite materials*, vol. 46, n. 8, pp. 973-986, 2011.
- [154] R. Bernabini, A. Benedetti and F. Marani, «Analisi sperimentale di fattibilità di elementi strutturali rinforzati con fibre naturali», Bologna, 2010.
- [155] A. C. Corbin, D. Soulat, M. Ferreira, A. R. Labanieh, X. Gabrion, P. Malécot and V. Placet, «Towards hemp fabrics for high-performance composites: Influence of weave pattern and features», *Composites Part B Engineering*, vol. 181, 2020.
- [156] K. B. Katnam, H. K. Mohmoud and P. Potluri, «Towards balancing in-plane mechanical properties and impact damage tolerance of composite laminates using quasi-UD woven fabrics with hybrid warp yarns», *Composite Structures*, vol. 225, 2019.
- [157] A. P. Mouritz, M. K. Bannister, P. J. Falzon and K. H. Leong, «Review of applications for advanced three-dimensional fibre textile composites", *Composites Part A: Applied Science and Manufacturing*, vol. 30, no. 12, pp. 1445-1461, 1999.
- [158] ASTM, D 3039/D 3039M-00, «Standard Test Method for Tensile Properties of Polymer Matrix Composite Materials», 2000.
- [159] A. Borri, M. Corradi and E. Speranzini, «Reinforcement of wood with natural fibers», *Composites Part B Engineering*, vol. 53, pp. 1-8, 2013.
- [160] X. Gabrion, G. Koolen, M. Grégoire, S. Musio, M. Bar, D. Botturi, G. Rondi, E. de Luycker, S. Amaducci, P. Ouagne, A. Van Vuure and V. Placet, «Influence of industrial processing parameters on the effective properties of long aligned European hemp fibres in composite materials», *Composites Part A*, n. 157, 2022.
- [161] EN ISO 139, +A1, «Textiles- Standard atmospheres for conditioning and testing», Brussels, Belgium: European Committee for Standardization (CEN), 2011.
- [162] G. A. Sivasankar, P. A. Karthick, C. Boopathi, S. Brindha, R. J. T. Nirmalraj and A. Benham, «Evaluation and comparison on mechanical properties of abaca and hemp fiber reinforced hybrid epoxy resin composites», *Materials Today: Proceedings*, 2023.
- [163] J. P. Shebaz Ahmed, S. Shanmugavel, P. Elumalai, T. Evgeny and B. Sridhar, «Exploration of mechanical properties of hemp fiber/flax fiber reinforced composites based on biopolymer and epoxy resin», *Materials Today: Proceedings*, 2023.

- [164] H. Ruihua and L. Jae-Kyoo, «Fabrication and Mechanical Properties of Completely Biodegradable Hemp Fiber Reinforced Polylactic Acid Composites», *Journal of Composite Materials*, vol. 41, no. 13, pp. 1655-1669, 2007.
- [165] B. Baghaei, M. Skrifvars and L. Berglin, «Characterization of thermoplastic natural fibre composites made from woven hybrid yarn prepregs with different weave pattern», *Composites*, no. 76, pp. 154-161, 2015.
- [166] L. Y. Mwaikambo and M. P. Ansell, «Hemp fibre reinforced cashew nut shell liquid composites», *Composites Science and Technology*, vol. 63, no. 9, pp. 1297-1305, 2003.